Stress Analysis of ASME B16.5 class 900 Bolted Flange Joints Subjected to Bolt-up and Pressure

by

Abdul Fattah ALARNOUS

THESIS PRESENTED TO ÉCOLE DE TECHNOLOGIE SUPÉRIEURE
IN PARTIAL FULFILLMENT FOR A MASTER'S DEGREE
WITH THESIS IN MECHANICAL ENGINEERING
M.A.Sc.

MONTREAL, AUGUST 24, 2023

ÉCOLE DE TECHNOLOGIE SUPÉRIEURE
UNIVERSITÉ DU QUÉBEC

BOARD OF EXAMINERS

THIS THESIS HAS BEEN EVALUATED

BY THE FOLLOWING BOARD OF EXAMINERS

Mr. Hakim A. Bouzid, Thesis Supervisor
Department of Mechanical Engineering, École de technologie supérieure

Mr. Lucas Hof, Member of the jury
Department of Mechanical Engineering, École de technologie supérieure

Mr. Wahid Maref, President of the jury
Department of Construction Engineering, École de technologie supérieure

THIS THESIS WAS PRESENTED AND DEFENDED

IN THE PRESENCE OF A BOARD OF EXAMINERS AND PUBLIC

ON AUGUST 4, 2023

AT ÉCOLE DE TECHNOLOGIE SUPÉRIEURE

ACKNOWLEDGMENT

I would like to extend my heartfelt gratitude and appreciation to the following individuals who have been instrumental in the completion of my thesis.

First and foremost, my sincere thanks go to my esteemed professor, Hakim A. Bouzid. I greatly appreciate his willingness to share his expertise and experience with me. More specifically, his priceless advice, constant support, and significant guidance have profoundly influenced the course of my work throughout the research process.

Furthermore, warmest thanks to my family are in order. I am forever grateful for my parents, Mohamad Imad Alarnous and Nelly Arnaout, who have always been my greatest inspiration with their unconditional love, steadfast faith in my skills, and everlasting support. Your advice, sacrifices, and unfailing confidence in my talents are and will always be immensely appreciated.

Last but not least, my sisters, Sally Alarnous and Jana Alarnous, as well as my beloved, Mira Yakan, have been my backbones and my biggest support system through their love, encouragement, and faith in my skills. I appreciate all the feedback, advice, and motivation that you have offered me along this journey.

Analyse de contrainte des joints de brides boulonnés de classe 900 selon la norme ASME B16.5 soumis à l'assemblage des boulons et à la pression

Abdul Fattah ALARNOUS

RÉSUMÉ

Les assemblages à brides boulonnées munis de joints d'étanchéité sont largement utilisé dans les différentes industries, mais principalement dans les installations pétrolières, gazières et de production d'électricité. Le rôle principal d'une bride boulonnée consiste à connecter la tuyauterie et les vaisseaux sous pression entre eux. Malgré le fait que ses principaux domaines d'utilisation semblent simples, les brides boulonnées peuvent encore rencontrer de nombreux problèmes qui peuvent causer des dommages importants à l'environnement et aux humains. En effet, soumis à la haute pression et la haute température des fluides ces assemblages et tuyauteries, sont sujet à des fuites qui peuvent compromettre la sécurité et l'environnement.

Lors de la conception des brides, l'intégrité structurelle et l'étanchéité sont considérées comme les deux paramètres à considérer pour assurer leur bon fonctionnement. Au niveau de la conception du modèle, l'inspection des résultats analytiques est cruciale et est obtenue en les comparants aux résultats obtenus par la méthode des éléments finis. Enfin, il est essentiel de mentionner à quel point il est important d'examiner les contraintes au niveau des jonctions, car cela peut compromettre considérablement l'intégrité de la bride. Pour toutes ces raisons et paramètres, cette étude a été conçue dans le but d'évaluer l'intégrité de la bride et son étanchéité en appliquant la méthodologie à différentes tailles de brides boulonnées appartenant à la classe 900.

De nombreux paramètres ont été étudiés dans cette étude, notamment la contrainte de contact du joint d'étanchéité, la contrainte dans les boulons, la rotation de la bride, le déplacement radial et les contraintes longitudinales et tangentes le long de la distance axiale de la bride. À noter, la bride à collet soudé et le joint spiralé sont utilisés dans cette étude pour toutes les brides étudiées.

La forme de la bride est la même pour toutes les brides, composées de l'anneau, du moyeu et de la coque reliés aux jonctions. Ainsi, la bride à collet soudé (WNF) et le joint spiralé (SWG) sont assemblés en plaçant le joint entre les deux brides, puis en plaçant les boulons dans les trous avec un serrage approprié dans le but d'éviter toute fuite possible. Cependant, sept exemples sont utilisés tout au long de l'étude pour étudier l'influence de taille des brides et leur intégrité. Ainsi les brides NPS 4, 8, 10, 14, 16, 20 et 24 classe 900 de la norme ASME B16.5 sont modélisés et simulés sur ANSYS (logiciel d'éléments finis) pour obtenir les résultats lesquels sont ensuite comparés aux résultats analytiques pour vérifier la validité du modèle analytique développé précédemment.

Mots-clés : Assemblages à brides boulonnées, intégrité des brides, étanchéité, contrainte de contact de la garniture d'étanchéité, contrainte des boulons, rotation des brides, déplacement radial, distribution des contraintes, bride à collerette soudée, garniture spiralée

Stress Analysis of ASME B16.5 class 900 Bolted Flange Joints Subjected to Bolt-up and Pressure

Abdul Fattah ALARNOUS

ABSTRACT

Bolted flange joint assemblies are used in many industries, mainly in oil, gas, and power generation facilities. The main role of a bolted flange manifests in connecting pipes, valves, and pressure equipment to ensure the pressurized substance flowing in the pipes. Although their usage may seem simple, bolted flanges are subjected to harsh conditions that may lead to leakage and environment damage. The high pressure and high temperature of the confined fluid inside the pipes can notably compromise human health, safety, and the environment. On the other hand, structural integrity and leakage tightness are two main criteria that must be taken into consideration to prevent catastrophic failure when designing bolted flange joints. At the design level, it is crucial to compare the analytical results to the ones obtained from the numerical finite element method. Finally, from the structural integrity standpoint, it is important to examine the stresses at the junctions since they are the weakest regions of the flange. This study focuses on the evaluation of the integrity and leakage tightness of some ASME B16.5 class 900 flanges when subjected to pressure.

This study investigated many parameters: the gasket contact stress, the bolt stress, the flange rotation, the radial displacement, and the distribution of the longitudinal and tangential stresses along the axial flange distance. It is to be noted that the welding neck type of flange and the spiral wound type of gasket are used to analyze all flange sizes. The flange is composed of the ring, hub, and shell that are connected at the two junctions. The welding neck flange (WNF) and the spiral wound gasket (SWG) are tightened to the recommended bolt stress of 50 ksi to prevent any possible leaks. Seven flanges of the size NPS 4, 8, 10, 14, 16, 20, and 24 of ASME B16.5 standard are modeled and simulated on ANSYS (finite element software) to obtain the results which are then compared to the analytical results to check the validity of the already developed analytical model.

Keywords: Bolted flange joint, flange integrity, leakage tightness, gasket contact stress, bolt stress, flange rotation, radial displacement, stress distribution, welding neck flange (WNF), spiral wound gasket (SWG)

TABLE OF CONTENTS

LIST OF TABLES

LIST OF FIGURES

LIST OF ABREVIATIONS

ASME	American Society of Mechanical Engineers
CPU	Central Processing Unit
NPS	Nominal Pipe Size
PTFE	Polytetrafluoroethylene
ROTT	Room Temperature Tightness Test
FEA	Finite Element Analysis
UGR	Universal Gasket Rig
MMC	Metal-to-Metal Contact
BFC	Bolted Flange Connection
SWG	Spiral Wound Gasket
WNF	Welding-Neck Flange
OD	Outer Diameter
PVRC	Pressure Vessel Research Council

LIST OF SYMBOLS

α	Cone angle (rad)
β_S	Shell flexural rigidity (mm^{-1})
θ	Flange rotation (deg)
ν	Poisson's ratio
σ, τ	Longitudinal and tangential stresses (MPa)
A_r	Root stress area of the bolt (mm^2)
A_S	Tensile stress area of the bolt (mm^2)
A_p	Pressurized area (mm^2)
D_b	Nominal diameter of the bolt(mm)
E	Young's modulus (MPa)
E_g	Gasket compression modulus (MPa)
H_B	Bolt force (N)
H_G	Gasket force (N)
K	Ratio of outside to inside diameter of the flange
K	Stiffness (N/mm)
M_f	Twisting moment of flange ring (N.mm/mm)
M_θ, M_ϕ, M_s	Bending moments around θ, ϕ, s directions respectively (N.mm)
N_θ, N_ϕ, N_s	Normal forces in θ, ϕ, s directions (N/mm)

Q	Shear force (N/mm)
r_b	Bolt circle radius (mm)
r_g	Average radius of gasket (mm)
r_h	Hub radius (mm)
r_s	Cylinder radius (mm)
R_i	Inside radius of flange (mm)
R_m	Average radius of flange (mm)
R_o	Outside radius of flange (mm)
S_g	Gasket stress (MPa)
t	Thickness (mm)
t_f	Flange thickness (mm)
U	Axial displacement (mm)
w	Radial displacement (mm)
P	Internal Pressure (MPA)
P_b	Pitch of the bolt threads (mm)

W_M, W_P, W_Q	Displacement due to edge moment, internal pressure, and edge load at the junction (mm)
y_S	Yield stress (MPa)
Y	Factor involving

INTRODUCTION

Bolted flange connections are mechanical joints that are frequently used in pressure vessels and piping systems of the chemical, petrochemical, and oil and gas industries. An assembly of two flanges, with a gasket in between tightened together by bolts is called a bolted flange joint. The gasket, on the other hand, positioned between the two flanges prevents leaks by plastic deformation and penetration creating a perfect seal. For this reason, the initial tightening of the bolts in a bolted flange joint is essential to achieve a reliable and leak-free connection. The bolts must be tightened to the prescribed torque value to ensure joint mechanical integrity and leak tightness. Unfortunately, the type of fluid being conveyed, the working conditions, and the external solicitations can cause leakage in a bolted flange joint which may result in severe environmental damage, severe accident safety hazards and even loss of revenue.

Hence, it is important to select the right material and the appropriate components, ensure proper installation, and routinely check the connection for leaks, wear, and damage to avoid catastrophic failure of the bolted flange joint. These measures help reduce the risk of danger or damage and, as a result, increase pipeline system safety, and its effective functioning. It seems a bit vague many techniques have been investigated to study the behavior of bolted flange joints of piping systems, and a useful technique that is offered via finite element analysis (FEA) can be implemented through the ANSYS software. FEA may not only offer a thorough knowledge of bolted joint performance and possible concerns in the design and proper modeling under various loading conditions, but can also improve piping systems' reliability, safety, and problem-solving potential. The latter, however, can hold several advantages to prevent leaks in bolted flange joints, notably by reducing the possibility of hazards like fire, explosions, and poisonous gases while also improving the safety of use. In addition, dependability is increased through the prevention of equipment breakdowns and the reduction of production downtime. FEA works as well by minimizing soil and water pollution which lessens its negative environmental impact. Once leaks are avoided, the overall running expenses are reduced, and the effects of leaks can be minimized by putting in place efficient leak prevention procedures. Consequently, the easiest way to predict the real consequences

that might occur would be by conducting a simulation using the computational finite element method (FEA) under realistic conditions.

Figure 0-1 Bolted flange joint

On the other hand, the gaps between floating flanges, variations in flange flatness, surface finish, geometry discontinuities, and poor bolt tightening can all contribute to weakening bolted flange joints, resulting in stress concentration and joint failure. Therefore, for bolted flange joints to be safe under loads, it is essential to examine the stress in certain bolted joints. For instance, improving the design and pinpointing probable failure mechanisms requires studying the stress distribution in the flange, bolts, and gasket although being a difficult task that demands a good knowledge of mechanics and testing its analytical techniques.

It is also important to consider the stresses occurring in the bolted joint and identify the most critical locations throughout analytical or FE modeling. Both longitudinal and tangential stresses exist during the bolting up and pressurization of the bolted joint because of the axial load exerted by the bolts or the internal pressure. In comparison, radial stress is often insignificant. As a result, the radial stress analysis is frequently overlooked in favor of the more important longitudinal and tangential stresses. To make sure the joint can bear anticipated loads without failure, these stresses must be accurately predicted during the design phase, and they can be supported by the structure if the right material and geometry are well selected.

In addition, the flange rotation is considered one of the main important parameters to investigate and it is defined as the angular distortion or cupping of the flange around the

circumferential direction because of the applied loads to a bolted flange connection. The suggested flange rotation limitations, which are commonly represented as a percentage of the bolt circle diameter, must be maintained to prevent issues including gasket crushing, joint separation, and uneven bolt loading. According to ASME PCC-1, these limitations typically range between 0.5% and 1% for metallic gaskets and up to 3% for non-metallic gaskets, depending on the gasket type, flange size, and maximum permitted bolt stress. The bolted flange joint can function as designed if flange rotation is kept within acceptable bounds.

When simulating bolted flange joints, the pressure that the flange faces generate on the gasket during bolt-up is known as gasket contact stress. However, variables like the type of gasket used, the flange surface finish, and the bolt preload, among other variables, can highly impact the contact stress distribution, which can compromise joint sealing and integrity. The gasket contact stress analysis using FEA models helps joint design optimization and material selection to guarantee that the contact stress stays within safe and predictable ranges. It is proposed to analyze the integrity of some of ASME B16.5 class 900 flanges by looking at the parameters that have been described previously such as bolt and gasket stress, flange rotation, and the stresses distribution in the different parts of the flange, namely the hub, the shell and flange ring during bolt up and pressurization.

The focal points of each of the following chapters are the different elements of the bolted flange joint which major contributions and conclusions are outlined in a brief summary.

More specifically, chapter 1 comprises a thorough analysis of the literature on bolted flange joints as a crucial part of pipes and pressure vessels; it serves as a summary of the development, design, and use of bolted flange joints throughout history. This segment particularly examines the various flange and gasket designs implemented in bolted flange joints and the materials often employed in their production. It also covers the numerous rules and standards that control the design and fabrication of bolted flange joints. In addition, it gives an insight into the main difficulties and problems associated with the use of this pressure vessel component. The literature review, on the other hand, introduces the need and justification of the chapters that follow.

Consecutively, chapter 2 proposes the use of a sophisticated analytical model based on the shell and plate theories for the analysis of the bolted flange joints to validate the FE study. The

elastic interaction between the different elements of the flange connection, namely the flange gasket and bolt, is considered. The model and its supporting assumptions are detailed.

Chapter 3 describes the FEM model and the stress analysis methodology. It provides the dimensions of the seven selected flange models that are representative of ASME B16.5 class 900 flanges NPS 4, 8, 10, 14, 16, 20, and 24 and gives an insight to the detailed ANSY elements used constraints and loading applied to the models.

Last but not least, chapter 4 discusses the results obtained from ANSYS for all the different flange sizes and their comparison with the analytical model counterparts. The longitudinal and tangential stress distributions, the flange rotation, gasket contact stress, bolt stress, and radial displacement are compared to validate the study.

Finally, a conclusion summarizing the major findings and a recommendation for future work to help take the research a step further follows the above-mentioned chapters.

CHAPTER 1

LITERATURE REVIEW

1.1 Bolted Flange Joints

Fluid transport and management are critical and crucial tasks when it comes to safety, given that various industrial fluids are either hazardous, poisonous, or highly inflammable. To ensure safe transportation and handling of fluids, pressure vessels and piping systems are used. To connect the different parts of this pressure equipment, bolted flange joints are used as the most popular means to achieve this task. These components utilize flanges that compress a gasket with bolts to create a tight seal. Hence, the main purpose of a bolted gasketed joint is fluid containment in pipes, and leakage prevention to the outer boundary or surrounding environment (Galai, 2009). Galai (2009) adds that leakage may cause health and hazard issues and contamination to the environment and humans. Thus, the efficiency of this installation is dependent on the success of fluid containment and the prevention of any possible harmful leakages. Bolted flange joints, which body design is demonstrated in Figure 1-1, are considered a must in pipping systems, creating a connection between several pipes while offering disassembly for access and maintenance that welding cannot provide.

Figure 1-1 Typical bolted flange joint assembly

According to Jaszak and Adamek (2019), bolted flange joints also enable a more complex system through measuring devices and processors, such as flowmeters, pumps, fans and pressure vessels. This complex system creates an inevitable leakage because there are over 100,000 joint connections in a typical process plant. Therefore, leakage should be countified in the design stage and, if possible, controlled with proper material choice and assembly procedures, in addition to compliance with regulations and calculation standards (Galai, 2009). Jaszak and Adamek (2019) elaborated that, during the design stage, leakage is predicted by the selection of the proper gasket, where the basic design data is:

- The nominal diameter of the pipeline
- Temperature
- Pressure
- The type of transported medium

Additional data:

- External loads (in the form of forces, thermal expansion of the components, bending, and friction conditions on the mating surfaces)
- Alterations in time
- Required tightness
- Durability of the joint

A typical bolted flange joint mainly consists of two flanges connected through bolts with a gasket between them that acts as a seal (Figure 1-2).

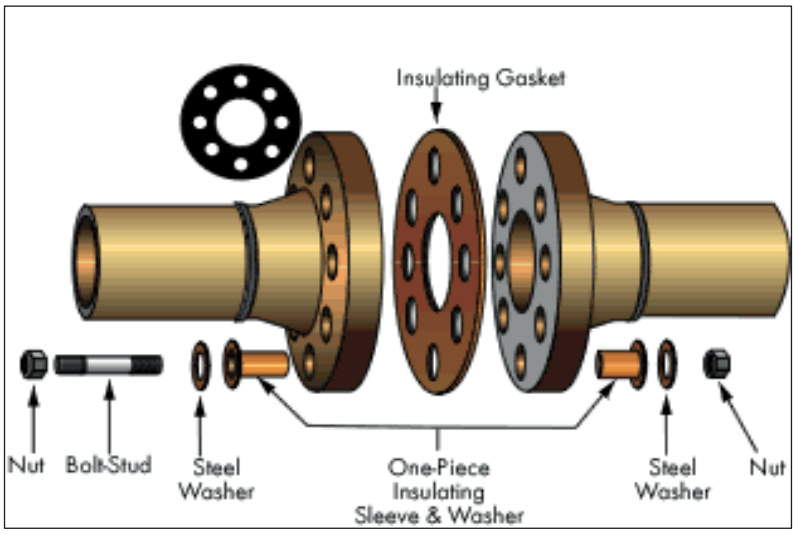

Figure 1-2 Insulated Flange Assembly

1.2 Selection Process of Piping Material

The selection process of proper piping is extremely essential since the passing liquids can be flammable, explosive, volatile, reactive, and even hazardous to human public health. Pipe selection depends on process conditions, such as types of fluid, service temperature, and operating pressure (*Pipe Material*).

- **First Process:** The type of passing fluid usually impacts the condition of the 1st process. For instance, corrosive fluids will require a higher resistance material in comparison to non-corrosive liquids:

1) Corrosive fluids like crude oil, seawater, H_2S, ammonia, acids, etc.
2) Non-Corrosive including normal carbon, lube oil, air, nitrogen, etc.

- **Second Process:** The temperature of fluids also impacts the material selection. These temperatures may vary from: a) cryogenic b) low c) medium and d) high temperatures. The listed levels of temperature control the mechanical properties of the pipe; hence, it is a must to provide the pipe with properties like impact resistance, elongation, and tensile strength.

- **Third Process:** The pressure of service fluids is the final factor in the selection of pipe material. In the case of high pressure, it is required to provide high-strength material or higher thickness.

1.3 Flange Material Selection

The performance of the flange is also dependent on the material used. The appropriate type of flange is linked to the required performance; as the determinant features are (*7 Materials for Constructing Flanges*, 2021):

- Durability
- Ease of assembly
- Weight

Flange connection selection relies on factors such as economy, flow pressure, operating temperature, and environmental corrosion. Therefore, there are 7 main materials used for constructing flanges:

a) **Copper** flanges can endure higher loads than other materials since they are non-magnetic and can sustain high-temperature services. Hence, they are great with electrical components and power generation.
b) **Titanium** is preferred for superior aircraft construction since it possesses extreme durability and lightweight properties. More importantly, titanium flanges have a high level of heat resistance which makes them perfect for aircraft engines. These assets allow titanium to be one of the most expensive industrialized materials.
c) **Aluminum** is the most used metal in the industry; it is used in marine equipment, wheels, and automotive frames. It is also lightweight and has an excellent weight-to-strength ratio which promotes higher corrosion resistance as it comes with microscopic oxide coating.
d) **Superalloys** like cobalt and nickel. These metals can withstand high heat and acid corrosion which increases susceptibility in harsh environments. They are best used in oil and gas, defense, aerospace parts, turbines, valves, piping systems, and marine industries.

e) **Stainless Steel** is used in medical tools, food service, nuclear, and desalination stations as it possesses high heat resistance.
f) **Tool Steel** comprises carbon and other alloys combined with iron. This mix makes it more resistant, susceptible, and durable. For instance, tool steel is highly efficient in machinery production.
g) **Alloy Steel** is an iron-based product that contains less than four percent chromium. It is resilient to wear and tear and is used in numerous industries like wind energy, military, aerospace, gas and oil, and nuclear industries.

1.4 Leakage

As previously stated by Bouzid and Chaaban (1993), the major challenge of flange joints is to limit or even prevent leaking. Unfortunately, whenever gas is involved in the piping system, leakage occurs to some extent since absolute zero leakage is a utopia. Thus, the most efficient and ideal design is one that minimizes leakage to a manageable level. Therefore, leakage in or out of the pipes may occur for several reasons:

1.4.1 Preload Relaxation

Preload relaxation is one of the most prevalent causes of bolted joint failure. A decrease in preload can cause a joint to open, resulting in leakage in bolted flange joints (Peth & Friedrich, 2018). When bolts are used to tighten flanges with even metallic gaskets, load relaxation occurs. According to Abid and Hussain (2008), a reduction in preload happens a few hours after bolting owing to the embedment of the asperities of the contact surfaces, which is caused by the locally high contact stress. The process of relaxation, even though inevitable, can be compensated for. Along these lines, Friedrich (2013), discussed how preload relaxation is influenced by superimposed damage mechanisms such as seating (roughness embedment during and within the first hours of tightening), load plastification (in this case caused by thermal loading), and creep (long-term permanent deformation caused by mechanical stress) (Figure 1-3).

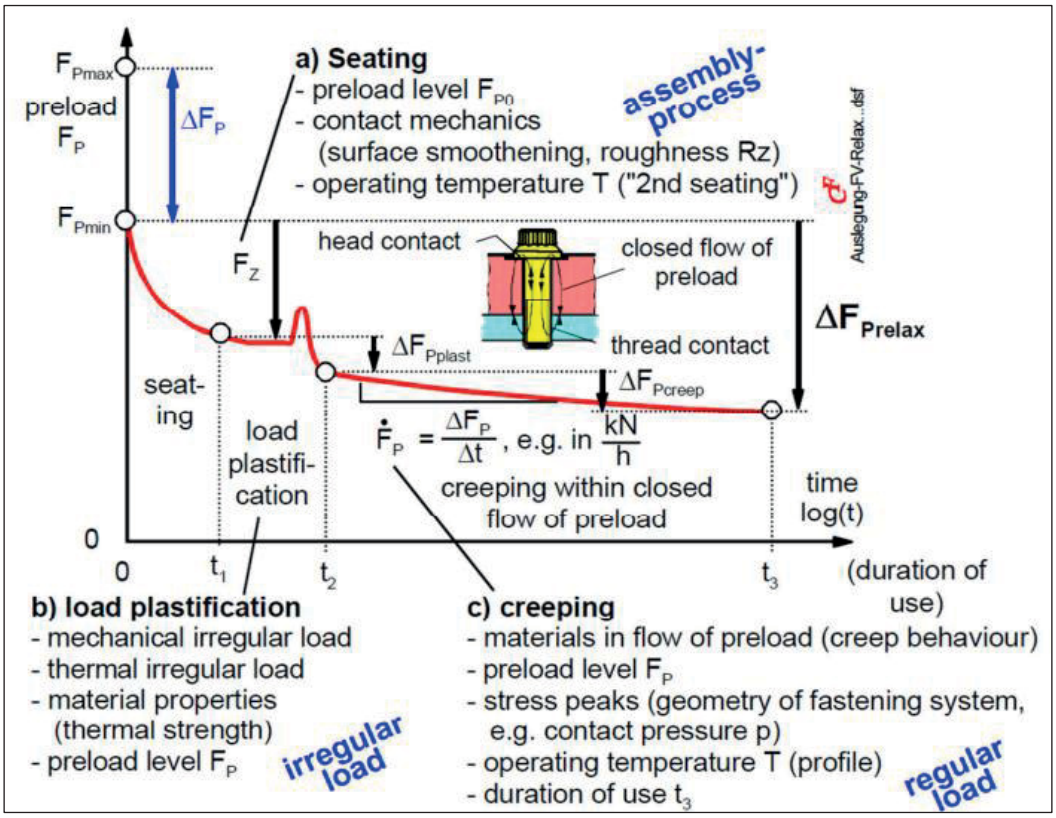

Figure 1-3 Preload Relaxation Behavior Taken from Friedrich and Hubbertz (2013, p. 339)

1.4.2 Gasket Creep

According to Peth and Friedrich (2018), creep is a permanent deformation due to mechanical stress. It's essential to distinguish between creep deformation and relaxation. During relaxation, an increase in plastic deformation to the detriment of elastic deformation causes a reduction in component stress. Unlike creep, however, the length of the components remains preserved. Creep deformation, also known as plastic deformation, is a gradual and continuous change in the shape of a material (Zacal & Jancar, 2020).

As the temperature rises and the gasket stress levels fall, gasket creep occurs several minutes after the bolts are tightened (Bouzid & al., 1995). Gaskets, like any other plastic material, can

crawl and flow when subjected to severe surface loads. The distortion that happens is vital for the gasket to function properly. Nowadays, all available gaskets on the market have acceptable loading curves and high unloading curves. On the other hand, when it comes to gasket design, physical qualities are crucial, and the primary gasket type selection is based on (Wasmi and al., 2016):

- Temperature of the media to be contained
- Pressure of the media to be contained
- Corrosive nature of the application
- Criticality of the application

1.4.3 Bolt Creep

Bolts experience creep in the same way that gaskets do. When the temperature rises beyond 650 degrees Fahrenheit, this process plays a significant role in joint relaxation (Nechache & Bouzid, 2007). A target preload is established when joining flanges for the first time, and bolts are tightened correspondingly. The gasket, on the other hand, responds to the forces exerted by the bolts. Bolts loosen in response to the reduction of gasket thickness, resulting in a risk of leakage.

Bolt creep occurs as the gasket load relaxes (Figure 1-4):

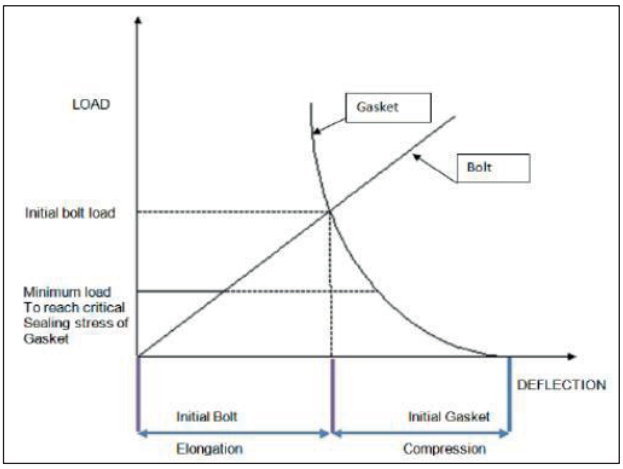

Figure 1-4 Gasket and bolt creep Taken from Wasmi et al. (2016, p. 3)

1.4.4 Vibration

Another source of load loss from bolted flange joints might be vibration. This is because mechanical vibration helps in relaxing the joints. In comparison to the initial preload, vibration-induced loosening occurs at a slow and steady pace. Philipps (2017) clarified that, when the bolt tension falls below a critical value, the effect of vibration intensifies.

1.4.5 Elastic Interaction

Another source of leakage is the elastic interaction of the joint elements, which should be properly handled. The elastic interaction prevents the objective of tightening uniformity and the target bolt preload from being met (Zhu et al., 2018). Elastic interaction, as defined by the authors, is a load variation event that occurs between joint components and bolts because of tightening. The phenomenon, also known as crosstalk, occurs when two bolts are tightened at opposite ends, causing the load of the already tightened bolts to change. Nevertheless, other experts feel that the order in which bolts are put has a significant impact on the outcome. Alkelani et al. (2009), found that the elastic interaction of a bolt, adjacently tightened to an already tightened one, decreases its initial preload by up to 98 percent. However, a three-pass tightening technique resulted in a 55 percent drop, while a four-pass tightening scheme resulted in a 28 percent loss.

1.4.6 Differential Thermal Expansion

In cryogenic or high-temperature applications, bolted-flange joints are still the preferred method to connect pipes. As a result, in addition to the relaxation caused by creep in bolted-flange joints, the temperature can influence the bolt load due to the thermal expansion difference between the bolts and the gasket and flanges. In a bolted joint, the flange rings act as a fin that transfers heat to the outer boundary. This causes the different parts of the bolted joint to expand differently in the radial and axial direction, causing a load change in the bolts. Thermal transitions have long been described as inducers of the fluctuations of the bolt load and consequently tightness of such joints for these reasons (Spetech, 2021).

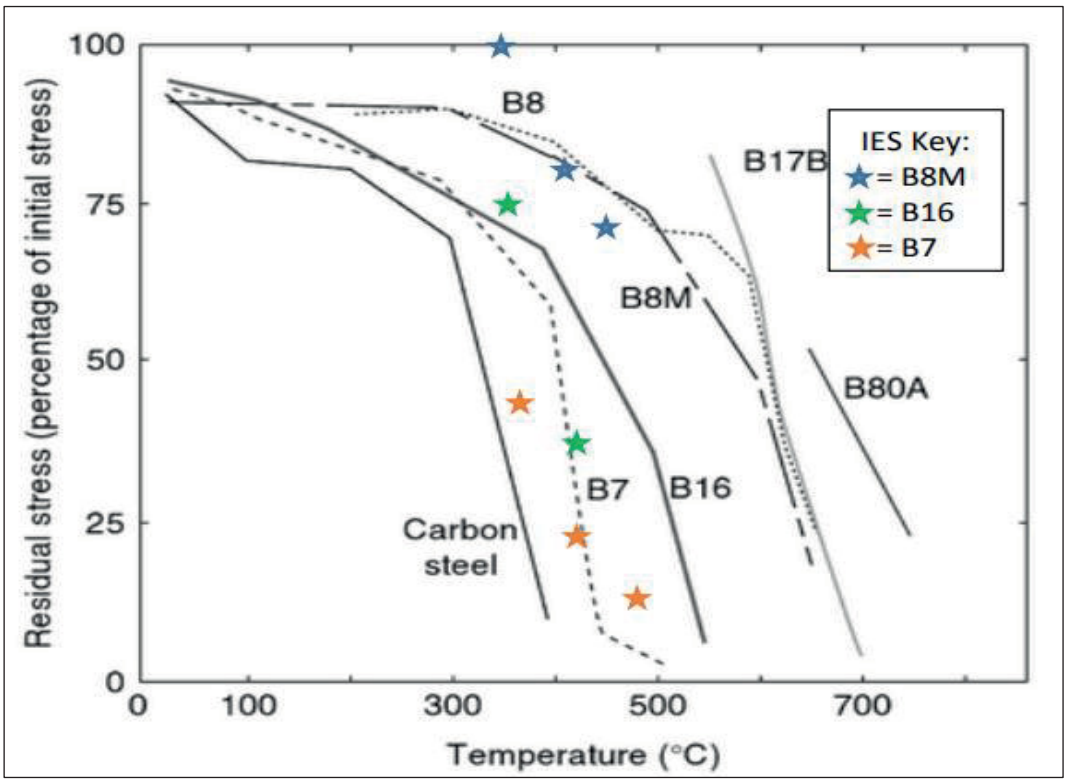

Figure 1-5 Relaxation of Materials with Temperature Taken from Brown and Lim (2017, p. 5)

Another aspect related to bolt load change during operation is the joint components' material properties change with temperature. For example, at high operating temperatures, Young's

modulus of elasticity changes, and therefore the stiffness of the joint changes (Zacal & Jancar, 2020). The operating temperature has a major impact on bolt pretension and gasket stress in heat exchangers. It generally increases for these factors during heat-up since their temperature is virtually lower than that of flanges and vice versa. The cool-down frequently reduces the load, increasing the bolted joint vulnerability to leakage. Figure 1-5, for example, depicts relaxation for various bolt materials.

Where:

- B7 is chromium molybdenum alloy steel
- B16 is a chromium, molybdenum, vanadium alloy steel
- B8 is AISI 304 stainless steel
- B8M is high tensile 316/316L stainless steel bolts
- B17B is a stud bolt
- B80A is a polyester based Thermoplastic polyurethane

1.5 Flange Design Methods

When designing flanges, in addition to structural integrity, tremendous care must be taken to ensure tightness by generating adequate sealing for the application under consideration. The current method for flange design that has been in use for a long time will be first presented, followed by the new proposed PVRC design method based on leakage tightness. In general, for most applications, the current ASME flange design procedure (ASME,2001) has worked out well. However, there are a few critical applications mainly related to heat exchangers that raised questions on the validity of this method. Temperature effects, gasket degradation with time, and joint assembly difficulties are other parameters that are responsible for most joint failures in recent years (Brown, 2007).

1.5.1 The Taylor Forge m & y Design Method

According to Brown (2007), pressure vessels and non-standard pipe flanges have been constructed utilizing two gasket factors, "***m***" and "***y***", in conjunction with the rudimentary

strength design of the joint components, based on the Taylor-Forge technique. This method has been in use across North America and much of the rest of the globe since the early 1940s. More precisely, when sizing the bolts of a bolted flange connection, the design necessitates the use of gasket constants referred to as m and y in the computation. The gasket must fit the flange surface and be able to compress sufficiently to fill any cavities or crevices and is obtained by meeting the seating stress y requirement. Moreover, y is the least compressive stress on the effective gasket contact area required to produce a seal at an internal pressure of 2 psig, which is basically used to compress the gasket voids to conform to the flange surface (Harrison, 2019).

The maintenance factor, on the other hand, is represented by ***m*** and is a multiplier of pressure that ensures minimum stress on the gasket during operation. Harrison (2019) presented the seated gasket configuration as shown in Figure 1-6. He also stated that when the vessel is pressurized, the flange designer multiplies the ***m*** value to estimate the compressive stress on the gasket necessary to maintain a seal. This constant ensures that the flange has sufficient strength and bolt load to hold the joint together while enduring the impacts of hydrostatic end force and internal pressure. Under pressure, the forces from appropriate bolting as to maintain the flange together and put extra stress on the gasket equal to ***m*** multiplied by the internal pressure. The designer then calculates the bolt load necessary to seat the gasket with the ***y*** factor and consecutively uses the ***m*** factor with the design pressure to obtain the operating bolt load. The greater of the two numbers is typically used to create the flange.

However, this strategy frequently misses the real joint operating condition in favor of focusing entirely on the parameters at hand resulting in additional tightening in the field.

Figure 1-6 Seated Gasket

1.5.1.1 The Gasket Factor m

The gasket factor determines how much the residual load must exceed the internal pressure (i.e., the difference between the original load and the internal pressure). This factor is dimensionless and may be calculated by dividing the net load by the internal one (Harrison, 2019). The equation is displayed following:

$$m = \frac{\mathrm{W} - F_{hyd}}{A_g . P_{int}} \tag{1.1}$$

Where:

- W is the bold load (lbs)
- F_{hyd} is the hydrostatic end force (lbs)
- A_g is the Gasket contact area (in^2)
- P_{int} is the internal pressure (psi)

1.5.1.2 The Seating Stress Factor y

The y factor may be considered as the minimum stress required to conform the gasket and flange surfaces and compress the voids in the gasket. As indicated in the following equation, this factor may be measured by dividing the bolt load by the gasket contact area.

$$y = \frac{W}{A_g} \tag{1.2}$$

1.5.1.3 Design Calculations

Harrison (2019) mentioned that only after retrieving the values of m and y, it would be possible to resume the design calculations. Afterward, two formulas would be used to calculate the total bolt load:

$$W_1 = 0.785PG^2 + 2b\pi GmP \tag{1.3}$$

$$W_2 = b\pi Gy \tag{1.4}$$

Where:

- P is the pressure acting over the load reaction diameter (psi)
- G is the diameter (Figure 1-7) (in)- b is the effective gasket width (i.e., calculated according to the ASME code for pressure vessels) (in)

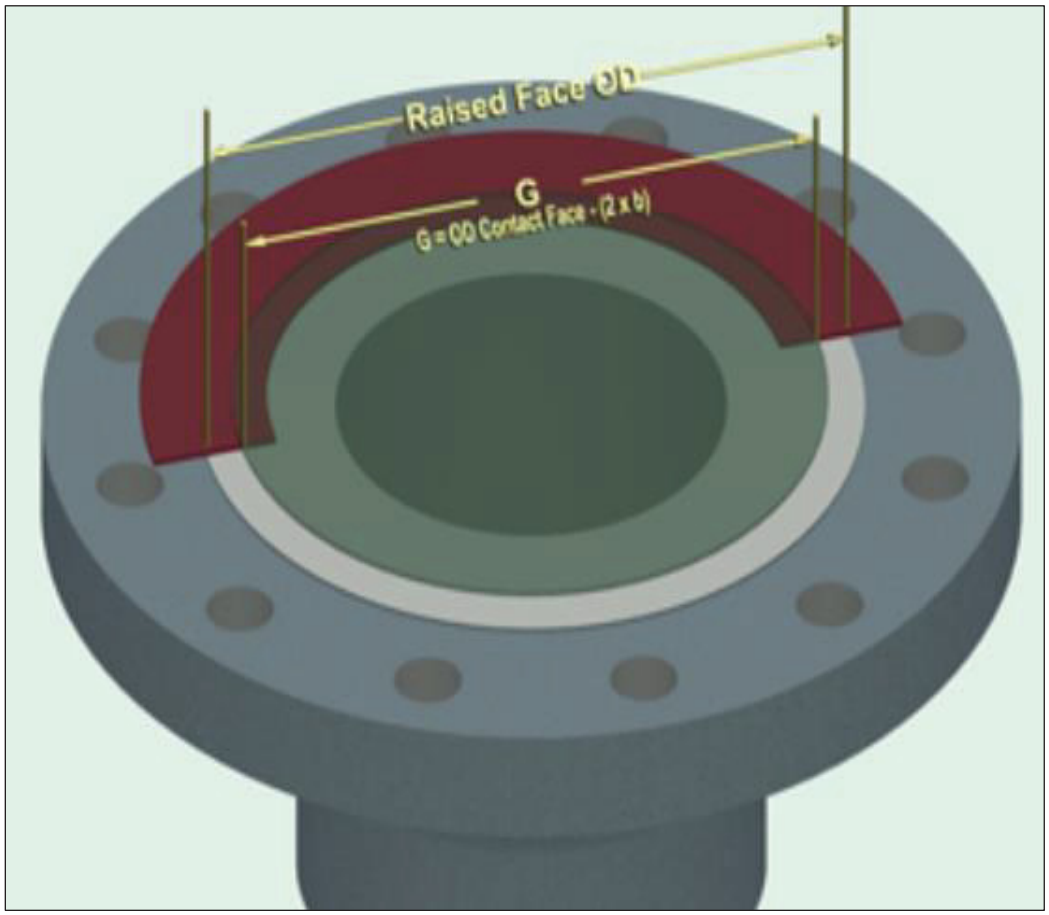

Figure 1-7 Load Reaction Diameter

Subsequently, the flange stresses are verified based on the largest value between the two calculated ones.

1.5.2 PVRC Flange Calculation Methods

For the design of flanges, the Taylor Forge technique has been and continues to be a standard in several countries that is still regarded as a viable approach. However, as previously mentioned, there are a few flaws in the accuracy of determining the bolt load under real operating conditions. As a result, while the gasket factor and seating stress remain the foundation of bolted joint calculations, advancements have yet to be made and additional tests must be conducted to improve the design method.

1.5.2.1 ROTT Test

The ROTT test, or Room Temperature Tightness Test, evaluates “real-world” gasket performance (Lidonnici, 2017). In addition to the new Gb and Gs constants, this test can also be used to determine the ASME m and y gasket constants ("Garlock", 2004). However, due to the incapacity of the m and y factors to predict the level of leakage, the PVRC developed this new method for implementation as an alternative procedure for the design of flanges. As a result, the new gasket parameters Gb a Gs (ROTT constants) were introduced. The last parameter refers to the operation when the gasket is discharged during pressurization and subsequent unloading cases, while the first two parameters are representative of the initial compression or seating condition of the gasket (Shu et al., 2001). In fact, the ROTT apparatus consists of a hydraulic system that applies a load to the gasket through platens or real flanges to evaluate its leakage performance under various contact stresses and pressures. A leak detection system and a pressure system are also part of the ROTT machine (Figure 1-8).

The technics for measuring gas leaks are flowmeter for high leak rates, pressure decay for gross leak rates, pressure rise for moderate to low leak rates, and mass spectrometry for fine leak rates.

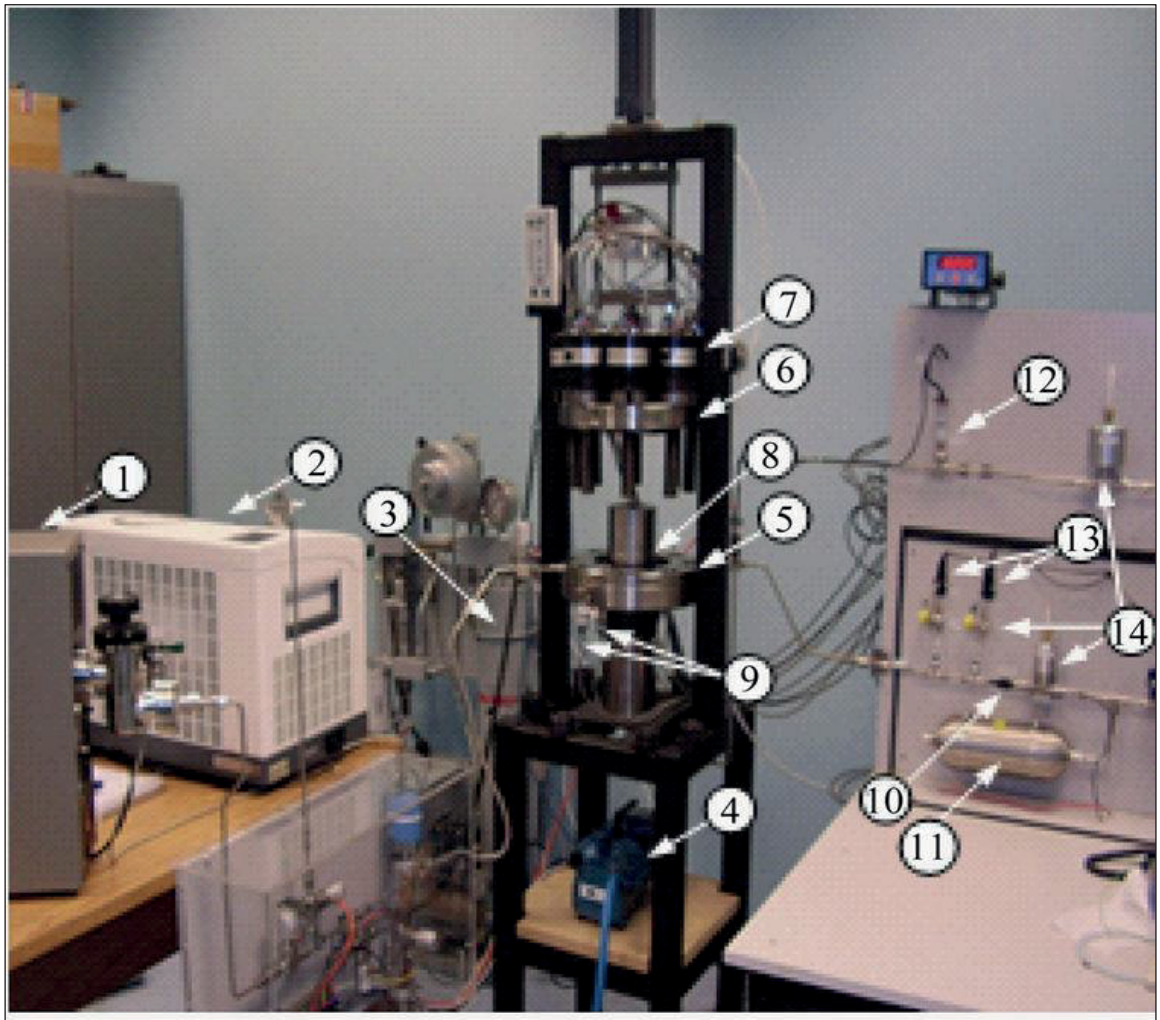

1 RGA	6 Upper flange	11 Tank
2 Alcatel	7 Hydraulic tensioner	12 Dif. Pressure transducer
3 Accumulator	8 O-ring Gasket	13 Pressure transducer
4 pump	9 LVDT	14 Pneumatic valves
5 Bottom flange	10 Thermocouple	

Figure 1-8 ROTT Machine Taken from Grine and Bouzid (2013, p. 35)

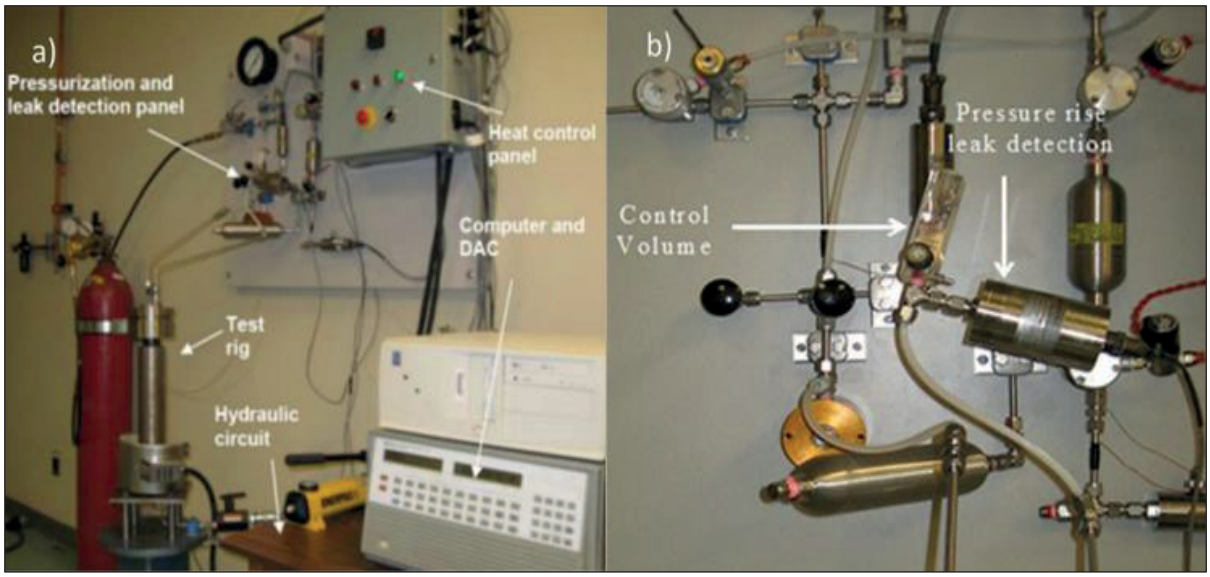

Figure 1-9 a) Universal Gasket Rig, b) Liquid leak measurement set-up Taken from Grine and Bouzid (2013, p. 36)

The ROTT is a test machine that subjects gaskets to gas pressure; however, it is not the only one. Other test fixtures are, in fact, designed to test liquids so that the correlation between gas and liquid leak rates is achieved. The UGR is a machine that consists of stiff platens through which a central stud travels, according to Grine and Bouzid (2013) (Figure 1-9, "a"). A hand pump is used to apply the load to a hydraulic bolt tensioner.

It is worth mentioning that there are two categories of leak detection systems, one of which is for liquids while the other one is for gases, depending on the type of fluid. All machines are equipped with an electric air-operated pressure regulator, pressure gage, bolt strain gages, LVDT displacement transducers, flowmeter pressure sensors (one for intake pressure and the others for leak chamber pressure), mass spectrometer, thermocouples, a data acquisition and control system, and a PC that are all included in the test rigs (Grine & Bouzid, 2013).

Testing Conditions:

The ROTT machine is pressurized with nitrogen or helium to reach pressures of 400 psig and 800 psig, as described by Shu et al. (2001). The gasket contact stress is systematically adjusted throughout the test to observe changes in its sealing characteristics. The gasket is loaded and

unloaded in a sequence of steps to mimic its behavior during operation. The test procedure is typically repeated twice for each pressure level. Throughout the test, the leak rate is measured under various stress and pressure combinations until stabilization is reached. By definition, stabilization is considered the state where the leak rate remains consistent without significant variations. The maximum dwell time, or the duration of stabilization, is set at a maximum of five hours. This ensures that the sealing performance of the gasket is maintained under prolonged exposure to the tested conditions.

Testing Procedures:

Bickford (1998) explained in his book that the ROTT test is divided into two sections: Part A and Part B.

Part A

Initial joint tightening and gasket seating are shown in Part A. Each successive level of gasket compression stress is higher than the one preceding it.

The seating behavior of a gasket during initial tightening is represented by the Part A sequence. As a result, Part A test data is used to establish the requisite seating load, which resembles the current ASME Code's ***y*** factor in this regard.

Part B

Unload-reload cycles at three different gasket seating stresses are used to stimulate the operating conditions in Part B as presented in Figure 1-10. The helium pressure is kept constant at 800 psig during these cycles, and the leak rate is recorded at predetermined stress levels. The unloading, relaxation, and retightening of a gasket during operation are referred to as Part B cycles. Part B leak data is like the ***m*** factor in the current ASME code in that it is utilized to establish the required operating bolt load (Bickford, 1998).

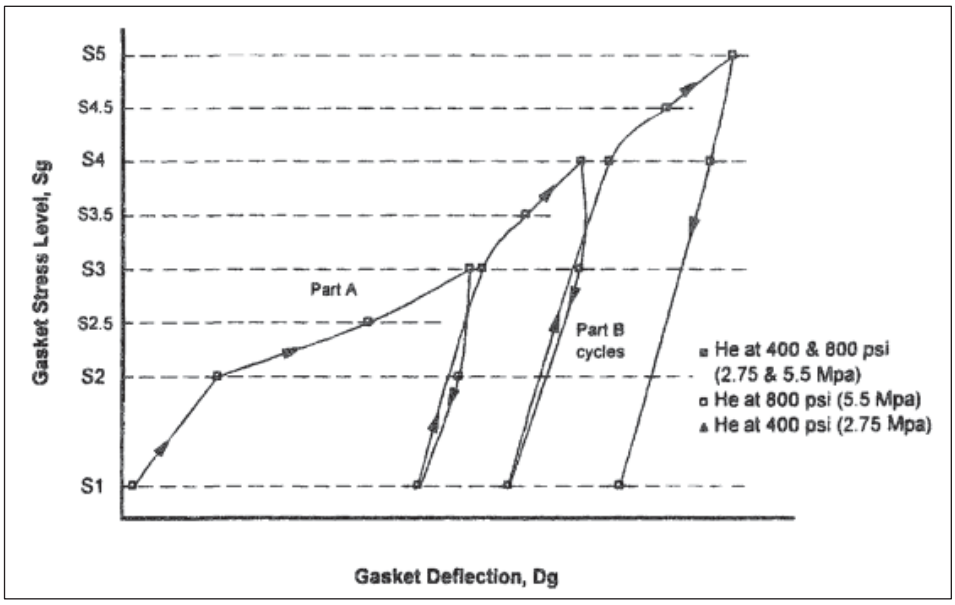

Figure 1-10 Generic ROTT Test Procedure Sequence
Taken from Bickford (1998, p.199)

Usually, the ROTT test contains five primary stress levels, ranging from S1 to S5, as well as intermediate levels S2.5, S3.5, and S4.5 as in Table 1-1. Bickford (1998) stated that the primary S levels represent a low-to-high range of typical pipe-fitter-imposed fastening stresses, and their values vary depending on the kind of gasket being tested. Additionally, three sets of S values are commonly in use: "soft," "standard," and "solid metal" tests. Except for the S1 level, where the applied He pressure is dependent on the gasket leakage at that level to avoid an uncontrolled gasket blowout, leakage is monitored at two distinct He pressures (400 and 800 psig) at each stress level.

For example, PTFE sheet gaskets go through a soft treatment, whereas metallic gaskets go through a hard procedure.

Table 1-1 ROTT test Procedure Stress Levels Taken from Bickford (1998, p. 200)

Stress Level	**Gasket Stress, *Sg***					
	Standard		**Solid Metal**		**Soft**	
	MPa	psi	MPa	psi	MPa	psi
S1	7.1	1,025	10.6	1,540	7.1	1,025
S2	31.4	4,560	47.1	6,840	20.9	3,040
S2.5	41.6	6,325	65.4	9,490	29.1	4,220
S3	55.8	8,090	83.7	12,140	37.2	5,390
S3.5	68.0	9,860	102.0	14,790	45.3	6,575
S4	80.2	11,630	120.3	17,450	53.5	7,750
S4.5	92.4	13,395	138.5	20,095	61.6	8,930
S5	104.2	15,160	156.8	22,740	69.7	10,110

1.5.2.2 CRUSH Test

The Crush Test is a term used to describe the progressive increase in stress levels. The latter refers to the maximum stress that may be applied to the gasket before it loses its tightness. There are several loading and unloading cycles, with tightness at level S1 being recorded. According to Bickford (1998), the CRUSH test involves cycling the gasket from high loads to a minimum of 1025 psi (ROTT stress level S1) as observed in Figure 1-11. The initial high-load level is the maximum ROTT S5 stress level, which is raised by 5000 psi. By applying 5000 psi to the cycling process, the maximum crush stress, Sc, is reached.

Every stage is monitored for gasket deflection and leakage using helium at 400 psig. It is not important to get exact leakage measurement values for the CRUSH test since the goal is to detect any large leaking situation caused by mechanical failure of the gasket.

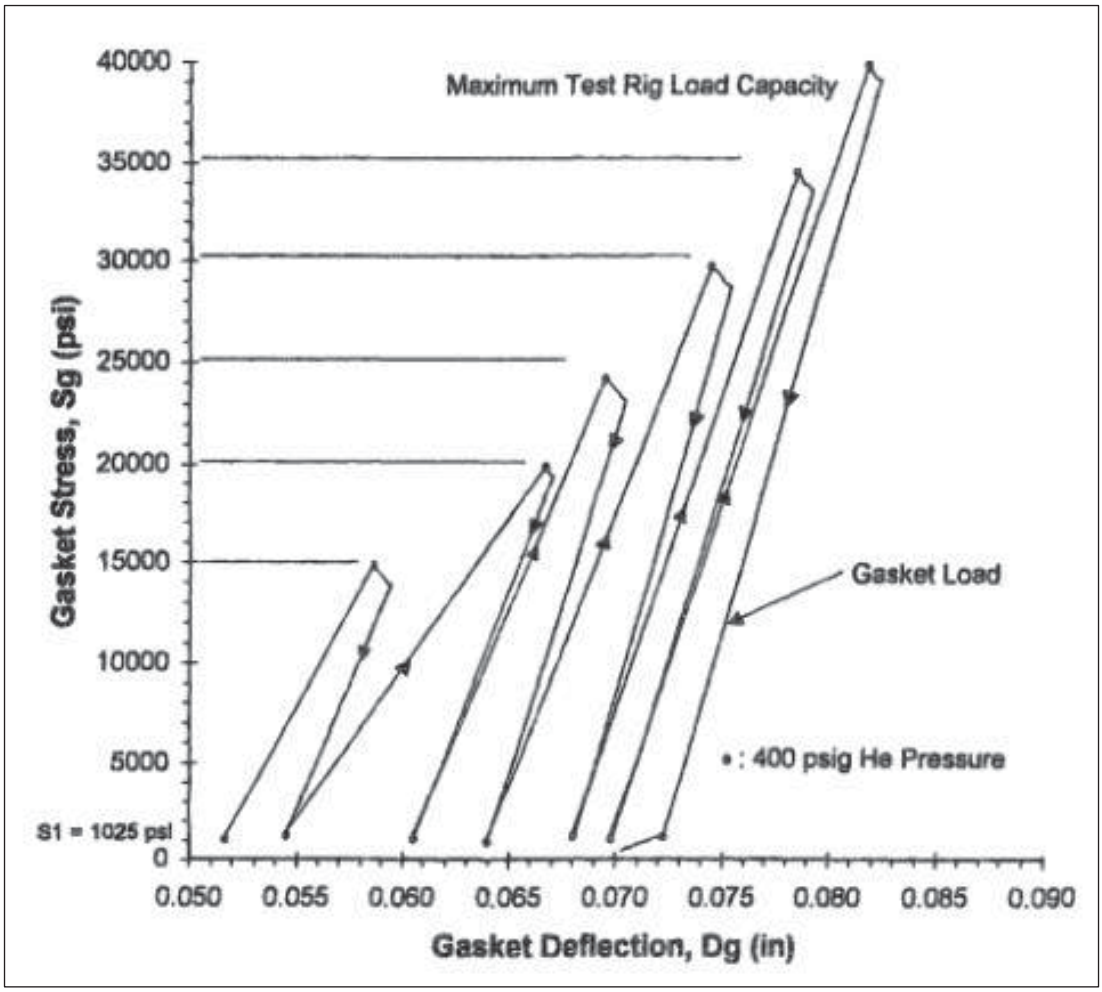

Figure 1-11 Generic CRUSH Test Procedure
Sequence Taken from Bickford (1998, p. 205)

Tightness Parameter:

As a result, as shown in Figure 1-12, a linear graph demonstrating the fluctuation in the tightness parameter as a function of gasket pressure is obtained.

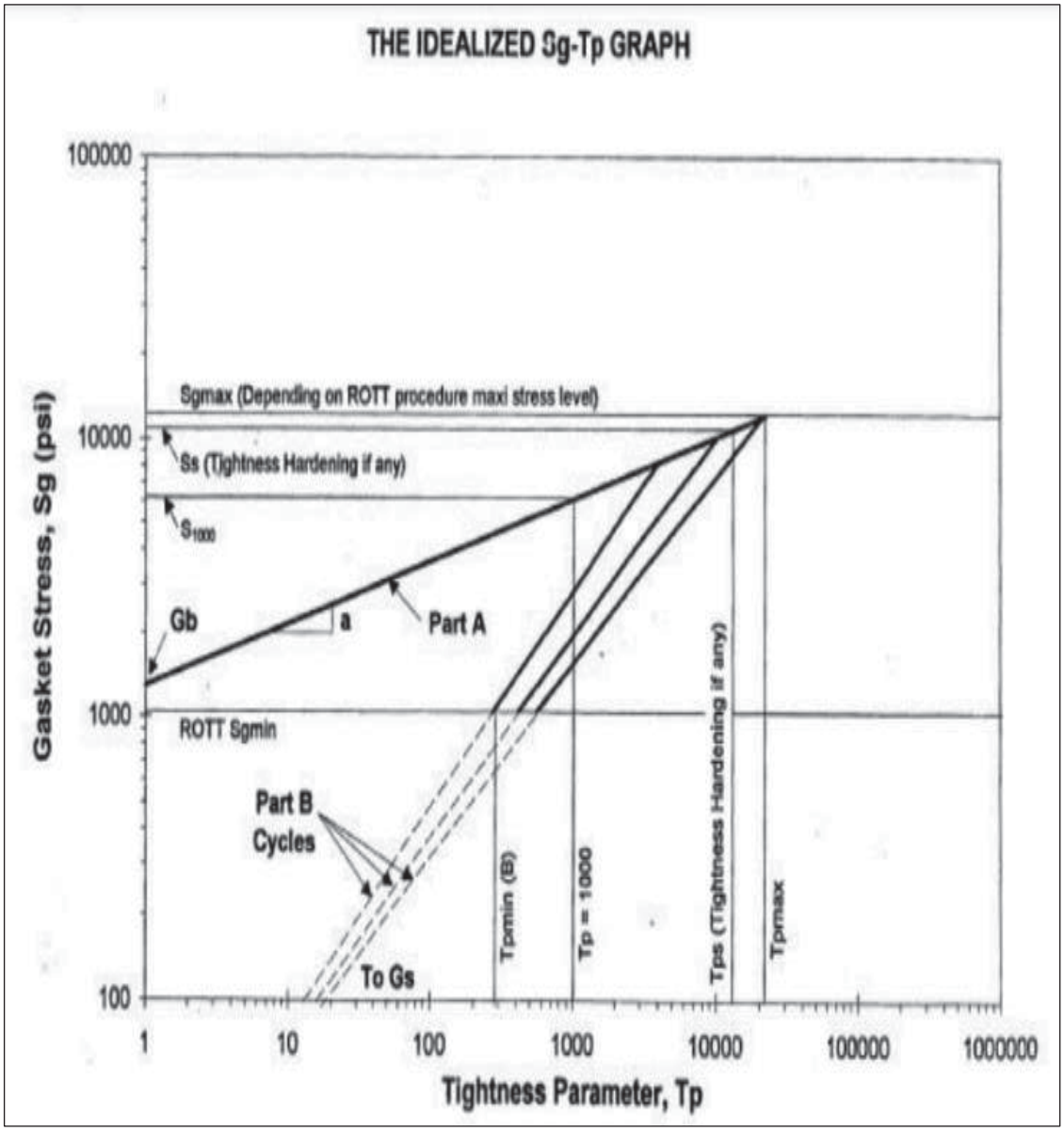

Figure 1-12 Idealized Sg-Tp graph Taken from Bickford (2004, p. 229)

The line depicts the link between the applied force and the leak that was discovered. When the line intersects the vertical axis, the intercept is Gb and the slope is “a”. For example, the higher the “a” value, the more the flange requires a bigger or greater number of bolts to achieve the necessary tightness (Garlock, 2004). Gs and Gb are both in psi and recovered at Tp = 1, which is dimensionless.

Tp refers to tightness and is a dimensionless measure. The greater this value, the less likely the gasket is to leak. For example, if a certain Tp is specified, the sitting stress may be determined using the equation:

$$S(T_p) = G_b \times (T_p)^a \tag{1.5}$$

However, Tp is usually calculated according to the obtained results. According to Shu et al. (2001), the following equation is defined as:

$$T_p = \frac{P_D}{P^*} \times \left(\frac{L^*}{L}\right)^d \tag{1.6}$$

Where:

- P_D is the fluid pressure (psia).
- P^* is the atmospheric pressure (14.7 psia).
- L^* is the standard leakage rate for gaskets with an outside diameter of 5.9 in (lbm/min/in).
- d is an empirical value that varies with the type of fluid in the pipes (i.e., d = 1- 0.5x where x is the vapor fraction of the fluid).
- L is the predicted leakage for gaskets with an outside diameter of 5.9 in (lbm/min/in) and is defined in Eq. 7.

$$L = Lrm \times Dt \tag{1.7}$$

Where:

- Lrm is the evaluated leakage rate of pipelines (lbm/min/in).
- Dt is the outside diameter of gaskets (5.9 in).

1.5.2.3 Simplified Equations

Numerous simplified equations for different types of pipelines, each with varying leakage rates, are compiled in Table 1-2.

Table 1-2 Simplified Equations

Parameter	Unit	Equation	Definitions
Minimum Tightness Parameter Tpmin	Under normal pressure	$0.1242 \times C \times P_D$	-
Minimum Tightness Parameter Tpmin	Different pressure unit	$1.8257 \times C \times P / P*$	-
Tightness Ratio Tr	-	$\frac{\log(1.5 \times \text{Tpmin})}{\log(\text{Tpmin})}$	-
Required Theoretical Seating Stress Sya	psi	$\frac{Gb}{e} \times (1.5 \times Tpmin)^a$	e depends on the method of bolt seating (0.75 for manual and 1 for machine)
Operating Stress Component Sm1	Psi	$(e \times Sya/Gs)^{1/Tr}$	
Seating Stress Component Sm2	psi	$Sya/1.5 - P_D \times A_H/A_G$	-A_H is the hydrostatic area (in^2) - AG is the gasket area (in^2)
Minimum Design Stress Sm	psi	MAX (Sm1, Sm2, $2P_D$)	-
Optimum Bolt Load Wm	lb_f	$P_D \times A_H + S_m \times A_G$	-
Actual Bolt Load Wmo	lb_f	$\frac{W_m}{0.85}$	-
Required Bolt Torque T	ft -lb_f/bolt	$[(Force/bolt) \times 0.2 \times D] /12$	D is the normal bolt diameter (in)

As for the designed parameter (C), it can be retrieved accordingly from Figure 1-13.

Tightness classes		
Seal classification	Leakage rate (mg/sec/mm)	Constant C
T_1	2×10^{-1}	0.1
T_2	2×10^{-3}	1
T_3	2×10^{-5}	10
T_4	2×10^{-7}	100
T_5	2×10^{-9}	1,000

Figure 1-13 Seal classification and leakage rate

1.6 Bolted Flange Joints

There exist several types of flanges, where the most common types are indicated in Figure 1-14 as:

- Welding Neck Flange
- Slip-on Flange
- Socket Weld Flange
- Lap Joint Flange
- Threaded Flange
- Blind Flange

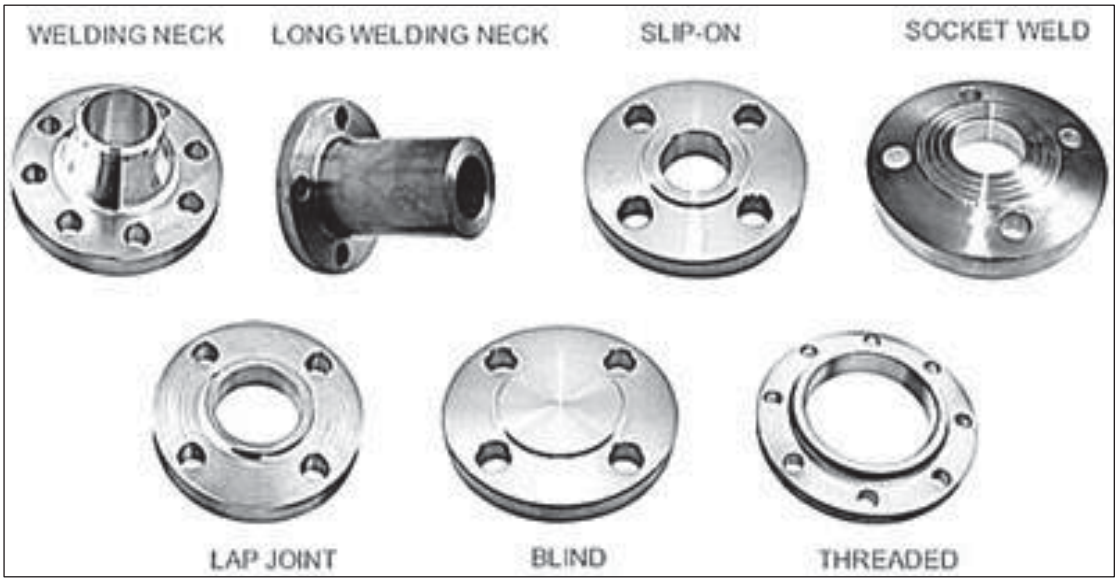

Figure 1-14 Common Flange Types (Metals)

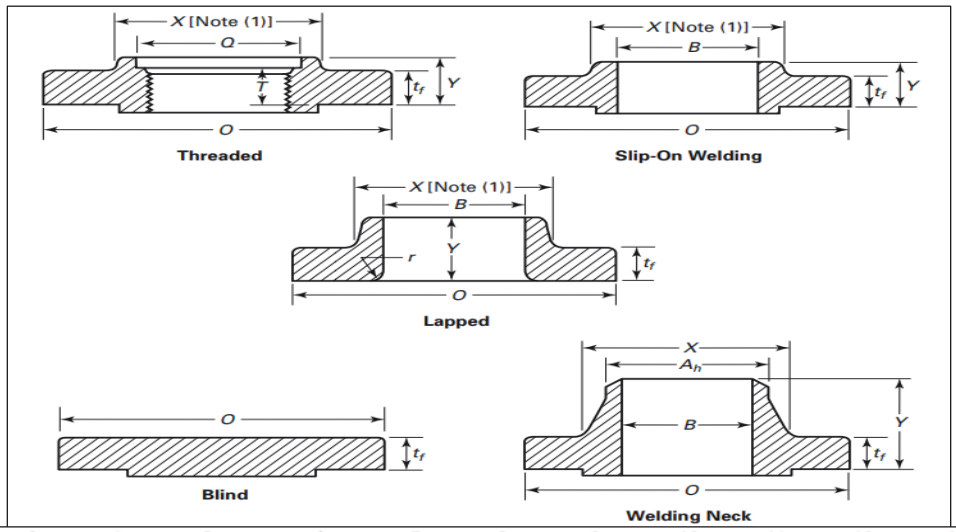

1	2	3	4	5	6	7	8	9	10	11	12	13	14
Nom. Pipe Size, NPS	Outside Diam. of Flange, *O*	Min. Thickness of Flange, t_f	Diam. of Hub, *X*	Hub Diam. Beginning of Chamfer Welding Neck, A_h [Note (2)]	Length Through Hub			Minimum Thread Length Threaded Flange, *T* [Note (3)]	Bore			Corner Bore Radius of Lapped Flange and Pipe, *r*	Minimum Counterbore Threaded Flange, *Q*
					Threaded/ Slip-On, *Y*	Lapped, *Y*	Welding Neck, *Y*		Min. Slip-On, *B*	Min. Lapped, *B*	Welding Neck, *B*		
½ ¾ 1 1¼ 1½ 2 2½	Use Class 1500 dimensions in these sizes [Note (4)]												
3	240	38.1	127	88.9	54	54	102	42	90.7	91.4	Note (5)	10	92.2
4	290	44.5	159	114.3	70	70	114	48	116.1	116.8	Note (5)	11	117.6
5	350	50.8	190	141.3	79	79	127	54	143.8	144.4	Note (5)	11	144.4
6	380	55.6	235	168.3	86	86	140	58	170.7	171.4	Note (5)	13	171.4
8	470	63.5	298	219.1	102	114	162	64	221.5	222.2	Note (5)	13	222.2
10	545	69.9	368	273.0	108	127	184	72	276.2	277.4	Note (5)	13	276.2
12	610	79.4	419	323.8	117	143	200	77	327.0	328.2	Note (5)	13	328.6
14	640	85.8	451	355.6	130	156	213	83	359.2	360.2	Note (5)	13	360.4
16	705	88.9	508	406.4	133	165	216	86	410.5	411.2	Note (5)	13	411.2
18	785	101.6	565	457.0	152	190	229	89	461.8	462.3	Note (5)	13	462.0
20	855	108.0	622	508.0	159	210	248	93	513.1	514.4	Note (5)	13	512.8
24	1,040	139.7	749	610.0	203	267	292	102	616.0	616.0	Note (5)	13	614.4

Figure 1-15 Dimensions of Class 900 Flanges Taken from ASME-B16.5 (2009, p. 95)

In this study, the welding neck flange joint is adopted while taking into consideration the dimensions. These calculations depend on the class and the corresponding nominal pipe size that is being used. This study also focuses on class 900 with its several nominal pipe sizes and the corresponding dimensions stated in Figure 1-15.

During service, bolted gasketed flange joints are exposed to a significant risk of leaking. Bolt relaxation, flange rotation, thermal transients, and gasket aging are thought to be among the primary causes of leaks (Ma et al., 2014). The two most common types of flange joints are floating and metal-to-metal contact (MMC).

Bolted flange joints are used in the petrochemical and nuclear sectors, but unfortunately, as mentioned earlier, they are prone to leaking at high temperatures due to the temperature influence on material creep and deformation (Chen and al., 2015). The main parameters that impact the proper function of the flange joints are established in Figure 1-16.

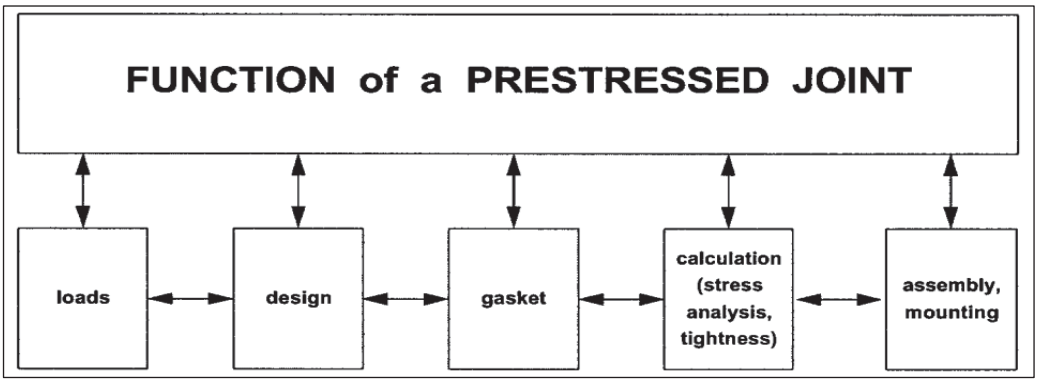

Figure 1-16 Parameters Affecting the Correct Function of Flanged Joints
Taken from Schaaf and Bartonice (2008, p. 6)

Previous research has shown that creep has a significant impact on the sealing performance of bolted joints. Because of bolt and gasket material creep, bolt load relaxation can reach up to 70% in some flange instances; the reduced bolt stress results in low gasket stress and higher leakage.

According to Roos et al. (2002), in contrast to floating-type flanged joints, where the entire bolt force is transferred via the gasket, just the portion of the bolt load required for MMC is taken over by the gasket (Figire 1-17). To minimize MMC loss, the additional bolt load

transmitted to the flange-flange contact must compensate for the unloading effects in service caused by internal pressure and external loadings. However, due to lack of standards for evaluating load losses caused by creep, hot torquing is used to recover load loss (Chen and al., 2015). However, all these studies have focused on the floating type of flanges, with little consideration made to the MMC kinds.

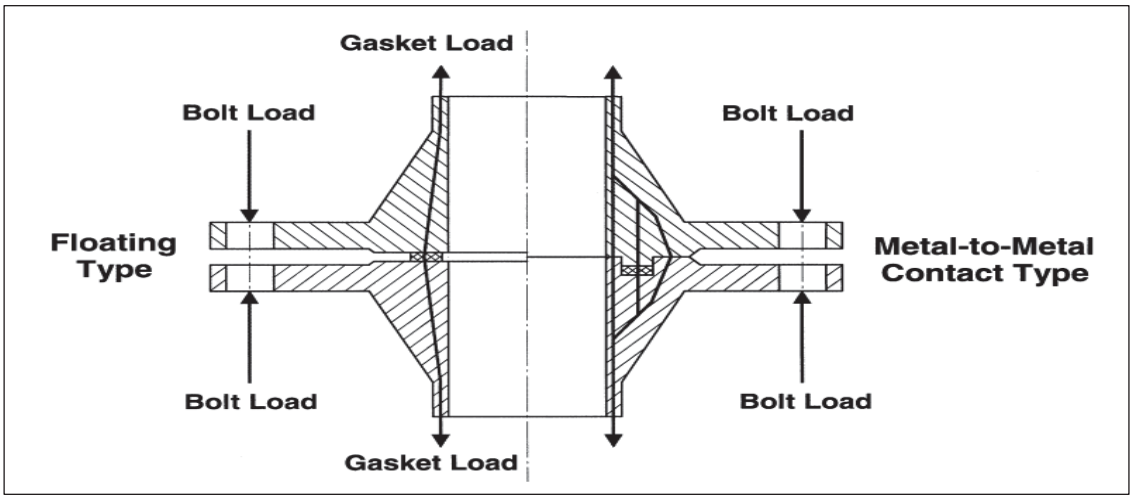

Figure 1-17 Bolted Flange Connections of Floating (left) and MMC type (right) flanged joints Taken from Roos and al. (2002, p. 46)

1.6.1 Calculation Parameters of MMC Bolted Flange Joints

The most crucial factors in flange calculation are typically the loads, the design of the individual components, and the material choice. The medium must be considered before anything else since it affects how resistant the flanges and gasket are. The properties of gasket tightness are also influenced by the media. In addition to the medium, other factors that affect the operating states include internal pressure, thermal gradients, expansion difference, and external forces and bending moments. They are essential in design loading consideration for both structural integrity (strength proof) and leak tightness (limiting the leak rate to the prescribed tightness class) (Schaaf & Bartonicek, 2003).

According to Schaaf and Bartonicek (2003), different gasket qualities are required for the MMC type of gasket. These unstandardized factors are as follows in Figure 1-18.

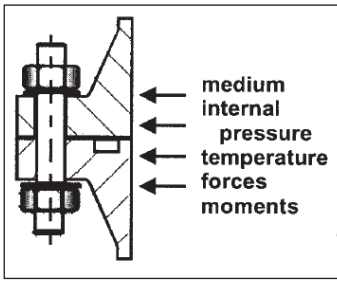

gasket factors	description
σ_{MMC}	minimum gasket stress to reach contact
$p_{MMC/L}$	maximum pressure for tightness class L
g_c	creep / relaxation factor

Figure 1-18 Gasket Factors for Use in Calculation: Metal-to-Metal Contact Type
Taken from Schaaf and Bartonicek (2003, p. 7)

These gasket variables are available material characteristics for the flange calculation that, while describing the tightness behavior of the sealing element, may also be considered analogical to the strength values of the flange and bolt material. Strength and tightness proofs may be made using these gasket variables.

Currently, specific testing techniques for flanges of the MMC type will be published soon (KTA 3211.2). There is no other calculating code that can manage MMC. On a linear elastic or elastoplastic base, finite element computations may be used to do detailed individual calculations, such as determining local stress distributions for fatigue analysis. If necessary, the behavior of the gasket can be efficiently characterized using elastoplastic analysis. However, these FEM calculations cannot be considered. The various analytical calculation processes are as follows (Schaaf & Bartonicek, 2003):

1.6.1.1 Design

For MMC, ensuring an acceptable rigidity and, thus, a constrained flange rotation, constitutes the verification of the flanges' sufficient dimensions. The ASME standard, which has influenced the national standards of certain European nations, is the one most used for the design of BFC (bolted flange connection) worldwide. The internal pressure as well as the

external forces and moments can be considered as loading conditions. With sufficient formal gasket variables (m and y), the behavior of the gasket is simulated. It is impossible to predict how the forces will change between assembly and operation. Flanges that were class-designed were calculated using ASME standards. The ASME calculation approach, which is based on elasticity theory, results in flanges with high stiffness. Finally, the ASME process was incorporated into the pressure vessel standard EN 13445.

1.6.1.2 Tightness Proof

The selection of calculating techniques for a tightness proof is rather constrained. Since the tightness qualities of the gasket aren't taken into adequate consideration, the ASME code is pure strength proof. Therefore, the KTA3201.2/KTA 3211.2 and EN 1591 both support the execution of a tightness proof to disposal. The stiffness of the individual components is first determined by considering their geometry and materials. Real loads, such as internal pressure, external loads, thermal expansions, and relaxation effects are then considered, and the resulting bolt and gasket strengths can therefore be determined by considering the force and deformation balance for each subsequent operation condition starting from the assembly condition. The gasket forces in every working condition result in operating gasket stresses. The tightness proof is obtained by checking the retention of the necessary operating gasket compression, which depends on the initial gasket stress during assembly.

The tightness proof for MMC is conducted using evidence of the MMC situation continued retention. If the MMC is retained, the tightness class that was achieved during assembly in the metal-to-metal contact condition will remain in effect. Therefore, it is sufficient to provide evidence that the two flanges maintain contact. The conditions for force and deformation are also taken into consideration.

1.6.1.3 Strength Proof

While the authorized bolt stress in service is limited to relatively low values, the pre-stress in the calculation technique according to ASME is connected to the highest allowable bolt stress rather than the needed bolt stresses for reaching the demanded tightness.

The provided statement suggests that there is no comprehensive confirmation of the entire connection, considering the rigidity of the components involved. However, slight positive evidence withdrawn from this experiment supports the practical applicability of this "pragmatic" technique.

When measuring the BFC's integrity using this approach which only considers global stresses, plastic deformations are excluded. Single flange cross-sections, bolting, and gasket cross-sections all have stress limits. The EN 1591 procedure is distinct in that it focuses more on the flanges' strength evidence. The nominal design stresses for the flange and bolt materials are not directly established in EN 1591; instead, the end-user must determine them by other standards.
Furthermore, the dispersion of the tightening device is considered in EN 1591. While the maximum scattering-related forces are used for the stress analysis in the assembly condition for all components, only the minimum forces are considered in the subsequent operational circumstances. The stresses under the subsequent circumstances are higher than these minimal values, but this is acceptable since these excessive stresses are secondary ("passive") stresses that are wiped off by plastic deformations.

The flange rotation and bolt load limitations for MMC might affect the strength proof. Only minuscule strains are created in the other flange cross-sections by the rotational flange constraint that is necessary for an MMC to operate safely.

1.6.2 Floating Flanges

A form of flange used in piping systems to join two pipes or fittings together is known as a floating flange. Instead of being welded to the pipes, they are simply slid onto the pipe ends and fastened there with bolts. Floating flanges accommodate thermal expansion, vibration, and misalignment by allowing for a small amount of movement and rotation of the connected pipes. They are appropriate for applications that need flexibility and regular repair or alterations since they are reasonably simple to install and maintain. While completely welded or enclosed flanges may offer a higher level of sealing performance, it's crucial to keep in mind that floating flanges might not. For a junction to be dependable and leak-free, precise bolt tightening and gasket selection are essential. It is worth mentioning that in industries, floating flanges are frequently used.

The two different types of flange connections utilized in plumbing systems are MMC (Metal-to-Metal Contact) flanges and floating flanges. Gaskets are not required since MMC flanges create a seal by direct metal-to-metal contact between the flange sides. In high-pressure and high-temperature applications, they frequently offer a high level of sealing performance. In contrast, floating flanges use gaskets to form a seal and provide some flexibility and tolerance for misalignment. In comparison to MMC flanges, they are simpler to install and maintain. Still, while floating flanges are convenient and ideal for situations where sealing requirements are less rigorous, MMC flanges excel in sealing performance. Specific system needs and industry norms usually determine which option is best for any given situation.

Floating flanges were chosen as the preferable flange connection method for the pipe systems under discussion. Their benefits in terms of adaptability, simplicity of installation, and maintenance are what influenced this decision. When compared to MMC flanges, floating flanges provide the required convenience while more successfully meeting the sealing criteria of the project.

Important factors to be considered when designing floating flanges include flange dimensions, material selection, gasket selection, bolt and nut specifications, proper flange alignment during

installation, testing, inspection, and adherence to industry standards. These elements are essential to the creation of a well-designed floating flange connection that satisfies the needs of the pipe system.

Several important elements have been suggested for consideration during the design process. In the early stages of this research, the significance of choosing the proper flanges was emphasized. The choice of gaskets and bolts will be covered individually in the sentences that follow. The present discussion, however, is concentrated on adhering to industry standards, extensive testing and inspection, and precise flange alignment during installation.

To guarantee a safe and dependable connection, these factors are essential. To begin with, the perfect fit and excellent sealing are ensured by proper alignment, reducing the possibility of leaks and weakened joint integrity. Also, comprehensive testing and inspection methods verify the functionality and reliability of the flange connection, allowing for the early identification of any possible problems. Adherence to industry standards provides a degree of quality assurance by guaranteeing compatibility, performance, and safety. The design strives to maximize the dependability and effectiveness of the flange connections within the pipe system by taking these factors into account.

1.6.3 Metallic Gaskets

According to a book titled “Flange Sealing Guide Gaskets and Bolted Connections” (2012), there are three types of metallic gaskets:

- Camprofile Gasket
- Corrugated metal Gasket
- Double Jacketed gasket
- **Spiral Wound Gasket :**

Spiral Wound Gasket, the type that was chosen for this study, is generally used at flange contact to compensate for surface defects. Because of its stability, the spiral wound gasket (SWG) with

graphite filler is favored for high pressure and temperature operations (Nelson et al., 2017). A spiral coiled gasket segment having inner and outer rings is shown in Figure 1-19.

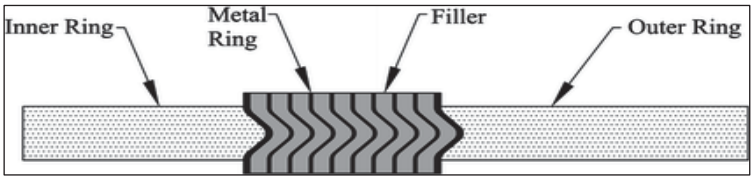

Figure 1-19 A Section of Spiral Wound Gasket Taken from Nelson and al. (2017, p. 84)

Spiral wound gaskets are prefabricated rings with windings of a chevron-shaped metal strip and a layer of filler material placed between them. Depending on the applications, these gaskets may be manufactured by a variety of specifications that define the manufacturer's practices to guarantee product consistency and quality. Due to their uniform manufacturing, gaskets built to these criteria ought to be of high quality. Dimensions, materials, labeling, and design of the gasket are determined by the specification. The gasket measurements are predetermined for a specific nominal pipe size and pressure class (Flange Sealing Guide Gaskets and Bolted Connections, 2012).

The seal is made by filler material molding to the flange face flaws. To withstand a broad range of chemicals and temperatures, the windings can be manufactured using a variety of metals including stainless steel. The most used filler materials are PTFE and flexible graphite, both of which have unique chemical resistance and temperature properties. Numerous variations of spiral-wrapped gaskets are available. The center ring type features a steel ring on the OD for raised or flat-faced flanges that functions as a compression gauge to avoid over-compression of the gasket and as a guide that fits inside the bolt circle to center the gasket on the flange face. The ring strengthens the gasket and aids in preventing blowout.

Furthermore, to offer additional over-compression protection, API 601 specifies that gaskets exceeding nominal pipe diameters in higher pressure classes should additionally be installed with an inner ring as it is shown in Figure 1-20 (Flange Sealing Guide Gaskets and Bolted Connections, 2012).

Typically, color coding is used on spiral wound gaskets to quickly distinguish between the winding and filling materials. Additional information, including the pressure class, nominal pipe size, the material of the winder, filler, and centering ring, a mark indicating the gasket specification, and the manufacturer's mark, is imprinted on centering guides for gaskets.

In higher-pressure applications, spiral wound gaskets are frequently employed. They are cost-effective and able to resist extremely high pressures, yet they still have significant disadvantages. Spiral wound gaskets are pre-made, and the stockroom must have all sizes and pressure classes of spiral wounds accessible to cover all uses in a plant (Flange Sealing Guide Gaskets and Bolted Connections, 2012).

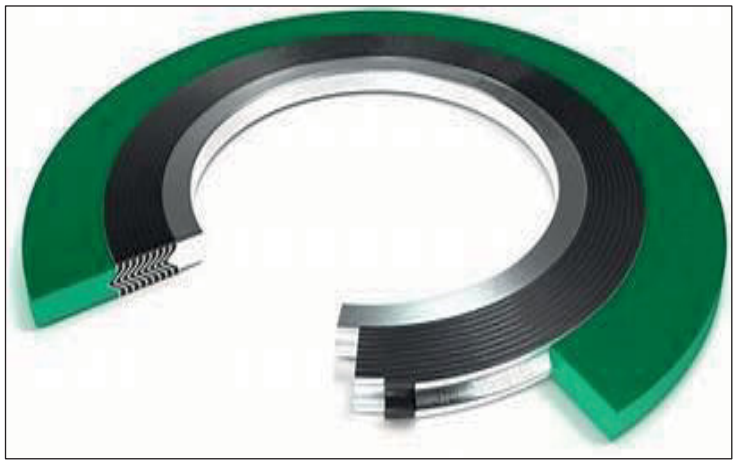

Figure 1-20 Spiral Wound Gasket

Furthermore, Spiral wounds are extremely sensitive to both good flange alignment and uneven bolt loading. In rare circumstances, if they are off-center, the windings may break, leading to catastrophic failure. Additionally, large stresses are needed to create a tight closure in spiral wounds. Because of their relative thickness and increased surface area exposed to pressure, they exert greater stresses on the gasket inside the flange (Flange Sealing Guide Gaskets and Bolted Connections, 2012).

1.6.4 Gasket Characteristics at Different Loading Rate

In comparison to other joint parts, flange joint gasket materials are often softer. They are very nonlinear and have considerable hysteresis. The deformation along the thickness direction has a significant impact on how flange joints behave in terms of leakage tightness. A compressive force is applied to the gasket specimen during the tests at various loading and unloading rates. With stainless steel (metal) rings and soft graphite (non-metallic) filling, the gasket is made of semi-metallic spiral-wrapped material. Inner and outer supporting rings are typically included with spiral-wrapped gaskets. On the other hand, the sealing ring is made of rings of radially damaged stainless steel and graphite, which helps to stop leakage (Nelson et al., 2017). As a result of the inner and outer supporting rings being present for stability and to avoid excessive compression, the deformation of the gasket is localized on the sealing ring.

In this regard, Nelson et al. (2017) tested on a gasket sealing ring of 4.5 mm thick, with a supporting ring of 3 mm thick. When a compressive force is applied, the sealing ring alone initially experiences compression. The gasket deformation behavior for various loading rates together with the accompanying stress levels is displayed in Figure 1-21. The gasket material exhibited a high viscoelastic behavior and hysteresis. Both elastic and plastic deformation of the gasket occur during loading; however, only elastic deformation is restored during unloading. With a reduction in loading rate, the gasket deforms more (Nelson et al, 2017).

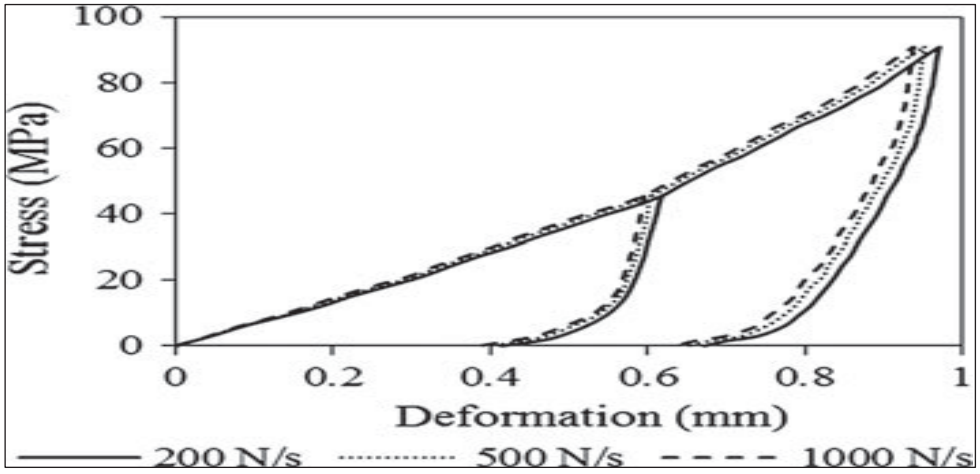

Figure 1-21 Stress Displacement Relation of SWG for Different Loading Rates Taken from Nelson and al. (2017, p. 87)

Possibly, when loaded at a low rate, the increased material flowability may be the cause. The recommended gasket contact surface finish for various gasket types is mentioned in Appendix 1.

1.6.5 Hex and Stud Bolts

Hex bolts are a specific kind of threaded bolt distinguished by its head with a six-sided hexagonal form. Hex bolts can be fully threaded or partly threaded (with a clear shank along part of the body) and can be used in a variety of applications, most frequently in equipment and construction (A Complete Guide to Hex Bolts, 2010). Typically, for flange connections, Stud Bolts and Hex Bolts are utilized in the chemical and petroleum industries. The Hex Bolt has a head with one nut, whereas the Stud Bolt has a threaded rod with two substantial hexagon nuts. Hence, the head has six sides, as do the nuts.

1.6.5.1 Bolts Threading

The helical structure that makes up the main body of a bolt is known as the thread or screw thread. It helps in offering a simpler entrance and departure into the material while also providing additional grip by using rotating force to push the bolt firmly and securely into position. There are two types of hex bolts.

- Partially Threaded Hex Bolts

Partially threaded hex bolts, displayed in Figure 1-22, are threaded just halfway down the bolt length to the end. The threaded shank and the head are joined by an unthreaded shank (also known as grip length). Partially threaded bolts offer high levels of resistance. In addition, the design prevents strain on the unthreaded area of the shank and guarantees that the segment has no weak points. However, the dimensions of these bolts fluctuate according to the flange size variations and are presented in Figure 1-24.

Figure 1-22 Partially Threaded Hex Bolts

- Fully Threaded Hex Bolts

Fully threaded hex bolts such as in Figure 1-23, are threaded from the end of the bolt to the head. They are ideally suited for installation in pre-threaded holes and are appropriate for use in heavy-duty fastening applications. Fully threaded hex bolts are designed to distribute pressure throughout the whole length of the bolt, providing better resistance than partially threaded alternatives.

Figure 1-23 Fully Threaded Hex Bolts

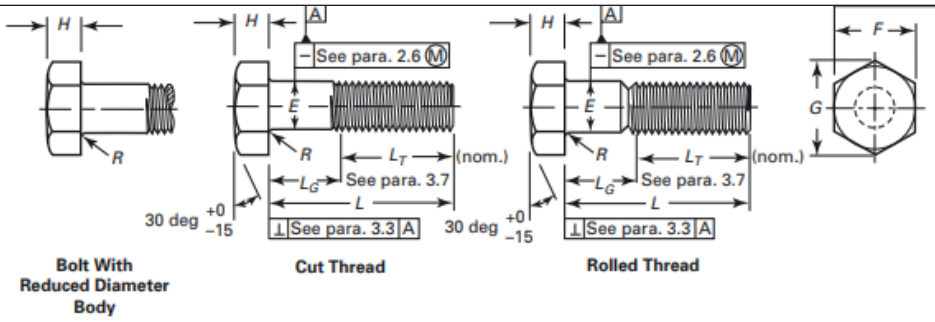

Nominal Size or Basic Product Diameter		Full-Size Body Diameter, *E* (See Paras. 3.4 and 3.5)		Width Across Flats, *F* (See Para. 2.1.2)			Width Across Corners, *G*		Head Height, *H*			Radius of Fillet, *R*		Thread Length for Bolt Lengths, L_T (See Para. 3.7)	
														6 in. and Shorter	Over 6 in.
		Max.	Min.	Basic	Max.	Min.	Max.	Min.	Basic	Max.	Min.	Max.	Min.	Nom.	Nom.
1/4	0.2500	0.260	0.237	7/16	0.438	0.425	0.505	0.484	11/64	0.188	0.150	0.03	0.01	0.750	1.000
5/16	0.3125	0.324	0.298	1/2	0.500	0.484	0.577	0.552	7/32	0.235	0.195	0.03	0.01	0.875	1.125
3/8	0.3750	0.388	0.360	9/16	0.562	0.544	0.650	0.620	1/4	0.268	0.226	0.03	0.01	1.000	1.250
7/16	0.4375	0.452	0.421	5/8	0.625	0.603	0.722	0.687	19/64	0.316	0.272	0.03	0.01	1.125	1.375
1/2	0.5000	0.515	0.482	3/4	0.750	0.725	0.866	0.826	11/32	0.364	0.302	0.03	0.01	1.250	1.500
5/8	0.6250	0.642	0.605	15/16	0.938	0.906	1.083	1.033	27/64	0.444	0.378	0.06	0.02	1.500	1.750
3/4	0.7500	0.768	0.729	1 1/8	1.125	1.088	1.299	1.240	1/2	0.524	0.455	0.06	0.02	1.750	2.000
7/8	0.8750	0.895	0.852	1 5/16	1.312	1.269	1.516	1.447	37/64	0.604	0.531	0.06	0.02	2.000	2.250
1	1.0000	1.022	0.976	1 1/2	1.500	1.450	1.732	1.653	43/64	0.700	0.591	0.09	0.03	2.250	2.500
1 1/8	1.1250	1.149	1.098	1 11/16	1.688	1.631	1.949	1.859	3/4	0.780	0.658	0.09	0.03	2.500	2.750
1 1/4	1.2500	1.277	1.223	1 7/8	1.875	1.812	2.165	2.066	27/32	0.876	0.749	0.09	0.03	2.750	3.000
1 3/8	1.3750	1.404	1.345	2 1/16	2.062	1.994	2.382	2.273	29/32	0.940	0.810	0.09	0.03	3.000	3.250
1 1/2	1.5000	1.531	1.470	2 1/4	2.250	2.175	2.598	2.480	1	1.036	0.902	0.09	0.03	3.250	3.500
1 5/8	1.6250	1.658	1.591	2 7/16	2.438	2.356	2.815	2.616	1 3/32	1.116	0.978	0.09	0.03	3.500	3.750
1 3/4	1.7500	1.785	1.716	2 5/8	2.625	2.538	3.031	2.893	1 5/32	1.196	1.054	0.12	0.04	3.750	4.000
1 7/8	1.8750	1.912	1.839	2 13/16	2.812	2.719	3.248	3.099	1 1/4	1.276	1.130	0.12	0.04	4.000	4.250
2	2.0000	2.039	1.964	3	3.000	2.900	3.464	3.306	1 11/32	1.388	1.175	0.12	0.04	4.250	4.500
2 1/4	2.2500	2.305	2.214	3 3/8	3.375	3.262	3.897	3.719	1 1/2	1.548	1.327	0.19	0.06	4.750	5.000
2 1/2	2.5000	2.559	2.461	3 3/4	3.750	3.625	4.330	4.133	1 21/32	1.708	1.479	0.19	0.06	5.250	5.500
2 3/4	2.7500	2.827	2.711	4 1/8	4.125	3.988	4.763	4.546	1 13/16	1.869	1.632	0.19	0.06	5.750	6.000
3	3.0000	3.081	2.961	4 1/2	4.500	4.350	5.196	4.959	2	2.060	1.815	0.19	0.06	6.250	6.500
3 1/4	3.2500	3.335	3.210	4 7/8	4.875	4.712	5.629	5.372	2 3/16	2.251	1.936	0.19	0.06	6.750	7.000
3 1/2	3.5000	3.589	3.461	5 1/4	5.250	5.075	6.062	5.786	2 5/16	2.380	2.057	0.19	0.06	7.250	7.500
3 3/4	3.7500	3.858	3.726	5 5/8	5.625	5.437	6.495	6.198	2 1/2	2.572	2.241	0.19	0.06	7.750	8.000
4	4.0000	4.111	3.975	6	6.000	5.800	6.928	6.612	2 11/16	2.764	2.424	0.19	0.06	8.250	8.500

Figure 1-24 Dimensions of Hexbolts Taken from ASME-B18.2.1 (2010, p. 6)

1.7 Previous and Current Studies

Bolted flange joints have been the subject of several research projects, each concentrating on certain aspects and presenting a different viewpoint. These papers include a wide variety of subjects, such as the choice of flange material, evaluation of gasket performance, methods for tightening bolts, and procedures for stopping leaks. A thorough understanding of bolted flange joints is made possible by the diversity of study in this area, which also makes it easier to create efficient design procedures. This work seeks to add to the body of knowledge by shedding new

light on the complex dynamics of bolted flange joints and the vital role they play in maintaining joint integrity and leak control.

This study is notable for its particular emphasis on a subset of bolted flange joints: ASME B16.5 class 900 flanges in various nominal diameters. This study is notable for its comprehensive methodology, which comprehensively examines crucial factors inherent in bolted flange couplings. It deviates from traditional study by delving into a variety of characteristics such as longitudinal and tangential stresses within bolts, gasket stress, radial displacement, and flange rotation.

Maintaining constant internal pressure and uniform limitations, such as similar bolt tension during bolt-up, allows for controlled parameter evaluation, showing their impact.

In essence, this study provides a comprehensive and rigorous assessment of ASME B16.5 class 900 flange joints. Examining linked factors across sizes and phases leads to a better understanding of bolted flange joint behaviour and performance under a variety of situations.

1.7.1 Previous Similar Studies

This study focuses on the bolted flange joints of the floating type with an NPS 4 and class 900. The results shape the tangential stress, longitudinal stress, radial stress, and gasket contact stress. Various present studies indeed investigate this field of research; however, the accessible ones are very broad and not specifically dedicated to the analysis of stresses in the different parts of ASME B16.5 Flanges.

Bouzid et al. (2009) discussed and experimented with the gasket contact stress on different types of NPS and classes. Their study results were luckily inclusive as the study focused on bolted flange joints as an assembly. Few other studies, unfortunately, presented the same acquired set of results. These studies also experimented on bolted flange joints of different NPS and classes, and they similarly obtained the tangential, longitudinal, radial, and gasket contact stresses though these studies were designed for a completely different type of bolted flange joints. For instance, Vafadar et al. (2020) and Bouzid et al. (2022) underwent their experiments specifically on fiber-reinforced polymer (FRP) bolted flange joints.

1.7.2 Current Study

The purpose of this research project is to carry out a thorough analysis and design study on bolted flange joints, with a focus on three essential parts: floating flanges, spiral-wrapped gaskets, and fully threaded bolts. Primarily, investigating and assessing the possible leakage hazards connected to various joint arrangements is the main goal. A thorough analysis of critical elements influencing joint integrity, such as longitudinal and tangential stress, gasket contact stress, and flange rotation, will be carried out using the ANSYS program.

According to the B16.5 standard, the research will focus on Class 900 flanges, which cover a wide range of pipe diameters from NPS 4 to 24. By using ANSYS software, thorough evaluations of these flange joints under various operational circumstances will be possible, giving important insights into their behavior and performance.

The goal of the research is to better understand the complex dynamics of bolted flange joints by thoroughly analyzing the stress distribution, gasket contact pressure, and flange rotation characteristics. This knowledge will make it easier to create design strategies that work and trustworthy leak prevention techniques for industrial applications.

Additionally, the results of this study will add to the body of knowledge by addressing knowledge gaps and particular difficulties related to floating flanges, spiral-wrapped gaskets, and fully threaded bolts in bolted flange joint systems. Engineers, designers, and business executives looking to improve the functionality, integrity, and leak resistance of bolted flange joints will find the findings to be a helpful resource.

1.7.3 Objectives and Sub-objectives of this study

The major goal of this study is to validate an analytical model developed to simulate the real behavior of bolted flange joints using the numerical finite element method using a general-purpose finite element program such as ANSYS on different size flanges extracted from the ASME B16.5 standard. The adopted methodology is designed to test the amount of agreement between the two approaches and validate the robustness of the analytical model.

In addition to the primary goal, numerous subsidiary goals guide the scope of this research. Firstly, the research intends to thoroughly assess the structural integrity of ASME B16.5 class 900 flanges when subjected to bolt-up and pressure conditions. The aim is to assess ASME standard flange ability to withstand these conditions by testing their structural integrity. Flange rotation, flange ring, hub, and shell tangential and longitudinal stresses as well as gasket and bolt stresses.

Secondly, the study aims to evaluate the leakage tightness of these flanges under pressure conditions, with a particular focus on the combination of welding neck flanges (WNF) and spiral wound gaskets (SWG) in preventing fluid leakage.

Furthermore, the study looks at the effect of the flange size on the performance of ASME B16.5 flanges.

CHAPTER 2

ANALYTICAL MODEL

2.1 Analysis of Elastic Interactions

According to Bouzid and Nechache (2005), the flange, the bolts, and the gasket are the three fundamental components that make up a bolted flanged junction. Similarly, the shell, hub, and flange ring are the three components that make up the flange. The hub-ring and cylinder-hub connections operate as geometrical discontinuities. Due to bolt-up and pressurization, various radial displacements and distortions are induced at these connections in the above-mentioned flange components, as explained by the authors. However, as illustrated in Figure 2-1, shear force P and moments M1 and M2 are generated to preserve the continuity of displacement and rotation at the two discontinuity locations.

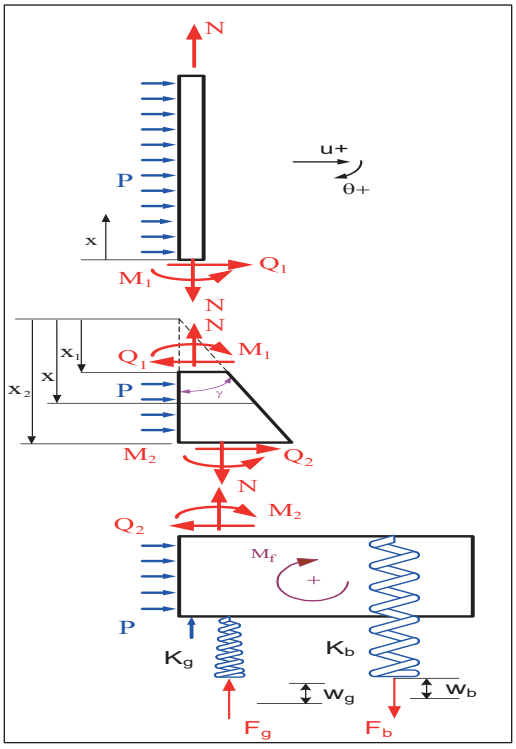

Figure 2-1 Analytical Model Taken from Nechache and Bouzid (2008, p. 2)

The bolt and the gasket are included in the model and are represented by springs of linear elastic and nonlinear non-elastic stiffness, respectively. The junction at the ring to the hub is not constrained. Circular ring and plate theories are considered for the flange ring depending on the flange width-to-thickness ratio. The gasket reaction is located at the mid-gasket-flange contact zone and the flange ring rotates rigidly without distortion.
The theoretical framework that was utilized to handle the various joint aspects should be noted before conducting the elastic interaction analyses (Bouzid & Nechache, 2005).

- The model is a statically indeterminate problem.
- The theory of beams on elastic foundations is used to treat the cylindrical shell.
- For small flanges, the flange is regarded as either a circular plate with a center hole or a circular ring for big-diameter flanges.
- The hub is handled using the theory of a cylindrical shell with linearly variable thickness.
- Linear elastic spring is used to simulate the gasket and bolt.

The analysis of the equilibrium during tightening and pressurization cannot be sufficient to solve the problem because it is a statically indeterminate problem. During tightening characterized by i the bolt force is equal to the gasket for

$$F_b^i = F_g^i \tag{2.1}$$

During pressurization characterized by f the axial equilibrium requires that

$$F_b^f = F_g^f + p\, A_p \tag{2.2}$$

These two equations come from the analysis of the separate components of the flange the free-body diagram which is shown in Figure 2.1. However, they are not enough to solve the problem and additional equations are required.

2.2 Radial Displacements, rotations, moments, and shear forces

According to the initial tightening and pressurization, the separate bolted joint components exhibit radial displacement, rotation moment, and shear forces. The values of these parameters vary depending on the specific tightening or pressurization case.

2.2.1 Shell

The equations of the radial displacement, rotation moment, and shear force of the cylinder shell caused by pressure at any axial location on the cylinder are given by the theory beam on elastic foundation applied to the thin shell (Bouzid & Nechache, 2005):

$$u_s^n = \frac{1}{2\beta_s^2 D_s} M_1 e^{-\beta_s x}(\cos\beta_s x - \sin\beta_s x) + \frac{1}{2\beta_s^3 D_s} Q_1^n e^{-\beta_s x}\cos\ \beta_s x + \frac{(2-\nu_s) r_i^2}{2E_s t_s} p \tag{2.3}$$

$$o_s^n = -\frac{1}{2\beta_s^2 D_s} Q_1^n e^{-\beta_s x}(\cos\ \beta_s x + \sin\ \beta_s x) - \frac{1}{\beta_s D_s} M_1 e^{-\beta_s x}\cos\ \beta_s x \tag{2.4}$$

$$M_s^n(x) = 2\beta_s^2 D_s \left[\frac{Q_2^n}{2\beta_s^3 D_s} e^{-\beta_s x}\sin\ \beta_s x + \frac{M_2^n}{2\beta_s^2 D_s} e^{-\beta_s x}(\cos\beta_s x - \sin\beta_s x)\right] \tag{2.5}$$

$$Q_s^n(x) = 2\beta_s^3 D_s \left[\frac{Q_2^n}{2\beta_s^3 D_s} e^{-\beta_s x}(\cos\beta_s x - \sin\beta_s x) - \frac{M_2^n}{\beta_s^2 D_s} e^{-\beta_s x}\sin\ \beta_s x\right] \tag{2.6}$$

Where:

$$\beta_s = \sqrt[4]{\frac{3(1-\nu_s^2)}{r_s^2 t_s^2}} \text{ and } D_s = \frac{E t_s^3}{12(1-\nu_s^2)} \tag{2.7}$$

2.2.2 Hub

The hub is treated using the theory of a cylindrical shell with a linearly variable thickness. The equation below determines its radial displacement u_h at any axial position (Bouzid & Nechache, 2005):

$$u_h^n = x^{-\left(\frac{1}{2}\right)}[C_1 \,\mathrm{ber}'(\varepsilon) + C_2 \,\mathrm{bei}'(\varepsilon) + C_3 \,\mathrm{ker}'(\varepsilon) + C_4 \,\mathrm{kei}'(\varepsilon)] + \frac{p r_h^2}{2E_f \gamma x}(2-\nu_f) \tag{2.8}$$

The hub thickness, t_h, at any point may be expressed in terms of the distance x, where x is displayed in Figure 2.1 and $x' = x_2 - x$. The taper angle γ may be defined in terms of the thickness of the cylindrical shell as $\gamma = t_s/x_1$,.

$$\varepsilon = 2\beta\sqrt{x}\ , \qquad \rho = \left[\frac{12(1-\nu_f^2)}{\gamma^2 r_h^2}\right]^{1/4}, \quad \beta_h = \sqrt[4]{\frac{3(1-\nu_f^2)}{r_h^2 t_h^2}} \tag{2.9}$$

The integration constants, C_1, C_2, C_3, and C_4, are determined by the boundary conditions. The real and imaginary components of the Bessel function are ber, bei, ber', and bei', as well as their derivatives. The real and imaginary parts, along with their derivatives, of the Bessel function $K_0\left(xe^{\pi i/4}\right)$ are represented as $J_0\left(xe^{3\pi i/4}\right)$, ker, kei, ker', and kei'.

The consecutive derivative of the displacement yields the rotation θ_h, bending moment M_h, and shear force P_h, which are then expressed as follows:

$$\theta_h^n = \frac{du_h}{dx} = x^{-\left(\frac{3}{2}\right)}[C_1S_1(\varepsilon) + C_2S_2(\varepsilon) + C_3S_3(\varepsilon) + C_4S_4(\varepsilon)] + \frac{pr_h^2}{2E_f y x^2}\left(2 - \nu_f\right) \tag{2.10}$$

$$M_h^n = \frac{E\gamma^3 x^3}{12\left(1-\nu_f^2\right)}\frac{d\theta_h}{dx} = \frac{E_f\gamma^3 x^{-(1/2)}}{48\left(1-\nu_f^2\right)}[C_1S_9(\varepsilon) + C_2S_{10}(\varepsilon) + C_3S_{11}(\varepsilon) + C_4S_{12}(\varepsilon)] + \frac{\left(2-\nu_f\right)pr_h^2y^2}{12\left(1-\nu_f^2\right)} \tag{2.11}$$

$$Q_h^n = \frac{dM_h}{dx} = -\frac{E_f\gamma^3\rho^2 x^{-(1/2)}}{24\left(1-\nu_f^2\right)}[C_1S_5(\varepsilon) + C_2S_6(\varepsilon) + C_3S_7(\varepsilon) + C_4S_8(\varepsilon)] \tag{2.12}$$

Where:

$$\begin{aligned} S_1(\varepsilon) &= -\varepsilon\mathrm{bei}\,(\varepsilon) + 2\mathrm{ber}'\,(\varepsilon) \\ S_2(\varepsilon) &= \varepsilon\mathrm{ber}\,(\varepsilon) - 2\mathrm{bei}'\,(\varepsilon) \\ S_3(\varepsilon) &= -\varepsilon\mathrm{kei}\,(\varepsilon) - 2\mathrm{ker}'\,(\varepsilon) \\ S_4(\varepsilon) &= \varepsilon\mathrm{ker}\,(\varepsilon) - 2\mathrm{kei}'\,(\varepsilon) \end{aligned} \tag{2.13}$$

$$\begin{aligned} S_5(\varepsilon) &= -\varepsilon\mathrm{ber}\,(\varepsilon) + 2\mathrm{bei}'\,(\varepsilon) \\ S_6(\varepsilon) &= -\varepsilon\mathrm{bei}\,(\varepsilon) - 2\mathrm{ber}'\,(\varepsilon)) \\ S_7(\varepsilon) &= -\varepsilon\mathrm{ker}\,(\varepsilon) + 2\mathrm{kei}'\,(\varepsilon)) \\ S_8(\varepsilon) &= -\varepsilon\mathrm{kei}\,(\varepsilon) - 2\mathrm{ker}'\,(\varepsilon)) \end{aligned} \tag{2.14}$$

$$\begin{aligned} S_5(\varepsilon) &= -\varepsilon\mathrm{ber}\,(\varepsilon) + 2\mathrm{bei}'\,(\varepsilon) \\ S_6(\varepsilon) &= -\varepsilon\mathrm{bei}\,(\varepsilon) - 2\mathrm{ber}'\,(\varepsilon)) \\ S_7(\varepsilon) &= -\varepsilon\mathrm{ker}\,(\varepsilon) + 2\mathrm{kei}'\,(\varepsilon)) \\ S_8(\varepsilon) &= -\varepsilon\mathrm{kei}\,(\varepsilon) - 2\mathrm{ker}'\,(\varepsilon)) \end{aligned} \tag{2.15}$$

2.2.3 Flange Ring

Given in terms of the applied loading, the flange ring radial displacement, rotation and moment are each calculated as follows:

$$u_f^n = \frac{R_i}{E_f}\left(P - \frac{P_2}{t_f}\right)\left(\frac{K^2+1}{K^2-1} + \nu_f\right) + \theta_f \frac{t_f}{2} \tag{2.16}$$

$$\theta_f^n = \frac{2\pi R_i Y}{E_f t_f^3} M_f^n \tag{2.17}$$

$$M_f^n = \frac{R_i}{R_m} M_2^n + \frac{R_i t_f}{2R_m} P_2^n + \frac{(r_b - r_g)}{\pi R_m} F_b^n + \frac{(r_g - R_i)}{2R_m}(r_g^2 + R_i^2)p \tag{2.18}$$

where for a plate

$$Y = \frac{1}{K-1}\left[\frac{3}{\pi}(1-\nu_f) + \frac{6}{\pi}(1+\nu_f)\frac{K^2 \ln K}{(K^2-1)}\right] \tag{2.19}$$

For a ring

$$Y = \frac{6}{\ln K} \tag{2.20}$$

with

$$K = \frac{R_o}{R_i} \tag{2.21}$$

2.3 Axial Displacements

Mechanical loads produce the axial displacements of the various components of the joint, and the gasket bolt and flange ring.

2.3.1 Gasket

The axial displacement of the gasket considered as a spring is as follows:

$$w_g^n = \frac{F_g^n}{K_g} \tag{2.22}$$

K_g is the equivalent gasket stiffness and is dependent on the stress level attained during bolt-up.

2.3.2 Bolt

The bolt axial displacement or elongation is obtained by considering a linear spring behavior and specified as follows:

$$w_b^n = \frac{F_b^n}{K_b} \tag{2.23}$$

Where:

$$K_b = \frac{nA_bE_b}{l_b} \tag{2.24}$$

2.3.3 Flange Ring

The following equations may be used to calculate the axial displacement of the flange ring at the bolt circle regarding the gasket reaction location produced by the tangential flange rotation while disregarding any local deformation or warping due to bending:

$$w_f^n = (r_b - r_g)\theta_f^n \tag{2.25}$$

2.4 Axial Displacement Compatibility

The final force of the bolt is determined by utilizing the axial compatibility relation. The number of nut turns performed during the initial tightening phase corresponds to an axial displacement of the nut. This displacement is a cumulative effect of the axial displacements of all the individual elements within the system. Once the nut reaches this displacement, it is assumed to have reached its desired position and should not be turned further during subsequent operating conditions. Therefore, the displacement of the nut remains constant throughout these conditions.

$$\Delta_n = \sum w_e^i = \sum w_e^f \tag{2.26}$$
$$\Delta_n = w_g^i + w_b^i + w_p^i + w_f^i = w_g^f + w_b^f + w_p^f + w_f^f$$

For the bolt and gasket:

$$w_e = \frac{F_e}{K_e} \tag{2.27}$$

Therefore

$$\frac{F_b^i}{K_b}+\frac{F_g^i}{K_g}+2\left(r_b-r_g\right)\theta_f^i=\frac{F_b^f}{K_b}+\frac{F_g^f}{K_g}+2\left(r_b-r_g\right)\theta_f^f \tag{2.28}$$

A system of 13 equations with 13 unknowns is ultimately discovered. Eight equations are produced utilizing equations 4, 6, 8, and 9 at the positions $x = x_1$ and $x = x_2$, as well as five more equations using equations 1, 2, 12, 13, and 23.

Compiling the above would resume solving a system of equations with 12 unknowns obtained for the bolt-up and 13 for the pressurization. During the bolt-up, the bolt force, F_b^i, is already known and therefore the last row and column of the system of equations defined by Eq. (23) are to be retrieved. To solve the unknowns, the equations are put into a matrix form.

$$[U^n] = [E]\backslash[V^n] \tag{2.29}$$

The exponent n in Eq. (2.28) refers to the initial bolt-up or pressurization condition. [*E*] is a 13x13 square matrix composed of matrix [*A,B*] and [*C,D*] appended together and [*V*] is a vector. During bolt-up, *n=i, p* is equal to zero in [V^n] to solve for the unknown matrix [U^i]. The elements of the unknown matrix [*U*] are used to determine the stresses in the different sections of the flange during the initial bolt-up and the pressurization conditions. Therefore

$$[E] = \begin{bmatrix} AB \\ CD \end{bmatrix} \tag{2.30}$$

With

$$A=\begin{bmatrix} x_1^{-\left(\frac{1}{2}\right)}\,\mathrm{ber}'(\varepsilon_1) & x_1^{-\left(\frac{1}{2}\right)}\,\mathrm{bei}'(\varepsilon_1) & x_1^{-\left(\frac{1}{2}\right)}\,\mathrm{ker}'(\varepsilon_1) & x_1^{-\left(\frac{1}{2}\right)}\,\mathrm{kei}'(\varepsilon_1) & 0 & 0 \\ \frac{x_1^{-\frac{3}{2}}}{2}S_1(\varepsilon_1) & \frac{x_1^{-\frac{3}{2}}}{2}S_2(\varepsilon_1) & \frac{x_1^{-\frac{3}{2}}}{2}S_3(\varepsilon_1) & \frac{x_1^{-\frac{3}{2}}}{2}S_4(\varepsilon_1) & 0 & 0 \\ -\frac{E_f\gamma^3\rho^2 x_1^{-\left(\frac{1}{2}\right)}}{24\left(1-v_f^2\right)}S_5(\varepsilon_1) & -\frac{E_f\gamma^3\rho^2 x_1^{-\left(\frac{1}{2}\right)}}{24\left(1-v_f^2\right)}S_6(\varepsilon_1) & -\frac{E_f\gamma^3\rho^2 x_1^{-\left(\frac{1}{2}\right)}}{24\left(1-v_f^2\right)}S_7(\varepsilon_1) & -\frac{E_f\gamma^3\rho^2 x_1^{-\left(\frac{1}{2}\right)}}{24\left(1-v_f^2\right)}S_8(\varepsilon_1) & 0 & 0 \\ \frac{E_f\gamma^3 x_1^{-\left(\frac{1}{2}\right)}}{48\left(1-v_f^2\right)}S_9(\varepsilon_1) & \frac{E_f\gamma^3 x_1^{-\left(\frac{1}{2}\right)}}{48\left(1-v_f^2\right)}S_{10}(\varepsilon_1) & \frac{E_f\gamma^3 x_1^{-\left(\frac{1}{2}\right)}}{48\left(1-v_f^2\right)}S_{11}(\varepsilon_1) & \frac{E_f\gamma^3 x_1^{-\left(\frac{1}{2}\right)}}{48\left(1-v_f^2\right)}S_{12}(\varepsilon_1) & 0 & 0 \end{bmatrix} \tag{2.31}$$

$$B=\begin{bmatrix} 0 & 0 & -1 & 0 & 0 & 0 & 0 \\ 0 & 0 & 0 & -1 & 0 & 0 & 0 \\ 0 & 0 & 0 & 0 & 0 & 0 & 0 \\ 0 & 0 & 0 & 0 & 0 & 0 & 0 \end{bmatrix} \tag{2.32}$$

$$C=\begin{bmatrix} x_2^{-\left(\frac{1}{2}\right)}\,\mathrm{ber}'(\varepsilon_2) & x_2^{-\left(\frac{1}{2}\right)}\,\mathrm{bei}'(\varepsilon_2) & x_2^{-\left(\frac{1}{2}\right)}\,\mathrm{ker}'(\varepsilon_2) & x_2^{-\left(\frac{1}{2}\right)}\,\mathrm{kei}'(\varepsilon_2) & 0 & 0 \\ \frac{x_2^{-\frac{3}{2}}}{2}S_1(\varepsilon_2) & \frac{x_2^{-\frac{3}{2}}}{2}S_2(\varepsilon_2) & \frac{x_2^{-\frac{3}{2}}}{2}S_3(\varepsilon_2) & \frac{x_2^{-\frac{3}{2}}}{2}S_4(\varepsilon_2) & 0 & 0 \\ -\frac{E_f\gamma^3\rho^2 x_2^{-\left(\frac{1}{2}\right)}}{24\left(1-v_f^2\right)}S_5(\varepsilon_2) & -\frac{E_f\gamma^3\rho^2 x_2^{-\left(\frac{1}{2}\right)}}{24\left(1-v_f^2\right)}S_6(\varepsilon_2) & -\frac{E_f\gamma^3\rho^2 x_2^{-\left(\frac{1}{2}\right)}}{24\left(1-v_f^2\right)}S_7(\varepsilon_2) & -\frac{E_f\gamma^3\rho^2 x_2^{-\left(\frac{1}{2}\right)}}{24\left(1-v_f^2\right)}S_8(\varepsilon_2) & 0 & 0 \\ \frac{E_f\gamma^3 x_2^{-\left(\frac{1}{2}\right)}}{48\left(1-v_f^2\right)}S_9(\varepsilon_2) & \frac{E_f\gamma^3 x_2^{-\left(\frac{1}{2}\right)}}{48\left(1-v_f^2\right)}S_{10}(\varepsilon_2) & \frac{E_f\gamma^3 x_2^{-\left(\frac{1}{2}\right)}}{48\left(1-v_f^2\right)}S_{11}(\varepsilon_2) & \frac{E_f\gamma^3 x_2^{-\left(\frac{1}{2}\right)}}{48\left(1-v_f^2\right)}S_{12}(\varepsilon_2) & 0 & 0 \\ 0 & 0 & 0 & 0 & \frac{1}{2\beta_s^3 D_s} & \frac{1}{2\beta_s^2 D_s} \\ 0 & 0 & 0 & 0 & \frac{-1}{2\beta_s^2 D_s} & \frac{-1}{\beta_s D_s} \\ 0 & 0 & 0 & 0 & 0 & 0 \\ 0 & 0 & 0 & 0 & 0 & 0 \\ 0 & 0 & 0 & 0 & 0 & 0 \end{bmatrix} \tag{2.33}$$

$$D$$

$$= \begin{bmatrix} 0 & 0 & 0 & 0 & -1 & 0 & 0 \\ 0 & 0 & 0 & 0 & 0 & -1 & 0 \\ -1 & 0 & 0 & 0 & 0 & 0 & 0 \\ 0 & -1 & 0 & 0 & 0 & 0 & 0 \\ 0 & 0 & -1 & 0 & 0 & 0 & 0 \\ 0 & 0 & 0 & -1 & 0 & 0 & 0 \\ -\frac{r_i}{E_f t_f}\left(\frac{K^2+1}{K^2-1}+\nu_f\right) & 0 & 0 & 0 & -1 & -\frac{t_f}{2} & 0 \\ -\frac{r_i t_f}{2R_m} & \frac{R_i}{R_m} & 0 & 0 & 0 & -\frac{E_f t_f^3}{2\pi R_i Y} & \frac{r_b - r_g}{\pi R_m} \\ 0 & 0 & 0 & 0 & 0 & C_5\left(r_b - r_g\right) & C_9 \end{bmatrix} \quad (2.34)$$

$$V = \begin{bmatrix} -\frac{r_h^2(2-v_f)}{2E_f\gamma x_1}p \\ -\frac{r_h^2(2-v_f)}{2E_f\gamma x_1^2}p \\ -\frac{\gamma r_i}{4}p \\ -\frac{r_h^2(2-v_f)\gamma^2}{12(1-v_f^2)}p \\ -\frac{r_h^2(2-v_f)}{2E_f\gamma x_2}p \\ -\frac{r_h^2(2-v_f)}{2E_f\gamma x_2^2}p \\ -\frac{\gamma r_i}{4}p \\ -\frac{r_h^2(2-v_f)\gamma^2}{12(1-v_f^2)}p \\ -\frac{(2-v_s)r_i^2}{2E_s t_s}p \\ -\frac{R_i}{E_f}\left(\frac{K^2+1}{(K^2-1)+v_f}\right)p \\ \frac{(r_i-r_g)(r_g^2+R_i^2)}{2R_m}p \\ \left(\frac{1}{K_b}+\frac{1}{K_g}\right)F_b^i + 2(r_b-r_j)\theta_f^i + \frac{A_p}{K_g}p \end{bmatrix} \quad (2.35)$$

With During initial bolt-up:

$$\left[U^i\right] = [\mathrm{C}_1^i\ \mathrm{C}_2^i\ \mathrm{C}_3^i\ \mathrm{C}_4^i\ \mathrm{Q}_2^i\ \mathrm{M}_2^i\ \mathrm{Q}_1^i\ \mathrm{M}_1^i\ \mathrm{u}_2^i\ \theta_2^i\ \mathrm{u}_1^i\ \theta_1^i\ \mathrm{F}_b^i]^T \tag{2.36}$$

And during pressurization:

$$[U^f] = \left[\mathrm{C}_1^f\ \mathrm{C}_2^f\ \mathrm{C}_3^f\ \mathrm{C}_4^f\ \mathrm{Q}_2^f\ \mathrm{M}_2^f\ \mathrm{Q}_1^f\ \mathrm{M}_1^f\ \mathrm{u}_2^f\ \theta_2^f\ \mathrm{u}_1^f\ \theta_1^f\ \mathrm{F}_b^f\right]^T \tag{2.37}$$

$C_1, C_2, C_3\ , C_4, P_1, M_1, P_2, M_2, u_{h1}, \theta_{h1}, u_{h2}, \theta_f$, and F_b^f are the thirteen unknowns that a system of thirteen equations is built to solve with. The ultimate gasket load is determined using the axial equilibrium relationship when the final bolt load F_b^f is known.

$$F_g^f = F_b^f + A_p p \tag{2.38}$$

CHAPTER 3

STRESS ANALYSIS METHODOLOGY AND FEM MODELING

3.1 Introduction

There seems to be a recurring issue with the bolted flange joint that needs further investigation. More precisely, at the junction of the shell and the flange ring, the integrated complex bolted flange joint is subjected to the highest stresses. Moreover, the integrity of the bolted flange joint may be compromised by an excessive flange rotation, which is a floating type of flange that increases during pressurization. Consequently, the generated stresses on the bolted flange joint during the bolt-up and pressurization stages must be investigated. Along these lines, Wagner et al. (2018) emphasize the need for a more accurate assessment study that considers a variety of service operating conditions, such as high pressure, high temperature, vibration, and external loads.

At the shell-to-flange junction, unforeseen high pressures can result in leaks and the emission of hazardous substances into the surrounding air. The geometry and shape of the flange ring, as well as the type of shell, have a major effect on the load redistributions and high stresses created at the junctions. Thus, the use of cylindrical pressure vessel shells is frequently optimized without any comparison; modeling all the active pressures and stresses on the flange is the key to guaranteeing a secure design of bolted joints. This is carried out in the presence of distinct shell connections to get an accurate estimate of the stresses. In addition, cornerstone characteristics of a successful design include an accurate estimation of the flange rotation, bolt, and gasket loads during operation.

3.2 Proposed Model of Bolted Flange Joint

This study evaluated the integrity and leakage tightness of the model by monitoring the behavior of the gasket. All the models have the same shape which consists of a shell, hub, and flange ring with all these components being attached to a raised face that is connected to the gasket. Despite setting a cylindrical shape for all the models, the sizes continue to vary between

each of the models. The main purpose of this study is to examine the stress distribution (longitudinal and tangential stresses) at the junctions, flange rotation, and the gasket contact stress. A pressure has been set to all the models on the inner surface of the pipe. However, the bolt pretension and the pressure on top of the shell are changing from one model to another. This variation is due to the change in dimensions and the fact that they are expanding from NPS4 to NPS24. According to Choulaei and Bouzid (2021), these shell connections are modeled using general-purpose finite element software to verify the analytical technique and analysis.

This chapter explains the numerical models used for validation as well as the analytical technique created to assess the behavior of the bolted flange joint, by determining the flange rotation, multiple stress components, and gasket contact stress. The numerical finite element bolted flange joint models were generated using the ANSYS software.

3.3 Analytical Method

This section discusses the theory adopted to obtain a similar result as the analytical solutions for the stresses in the shell-to-flange ring junction. The shape that has been implied for this project is a cylindrical-shaped pipe. As previously mentioned, the bolted flange joint consists of three main components: ring, shell, and hub. Each component consists of different characteristics concerning some conditions that are applied to it. Technically, “Ansys” is a FEA software that has been used to check the validity of the gasket contact stress and different kinds of stresses across the bolted flange joint.

The bolt and gaskets load changes, discontinuity edge loads, and stresses were assessed during both bolt-up and pressurization. This assessment was performed using continuity and equilibrium equations that were obtained from the bolted joint analysis.

The continuity conditions of radial displacement and tangential rotation of the shell and ring require that:

$$w_f = w_s \tag{3.1}$$

And

$$\theta_f = \theta_s \tag{3.2}$$

During Bolt-up, the gasket force is equal to:

$$H_G^i = H_B^i \tag{3.3}$$

And during pressurization:

$$H_G^f = H_B^f - pA_p \tag{3.4}$$

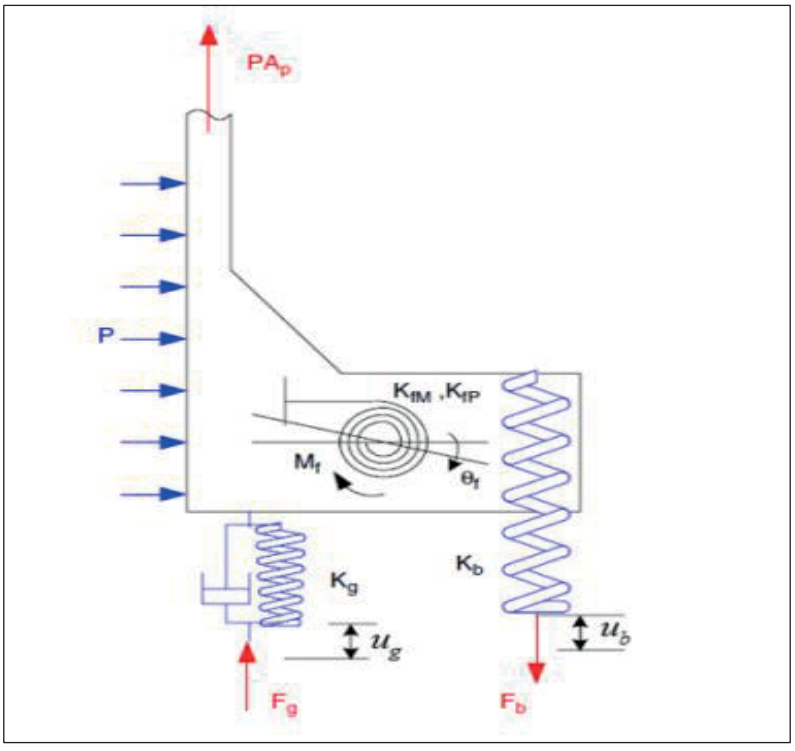

Figure 3-1 Bolted flange model Taken from Nechache and Bouzid (2007, p. 187)

A second equation is needed to solve the statistically complex indeterminate system represented by the bolted joint in Figure 3-1. To address this scenario, the compatibility of the axial displacement of the flange joint elements presented in earlier publications (Bouzid and Chaaban, 1993; Bouzid and Nechache, 2005) was applied, which specifies that the nut traveling axial distance Δ_e remains constant, and is given as follows:

$$\Delta_e = u_b^i + u_g^i + u_f^i = u_b^f + u_g^f + u_f^f \tag{3.5}$$

Regarding the linear stiffness and the ring rotation:

$$\frac{F_b^i}{K_b} + \frac{F_g^i}{K_b} + 2\theta_f^i(r_b - r_g) = \frac{F_b^f}{K_b} + \frac{F_b^f}{K_b} + 2\theta_f^f(r_b - r_g) \tag{3.6}$$

3.3.1 Bolt Load

A cross-sectional area named the stress area is utilized to gauge the rigidity of the bolt. By considering the normal 60 thread, the tensile stress area of the bolt is determined by (Bickford, 2008):

$$A_s = \frac{\pi}{4}(D_b - 0.938p_b)^2 \tag{3.7}$$

The bolt load can be calculated by using the equation for the stress area, as shown below:

$$F_B = \sigma_b . A_s \tag{3.8}$$

Where $\begin{cases} F_B \text{ is the resulting bolt load.} \\ \sigma_b \text{ is the applied bolt stress.} \end{cases}$

The root area, which is frequently used in ASME B31.1, is a more conservative stress area than the tensile stress area since it depends on the root of threads or a minor diameter. It aims to increase the estimations of thread strength safety margin.

The designer incorporates a root stress area that is less than the actual tensile stress area to ensure that the rod is not overstressed in service (Figure 3-2).

The bolt root area is specified by:

$$A_r = \frac{\pi}{4}(D_b - 1.22687p_b)^2 \tag{3.9}$$

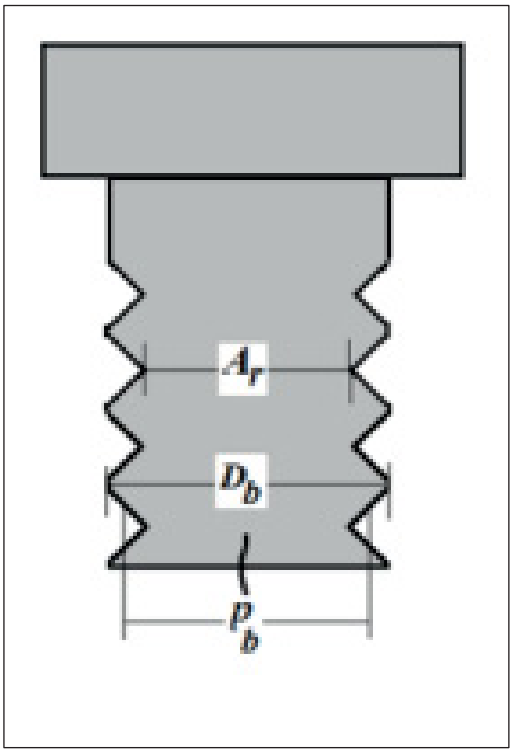

Figure 3-2 Bolt parameters

3.3.2 Gasket Modeling

To reasonably estimate the reaction load and contact pressure during service, it is important to model the gasket. The gasket is sufficiently pressed to seal the flange connection. While the

gasket material performs somewhat linearly during pressurization or unloading, it behaves nonlinearly during the bolt-up or seating stage.

The load compression curves for the corrugated metal sheet gasket with a flexible graphite layer are depicted in Figure 3-3. All the sizes of flanges that have been examined in this study have used the same loading-unloading curve. The Room temperature tightness test was set to observe the gasket behavior. The results obtained are demonstrated in Figure 3-3.

NPS 4, 8, 10, 14,16, 20, and 24 are the sizes used in this study where the same type of gasket was used, i.e. spiral wound gasket. The loading-unloading curve was acquired from the spiral wound gasket. However, it is assumed that all these sizes possess the same mechanical behavior.

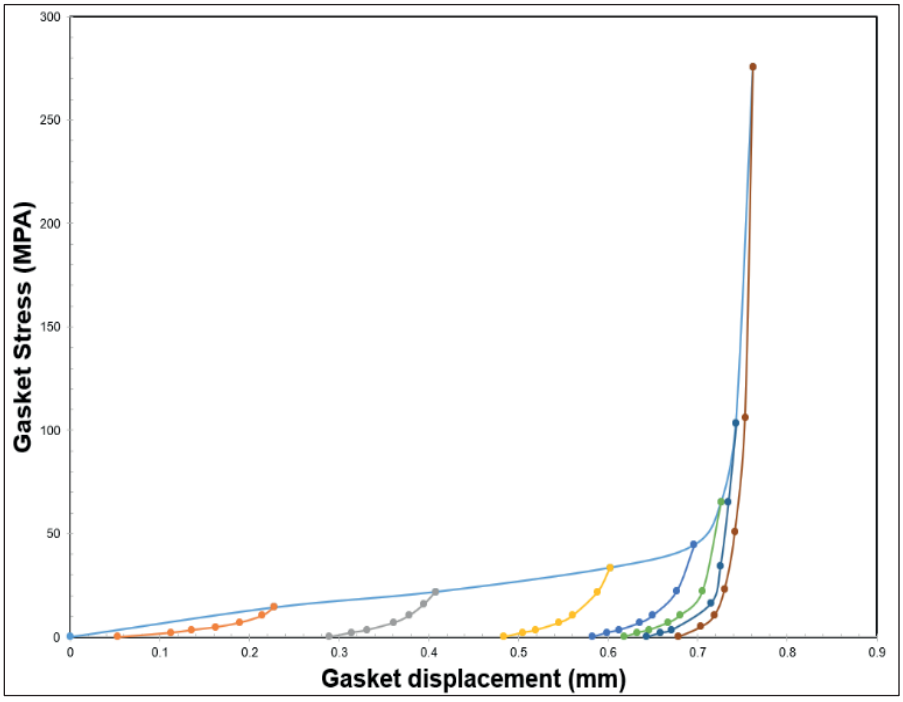

Figure 3-3 Nonlinear unloading–loading curve of the gasket

The analytical model assumed that the gasket unloading was linear, and the gasket compression modulus was calculated by using the slope of the unloading as follows (Bouzid & Chaaban, 1993):

$$E_g = \frac{\Delta S_g}{\Delta D_g} \times (t_g - D_s) \tag{3.10}$$

Where $\begin{cases} t_g \text{ is the initial gasket thickness.} \\ D_s \text{ is the displacement corresponding to the seating stress.} \end{cases}$

3.3.3 Flange Ring

In terms of regulations, the ASME code restricts the rotation of the flange ring to 0.2 degrees for flanges with a hub and 0.3 degrees for flanges without a hub, which is a crucial characteristic. By increasing the bolt preload and providing internal pressure, the flange rotation constantly rises. However, excessive rotation has a significant impact on the gasket contact stress and might result in a lift-off, and spiral wound gaskets are one example of a gasket type that has a limit stop to regulate compression.

Considering width-to-thickness ratio of the flange, the relevant theory for flange ring rotation was selected by employing the ring theory instead of the circular plate theory with the center hole, using the ratio to generate rotation (Timoshenko & Woinowsky-Krieger, 1989):

$$\theta_f = \frac{2R_i Y}{E_f t_f^3} M_f \tag{3.11}$$

Where the value of Y for a flange treated as a ring is given by:

$$Y = \frac{6}{\ln K} \tag{3.12}$$

Additionally, if a flange is viewed as a circular plate with a hole in the center:

$$Y = \frac{1}{K-1}\left[\frac{3}{\pi}(1-\nu_f) + \frac{6}{\pi}(1+\nu_f)\frac{K^2 ln\ K}{(K^2-1)}\right] \tag{3.13}$$

The following equation is used to determine the radial displacement of the flange at the junction with the shell:

$$W_f = (p + Q_0\frac{t_f}{2})\frac{R_i}{E}\left[\frac{k^2+1}{k^2\_1} + v\right] + \theta_f\frac{t_f}{2} \tag{3.14}$$

The flange ring tangential and radial stresses are calculated considering the effect of radial pressure *p* and edge load Q_2 and the bending due to the flange moment M_f

For a plate

$$\sigma_\theta^n = \frac{\left(1+\frac{R_o^2}{r^2}\right)}{K^2-1}\left(p - \frac{Q_2}{t_f} \mp \frac{M_f R_m}{R_i}\right) \tag{3.15}$$

$$\sigma_r^n = \frac{\left(1-\frac{R_o^2}{r^2}\right)}{K^2-1}\left(p - \frac{Q_2}{t_f} \mp \frac{M_f R_m}{R_i}\right)$$

for a ring

$$\sigma_\theta^n = \frac{\left(1+\frac{R_o^2}{r^2}\right)\left(p-\frac{Q_2}{t_f}\right)}{K^2-1} \mp \frac{12M_f y R_m}{r t_f^3} \tag{3.16}$$

$$\sigma_r^n = \frac{\left(1 - \frac{R_o^2}{r^2}\right)p}{K^2 - 1}$$

The rotation and radial displacement are given by:

$$w_c = w_p + w_{Q_0} + w_{M_0} \tag{3.17}$$

$$w_c = \frac{pR^2}{Et_s}(1 - \frac{v}{2}) + \frac{Q_0}{2\beta_s^3 D_s} + \frac{M_0}{2\beta_s^3 D_s} \tag{3.18}$$

And

$$\theta_c = -\theta_{Q_0}\text{-}\theta_{M0} \tag{3.19}$$

$$\theta_c = -\frac{2Q_0\beta_s^2}{k_s} - \frac{4M_0\beta_s^3}{k_s} \tag{3.20}$$

Where D_s and β_s are defined as below:

$$D_s = \frac{Et_s^3}{12(1 - v^2)}, \beta_s = \frac{\sqrt[4]{3(1 - v^2)}}{\sqrt{Rt_s}}, k_s = \frac{Et_s}{R^2} \tag{3.21}$$

There is no internal pressure or hydrostatic force during the bolt-up process. For each operational condition, the bolt and the gasket forces H_b and H_g, as well as the edge loads M_0 and Q_0, can be thus calculated.

As a function of the axial distance, the stresses, displacement, rotation, bending moment, and shear force obtained by the edge loads M_0 and Q_0 are determined by measuring:

$$w_s(x) = \frac{Q_0}{2\beta_s^3 D_s} f_1(\beta_s x) + \frac{M_0}{2\beta_s^2 D_s} f_2(\beta_s x) \tag{3.22}$$

$$\theta_s(x) = \frac{-Q_0}{2\beta_s^2 D} f_3(\beta_s x) - \frac{M_0}{\beta_s^3 D_s} f_1(\beta_s x) \tag{3.23}$$

$$M(x) = \frac{Q_0}{\beta_s} f_4(\beta_s x) + M_0 f_3(\beta_s x) \tag{3.24}$$

$$Q(x) = Q_0 f_2(\beta_s x) - 2M_0 \beta f_4(\beta_s x) \tag{3.25}$$

Where:

$$f_1(\beta_s x) = e^{-\beta_s x} \cos\ \beta_s x \tag{3.26}$$

$$f_2(\beta_s x) = e^{-\beta_s x} (\cos\ \beta_s x - \sin\ \beta_s x) \tag{3.27}$$

$$f_3(\beta_s x) = e^{-\beta_s x} (\cos\ \beta_s x + \sin\ \beta_s x) \tag{3.28}$$

$$f_4(\beta_s x) = e^{-\beta_s x} \sin\ \beta_s x \tag{3.29}$$

The axial distance from the junction is used to calculate the longitudinal and tangential stresses at the inner and outer surfaces of the cylindrical shell:

$$\sigma_l(x) = \frac{pR}{2t_s} \pm \frac{6M(x)}{t_s^2} \tag{3.30}$$

$$\sigma_t(x) = \frac{pR}{t_s} + \frac{Ew_s(x)}{R} \pm \frac{6\nu M(x)}{t_s^2} \tag{3.31}$$

Similar equations are used to determine the stresses in the hub by replacing the geometry and loading parameters with those of the hub.

3.4 Finite Element Modeling

The stress distribution in the bolted flange joint, the ring, the hub, and the shell were tested specifically at the junctions. In this study, these tests were performed by using different nominal pipe sizes (NPS) that belong to the same class, which is 900 in this research.

Table 3.1 displays the differences between the dimensions of each of the seven NPS that were used (NPS 4, 8, 10, 14, 16, 20, and 24) to test whether the results will be similar to the analytical results. It is worth noting that stainless steel is the material that has been used for all the elements in the bolted flange joints which are composed of two similar flanges attached by the bolts and connected to a gasket in the middle. Due to the symmetry between the two flanges, half of the gasket thickness is used in this study and, therefore, only one flange has been drawn to decrease the simulation central processing unit (CPU) time. Additionally, to further reduce the CPU time, only a small part of one flange was implied in this study because of the cyclic symmetry that occurred from the cylindrical shape of the pipe.

To conduct a good stress comparison between all the NPS 4, 8, 10, 14, 16, 20, and 24 (class 900), it is imperical to use the same material, pressure, and forces for all the flanges; hence, an identical internal pressure has been used for all the flanges. Still, the hydrostatic end effect on top of the shell will vary from one flange to another because all the flanges used are known to have a different shell thickness and a different radius. The hydrostatic pressure on top of the shell is calculated through an equation that comprises the shell thickness and the radius of the flange. Therefore, the axial stress applied to the end of the shell is given by

$$\sigma_{\ell} = \frac{P \times R}{2 \times t} \tag{3.32}$$

Moreover, the bolt pretension varies from one flange to another even though all the flanges possess the same initial bolt stress. Hence, the bolt pretension in Ansys is to be calculated using the following equation:

$$Bolt\ pretension = Bolt\ stress \times Root\ area\ of\ the\ bolt \tag{3.33}$$

When the bolt size changes, the root area of the bolt also changes as each flange requires a different bolt dimension. All flanges will be analyzed to observe the stress distribution (longitudinal, tangential, and radial stresses), along each element of the bolted flange joint and its junctions. The flanges were placed under the same conditions to monitor the effect of the flange size variation noting that the material properties, dimensions and loading are illustrated in Table 3-1 below.

Table 3-1 Properties, dimensions and loading

Model Properties							
Flange Size (in)	4	8	10	14	16	20	24
Outer diameter of flange (mm)	292.1	469.9	546.1	641.34	704.84	857.24	1041.4
Inner diameter of flange (mm)	102.26	202.72	254.5	336.56	387.36	488.96	590.56
Raised face diameter (mm)	157.074	269.88	323.84	412.76	469.9	584.2	692.14
Bolt circle diameter (mm)	102.26	393.7	469.9	558.8	615.94	749.3	901.7
Shell thickness (mm)	6.0198	6.0198	9.27	9.52	9.52	9.52	9.52
Length of the shell (mm)	127	177.8	203.2	228.6	254	279.4	304.8
Raised face height (mm)	6.35	6.35	6.35	6.35	6.35	6.35	6.35
Diameter of the hub (mm)	158.75	298.44	368.3	450.84	508	622.3	749.3
Length of the hub (mm)	60.808	86.282	100.39	112.85	112.72	125.42	138.12
Flange thickness (mm)	44.45	63.5	69.85	85.725	88.9	107.95	139.7
Bolt diameter (mm)	28.575	34.912	34.912	38.113	41.262	50.838	63.754

Number of bolts	8	12	16	20	20	20	20
Gasket height (mm)	4.572	4.572	4.572	4.572	4.572	4.572	4.572
Gasket width (mm)	14.285	17.46	17.4625	22.225	22.225	25.4	25.41
Inner diameter of the gasket (mm)	120.65	222.25	276.225	355.6	412.75	520.7	628.65
Outer diameter of the gasket (mm)	149.22	257.17	311.15	400.05	457.2	571.5	679.45
Bolt preload (N)	161915.27	257996.85	257996.85	313599.62	373650.61	511545.484	954143.533
Pressure on top of the shell (MPA)	53.00050633	77.319168	85.66032363	110.311765	126.949916	160.247395	193.5448
Internal pressure (MPA)	12.48	12.48	12.48	12.48	12.48	12.48	12.48

Boundary condition and Loading

Technically “Ansys workbench” is the software that has been used in this study with the aim of analyzing the stresses and deformations of selected flanges of class 900.

As mentioned earlier, because of symmetry, the portion of the flange considered is set based on the number of bolts. And since the bolted flange joint has a cylindrical shape, the angle of the portion that should be drawn is equivalent to 360 divided by the number of bolts to reduce the CPU time. The boundary conditions and loading that are set in this model are as follows:

- The bolt pretension is set in the middle of the bolt in the axial direction for the bolt-up (load case 1).
- The internal pressure is put on the inner surface of the pipe for the pressurization (load case 2).
- The hydrostatic end load is applied at the top surface of the shell for the pressurization (load case 2).
- The lower surfaces of the bolt and gasket are restrained in the axial direction or y-axis, but they are free on the x and z-axis.
- The two axial planes that represent the planes of symmetry are constrained with no radial rotation and tangential displacement.

All the cited se constraints are shown in Figure 3-4 and apply to the bolted flange joint in the bolt-up and pressurization stages accordingly. It goes without saying that the prestress is for the bolt-up phase while all pressure loads should be taken out.

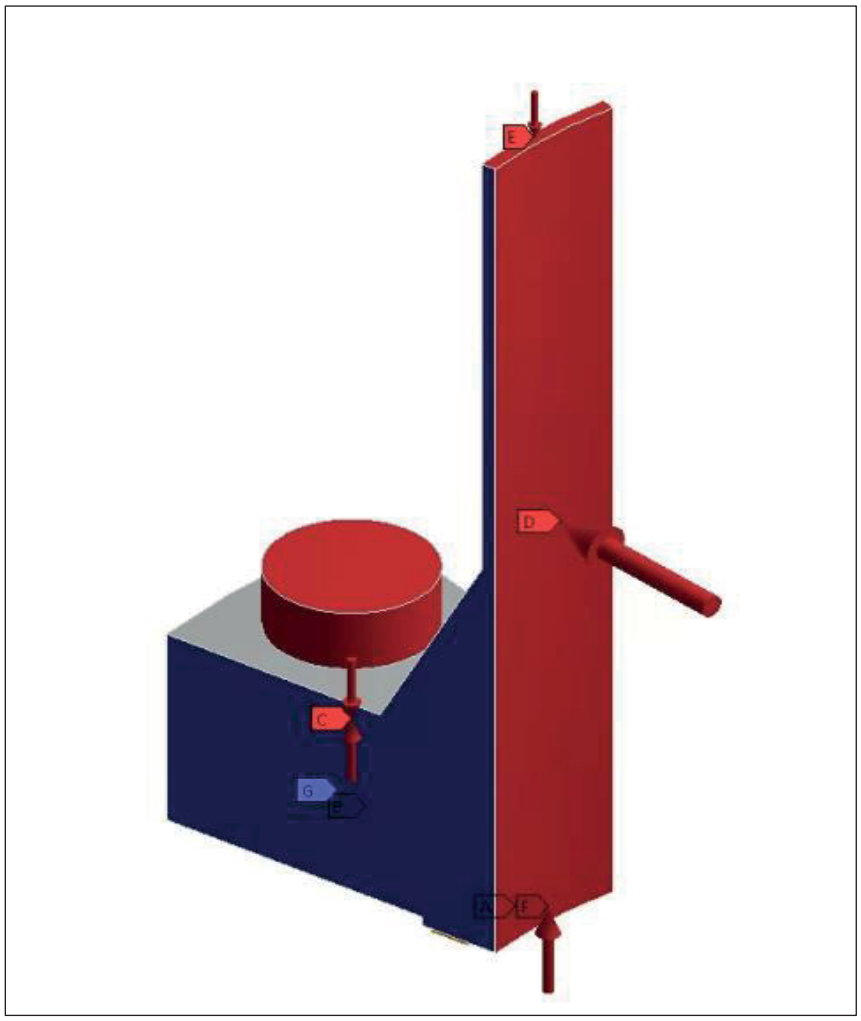

Figure 3-4 The loading and constraints that are applied to the model

An internal pressure of 1810 psi (12.48 MPA) is applied to the inner surface of the flange. The Young's modulus of the flange is 199.95 GPa, whereas that of the bolt is 209.95 GPa. The Poisson's ratio of the flange is set to be equal to 0.3 representing SA-280 or SS304 material.

In order to compare the analytical stress distributions to the numerical ones, the FEM model mesh was refined until a convergence of 1% was obtained. Therefore, it is a requirement indeed to use as many numbers of nodes per element as possible to accurately and rapidly obtain convergence. Consequently, since the higher the number of nodes per element, the higher the accuracy will be achieved, the SOLID186 elements consisting of 20 nodes per element were used to mesh the bolted flange joint. The PRETS179 elements were also used in the modeling of the bolt pretension. Specifically, CONTA174 is the type of contact elements used between the flange facing and the gasket, as well as between the lower surface of the bolt head and the flange upper surface. Figure 3-5 shows the bolted flange joint model on ANSYS from different angles.

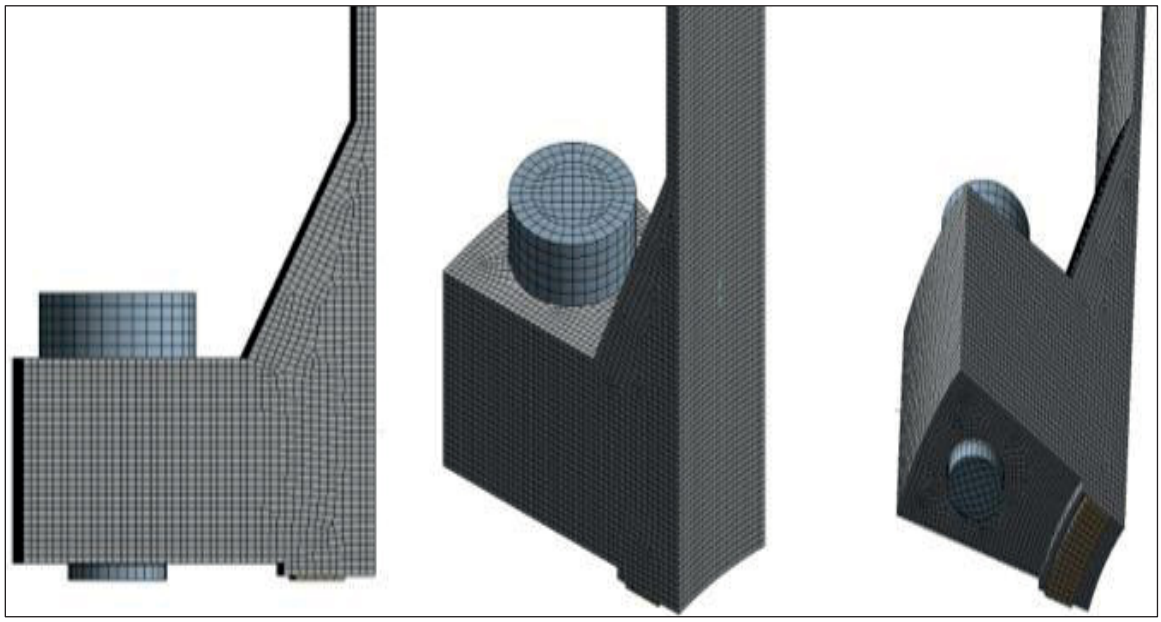

Figure 3-5 FEM bolted flange joint model in ANSYS

CHAPTER 4

RESULTS & DISCUSSION

This section displays and explains the results obtained from FEM, ANSYS (finite element analysis software) for all the sizes examined in this study and compared to the analytical model. The main purpose of this project is to examine the distribution of the stresses and deformations of bolted joints composed of selected flanges of class 900. The stress distributions in the longitudinal and tangential directions are plotted along the flange axial distance at both the inner and the outer diameter. The radial stresses are considered marginal and are not discussed in this paper. Indeed, for bolt-up, the radial stress is zero at both the flange inner and outer diameter. As for the pressurization, the radial stress is also zero at the outer diameter. In compression, however, the radial stress is equal to the pressure.

In addition, the flange rotation, the gasket contact stress, and the bolt stress are also discussed hereafter. The stress distributions of importance are those of the longitudinal and tangential directions. As displayed below, Figures 4-1 to 4-14 show the results of the tangential and longitudinal stresses along the axial position of the bolted flange joint at the inner and the outer diameters followed by the radial displacement of the flange ring hub and shell shown in the Figures 4-15 to 4-21. The stresses are given for both the bolt-up and pressurization at the inside and outside flange surfaces. The displacements are also given at both conditions at the inside surface, and eventually, the FEM results are compared to the analytical results.

NPS 4:

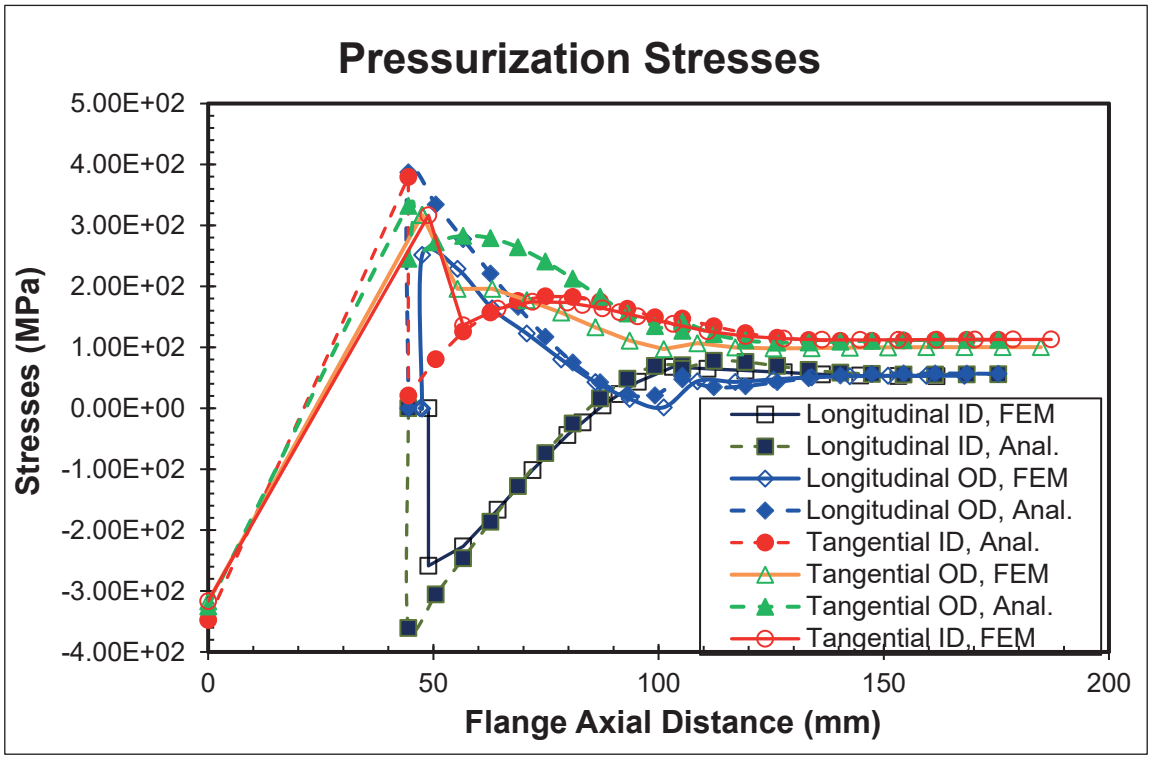

Figure 4-1 Pressurization stresses in function of the flange axial distance for NPS 4

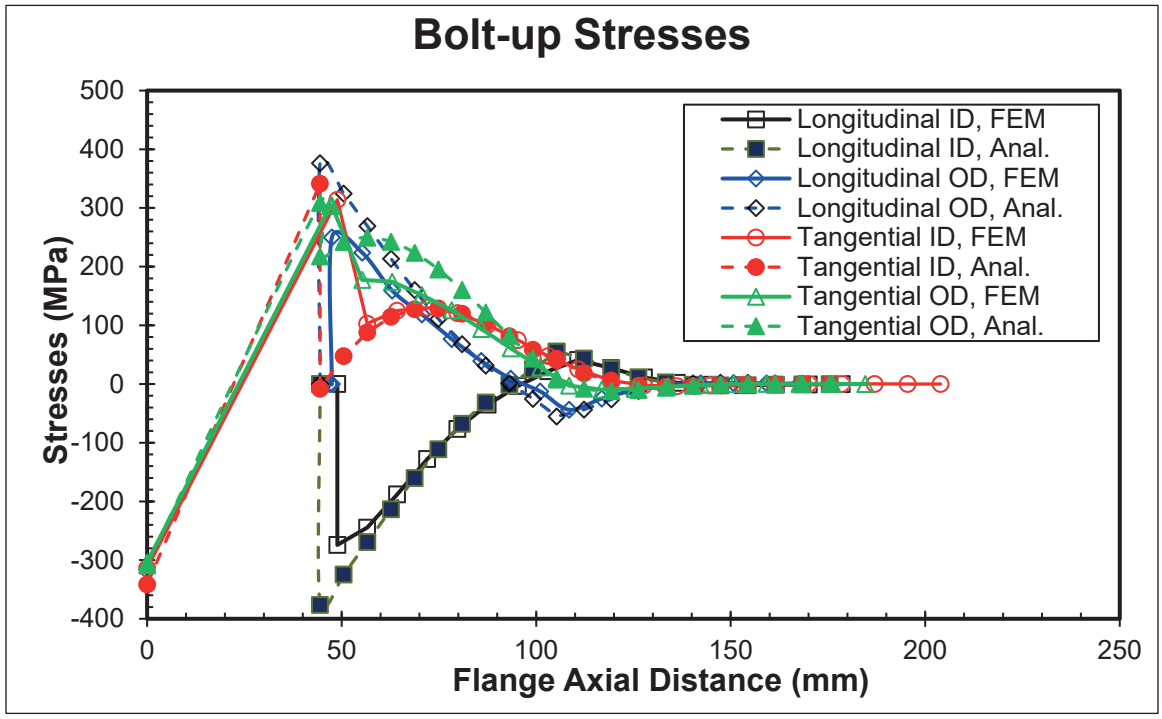

Figure 4-2 Bolt-up stresses in function of the flange axial distance for NPS 4

NPS 8:

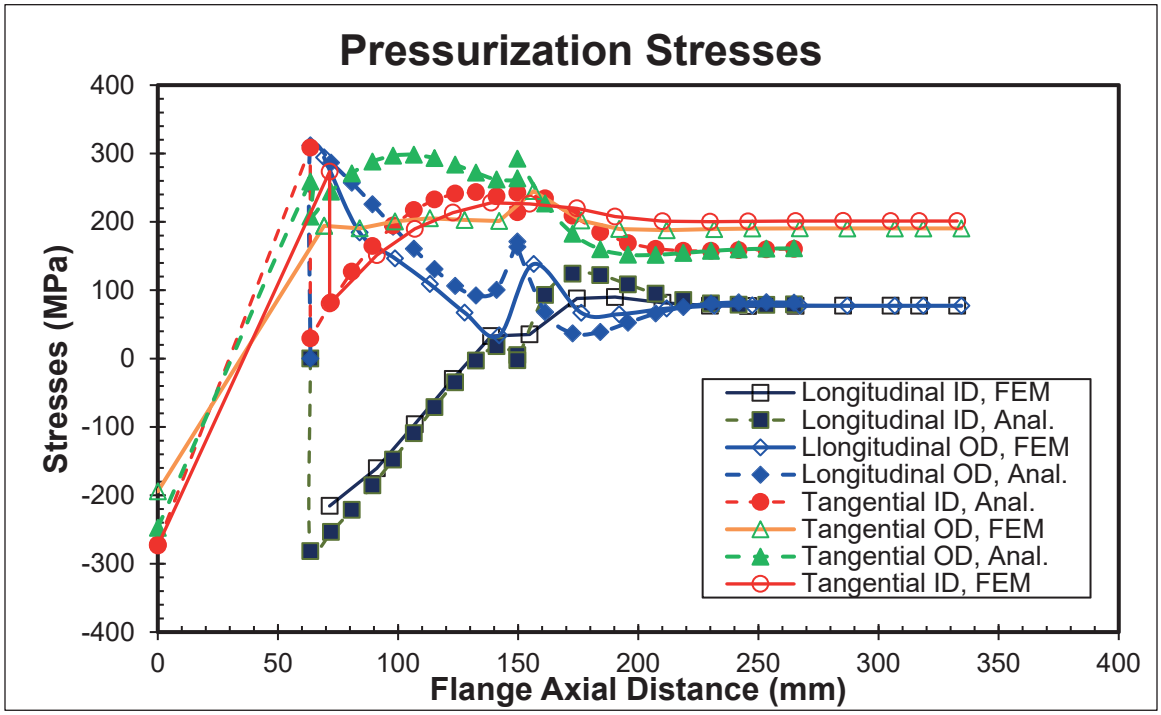

Figure 4-3 Pressurization stresses in function of the flange axial distance for NPS 8

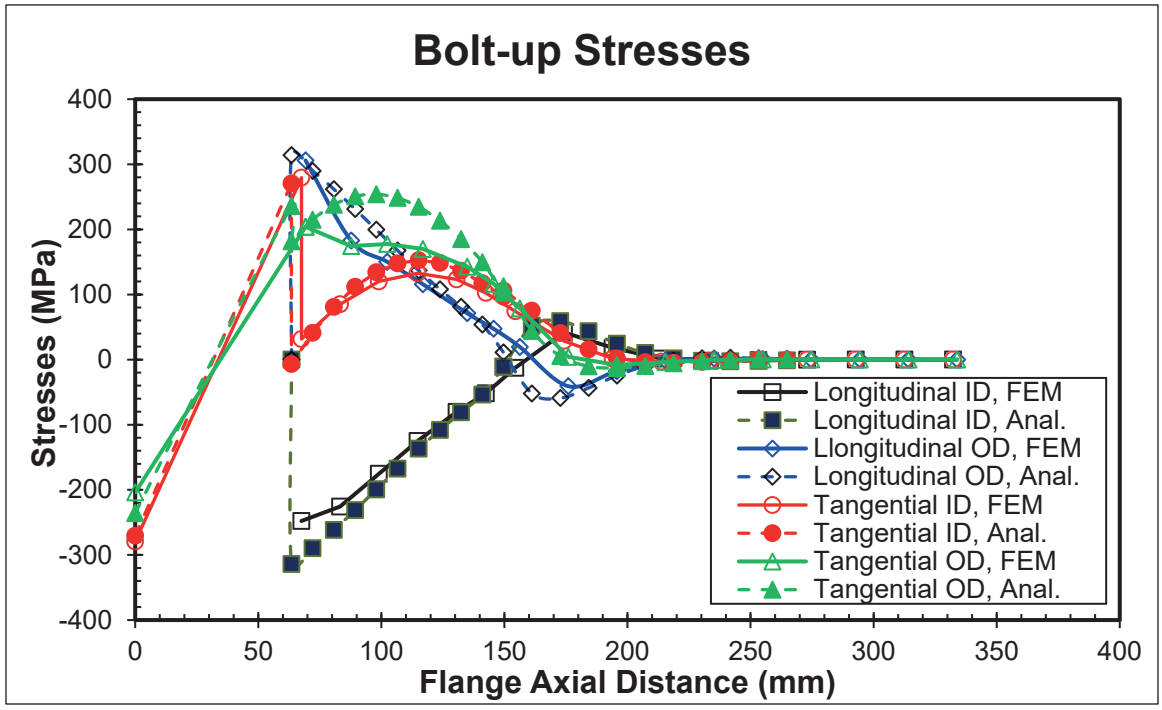

Figure 4-4 Bolt-up stresses in function of the flange axial distance for NPS 8

NPS 10:

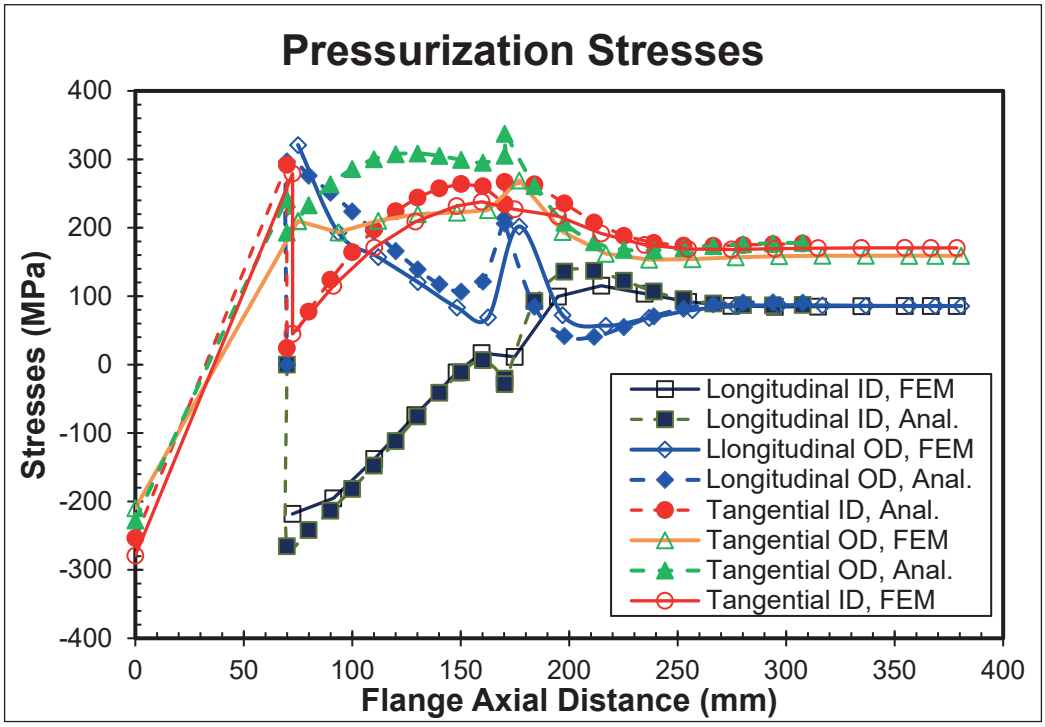

Figure 4-5 Pressurization stresses in function of the flange axial distance for NPS 10

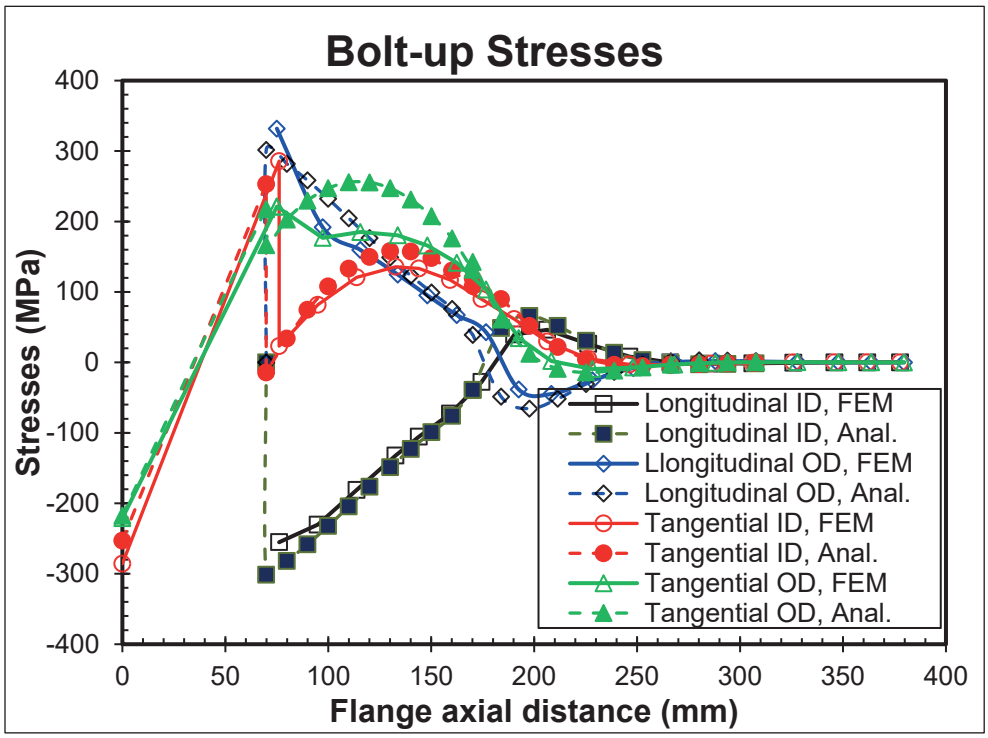

Figure 4-6 Bolt-up stresses in function of the flange axial distance for NPS 10

NPS 14:

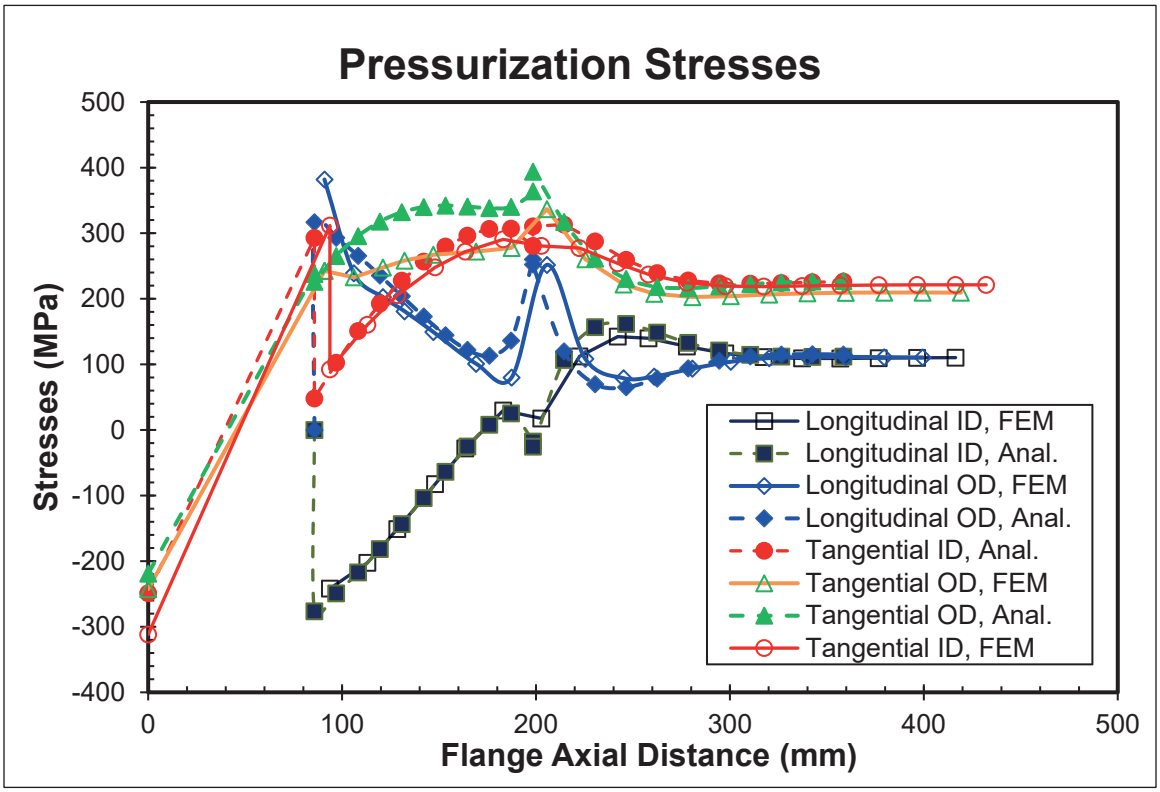

Figure 4-7 Pressurization stresses in function of the flange axial distance for NPS 14

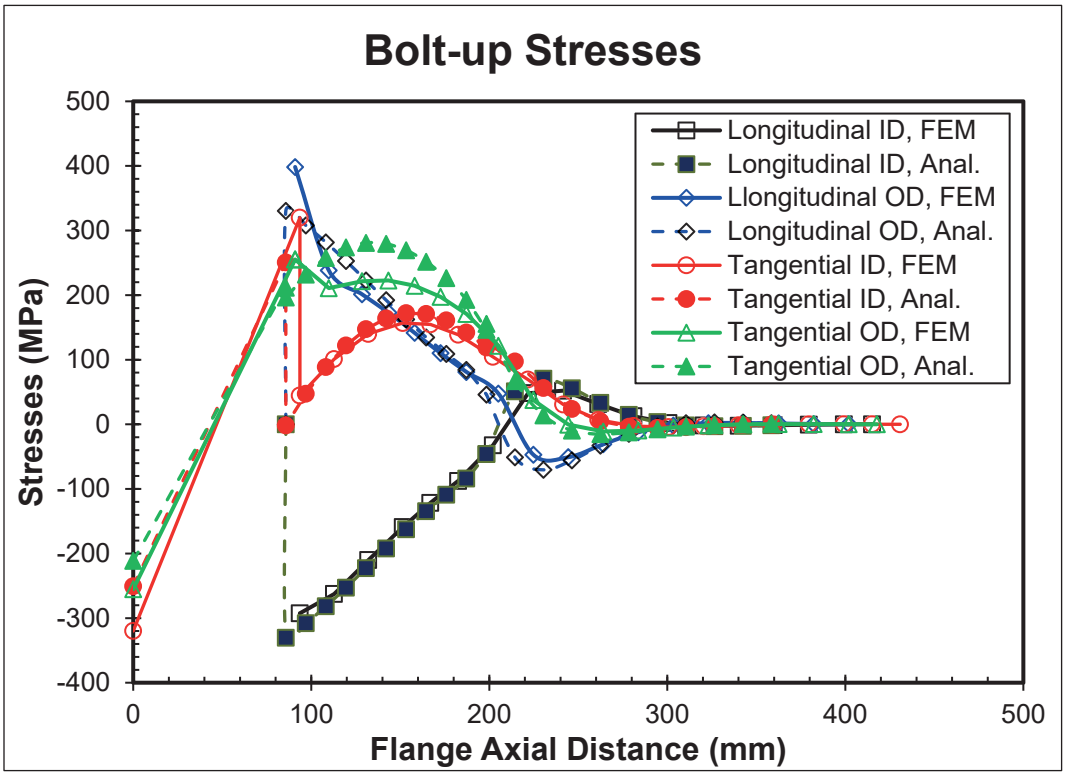

Figure 4-8 Bolt-up stresses in function of the flange axial distance for NPS 14

NPS 16:

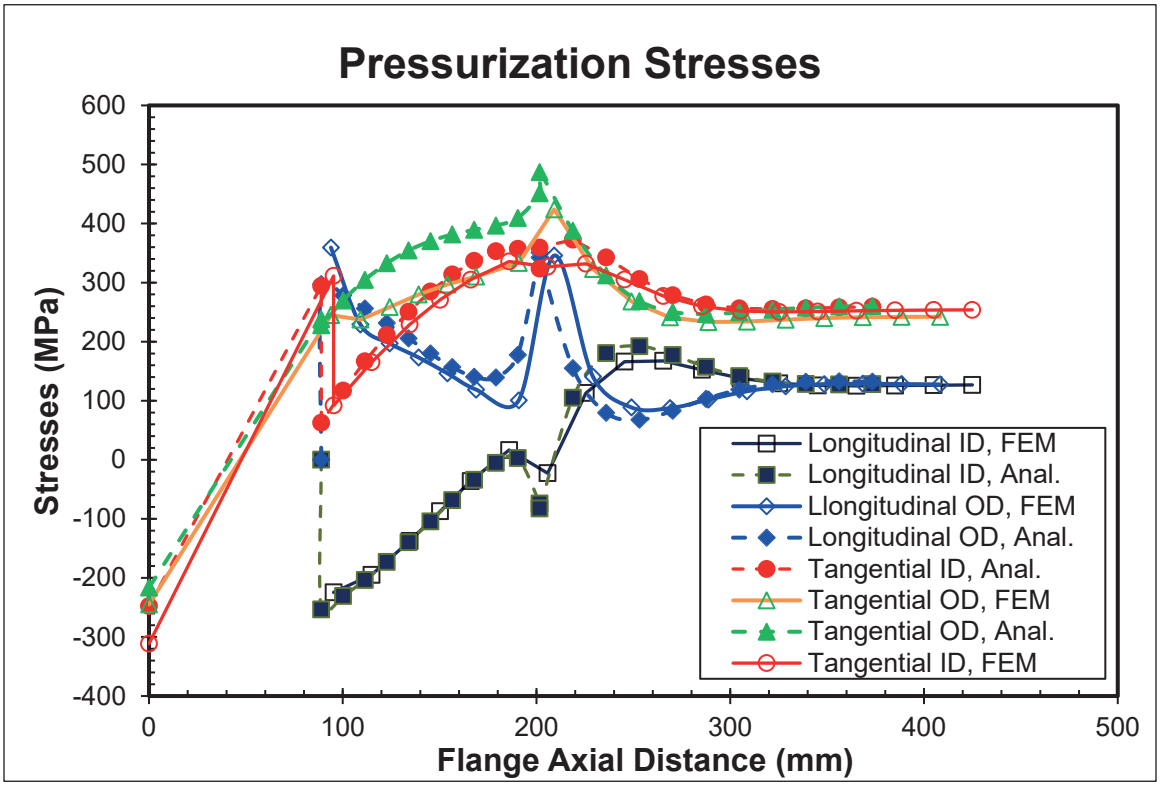

Figure 4-9 Pressurization stresses in function of the flange axial distance for NPS 16

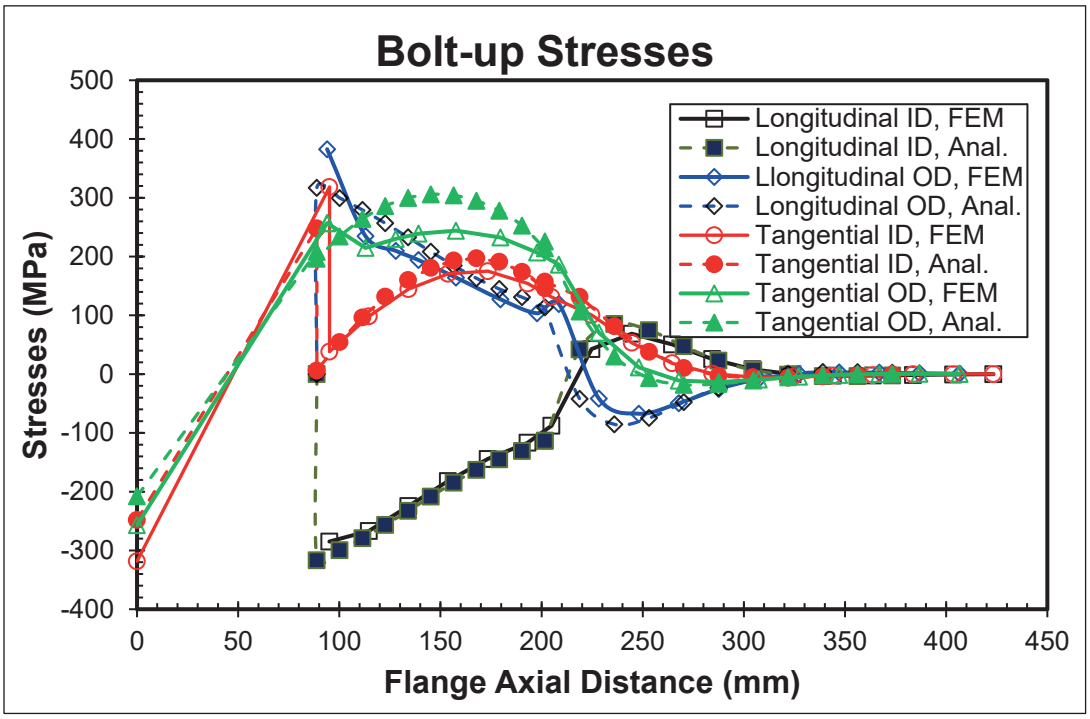

Figure 4-10 Bolt-up stresses in function of the flange axial distance for NPS 16

NPS 20 :

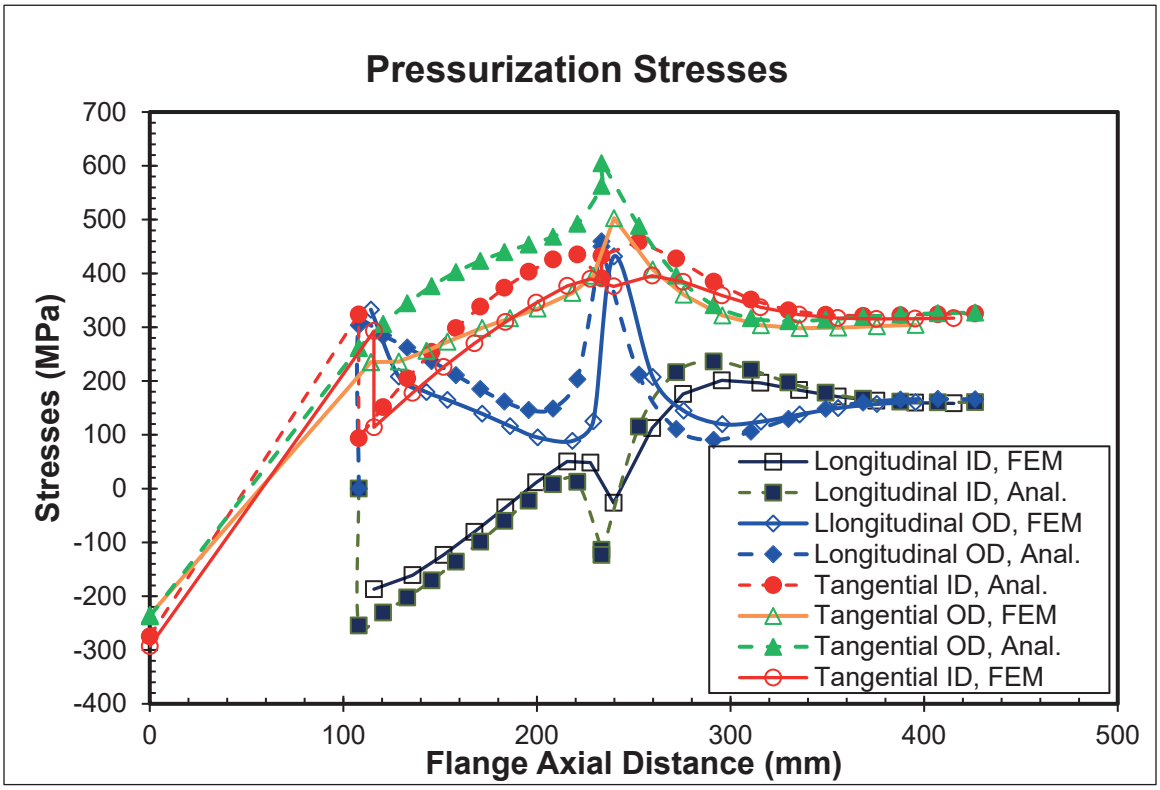

Figure 4-11 Pressurization stresses in function of the flange axial distance for NPS 20

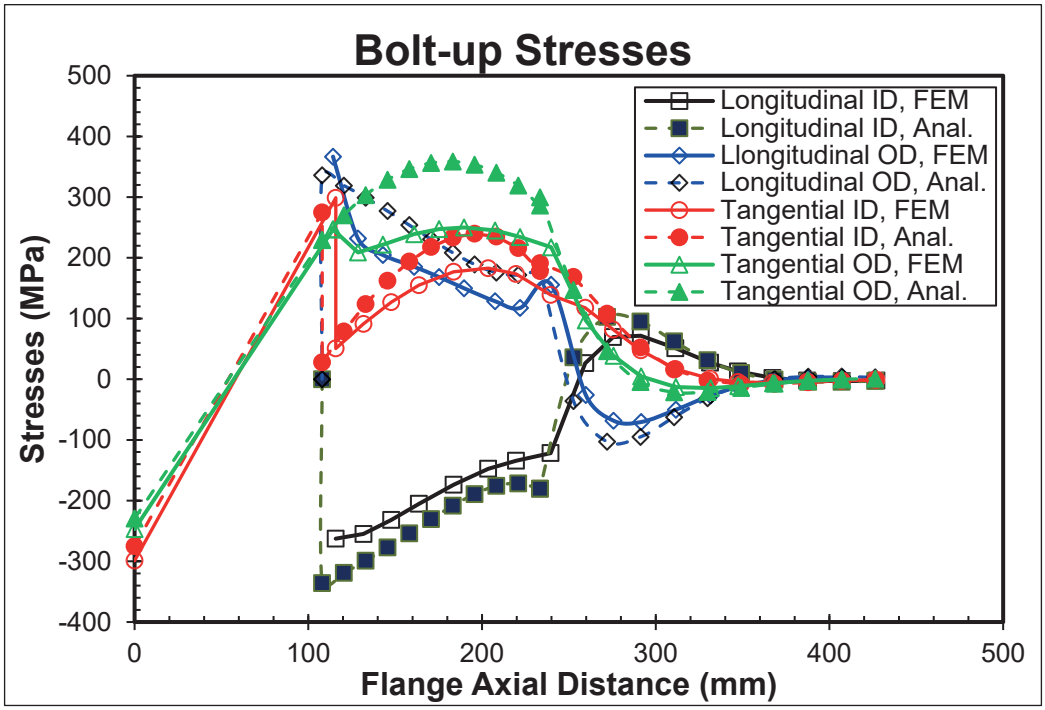

Figure 4-12 Bolt-up stresses in function of the flange axial distance for NPS 20

NPS 24:

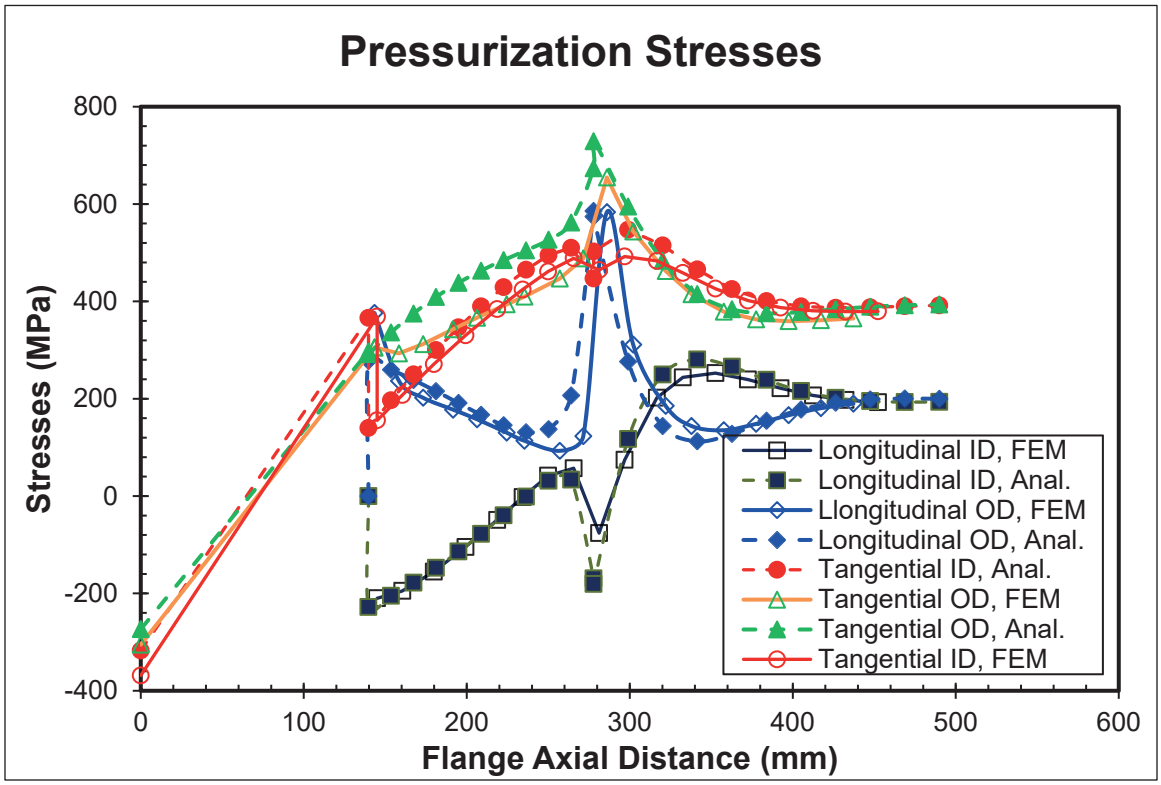

Figure 4-13 Pressurization stresses in function of the flange axial distance for NPS 24

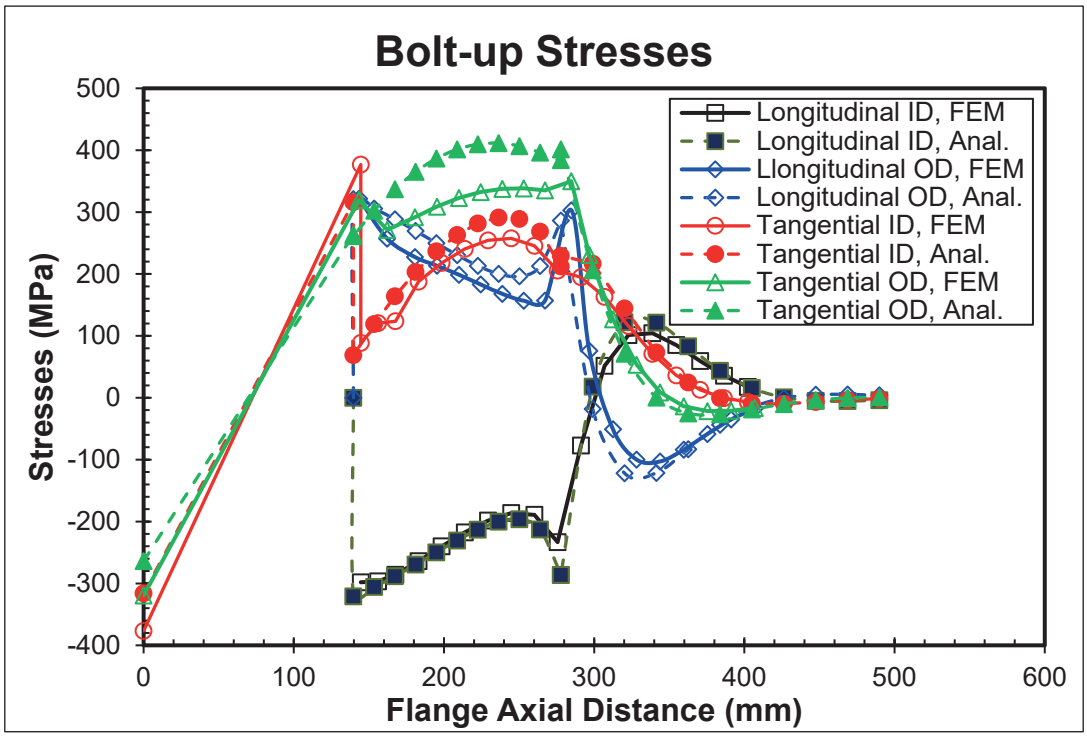

Figure 4-14 Bolt-up stresses in function of the flange axial distance for NPS 24

4.1 Longitudinal Stress Distribution

By looking at the results of any size shown above from Figures 4-1 to 4-14, one can easily observe that every graph obtained from ANSYS has its analytical counterpart for comparison, regardless of what stage it is. Having the analytical curves sheds the light on the validation of both methods. As observed in the previously mentioned figures, it is evident that all the distribution of the longitudinal stresses along the bolted flange joint axial direction is different for each flange size even though the general trends are rather similar. On the other hand, the FEM results compare well with the analytical results for both the inner and the outer surface of the flange and for both phases: bolt-up and pressurization. The maximum longitudinal stress occurs at the junction between the hub and the ring. This observation is noticed for all flange sizes of class 900 treated, as displayed in the previous graphs. Both the stresses at the inner and outer surfaces of the flange increase in the hub and at its two ends. Far from the junction, however, the longitudinal stress in the shell is uniform and relatively lower before it faces some disruptions due to the geometrical discontinuity that occurs at the junction between the hub and the shell. Far from the discontinuity, the longitudinal stress in the shell takes up a value of:

$$\sigma = \frac{P \times R}{2t} \tag{4.1}$$

when it is pressurized. In this equation, P stands for the internal pressure, R stands for the inner radius and t is the thickness of the shell noting that this stress is zero during bolt-up. The analytical and the FEM results of the longitudinal stress agree well, in general, for all treated flange sizes, except for the results of the small flanges because the theories used to model the hub are not appropriate for high hub angles.

4.2 Tangential Stress Distribution

Similarly, the results of the distributions of the tangential stress from the FEM are compared to the analytical ones and found in good agreement. As shown in Figures 4-1 to 4-14, the tangential stress distributions at the inner surface of the flange display higher values in comparison to the outer surface of the flange. Also, both the tangential stress curves of the

inner and the outer surfaces have the same trend in the flange ring, hub and shell. It is worth mentioning that the maximum tangential stress is in the big end of the hub or near the junction with the ring. Consequently, the tangential stress decreases in the shell near the junction with the hub until it reaches a certain value and remains steady upon it. The tangential stress is zero during the bolt-up phase and, for the pressurization, it is equal to:

$$\sigma = \frac{P \times R}{t} \tag{4.2}$$

where P is the internal pressure, R is the inner radius and t is the thickness of the shell. Thus, depending on the radius to thickness ratio the tangential stress can take different values from one flange to the other.

4.3 Radial Displacement

The results of the radial displacement along the flange axial distance from the analytical and the FEM are compared to each other in the different graphs and are shown in Figure 4-15 until Figure 4-21. The curves of the radial displacement during pressurization phase are higher than those of the bolt-up phase. The lateral pressure increases the radial displacement and causes the flange ring to rotate more. While the maximum radial displacement occurs in the hub during both the bolt-up and pressurization phases, in the shell far from the junction with the hub, it is zero for bolt-up and becomes equal to a constant value in the case of pressurization. In fact, during pressurization, the radial displacement can be calculated by the following equation for the thin-walled sections:

$$\Delta r = \frac{(2 - \nu)\mathrm{P} \times r^2}{\mathrm{E} \times \mathrm{t}} \tag{4.3}$$

Where

- P is the pressure (MPA)
- r is the radius of the shell (mm)
- E is the modulus of elasticity (MPA)
- t is the wall thickness (mm)

NPS 4:

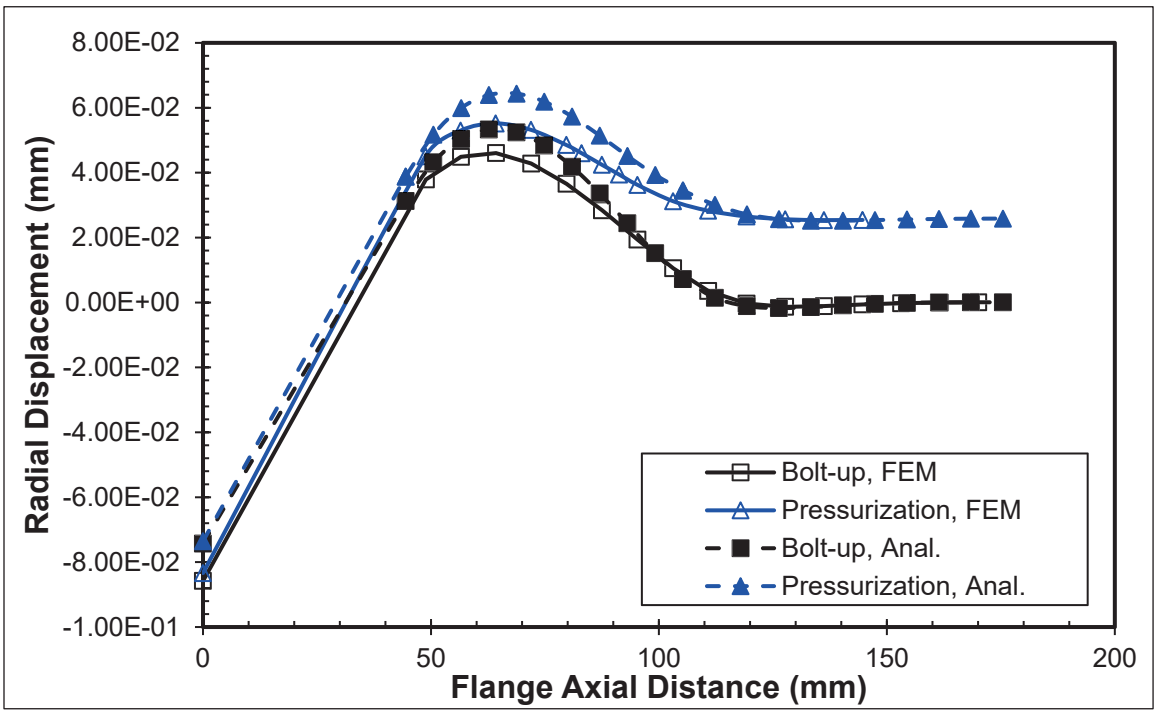

Figure 4-15 Radial displacement in function of the flange axial distance for NPS 4

NPS 8:

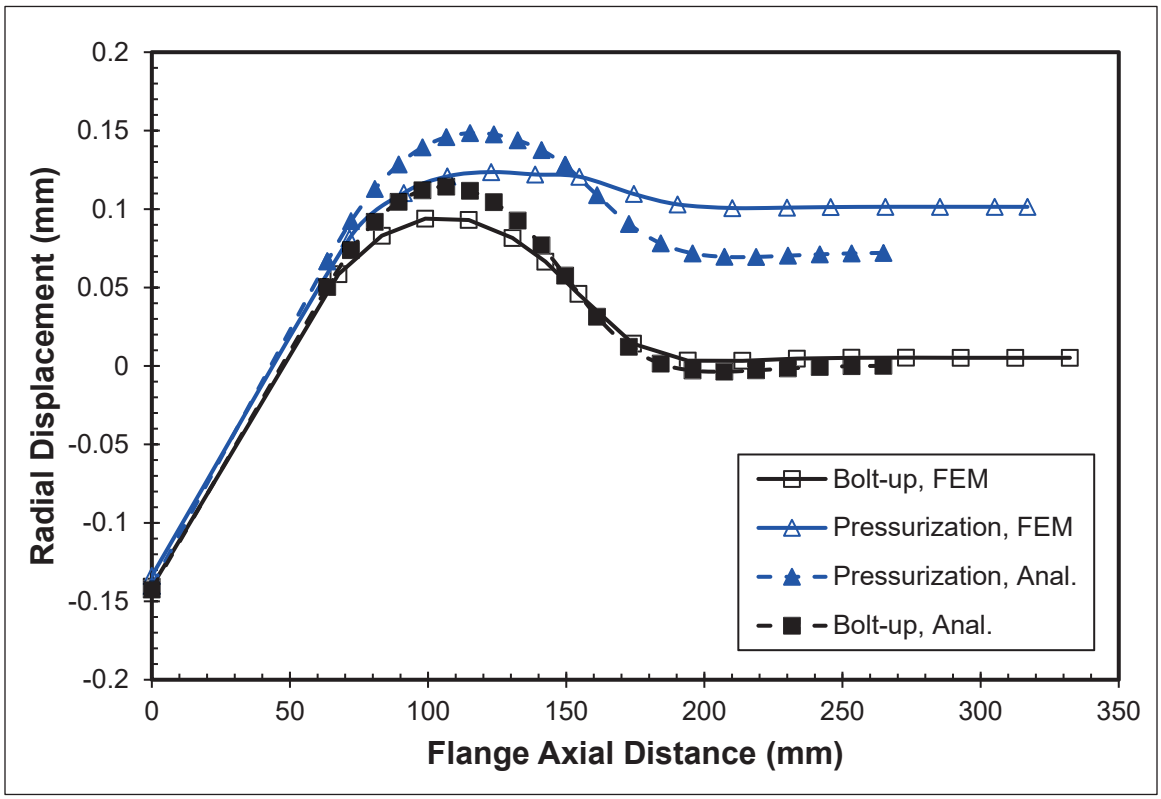

Figure 4-16 Radial displacement in function of the flange axial distance for NPS 8

NPS 10:

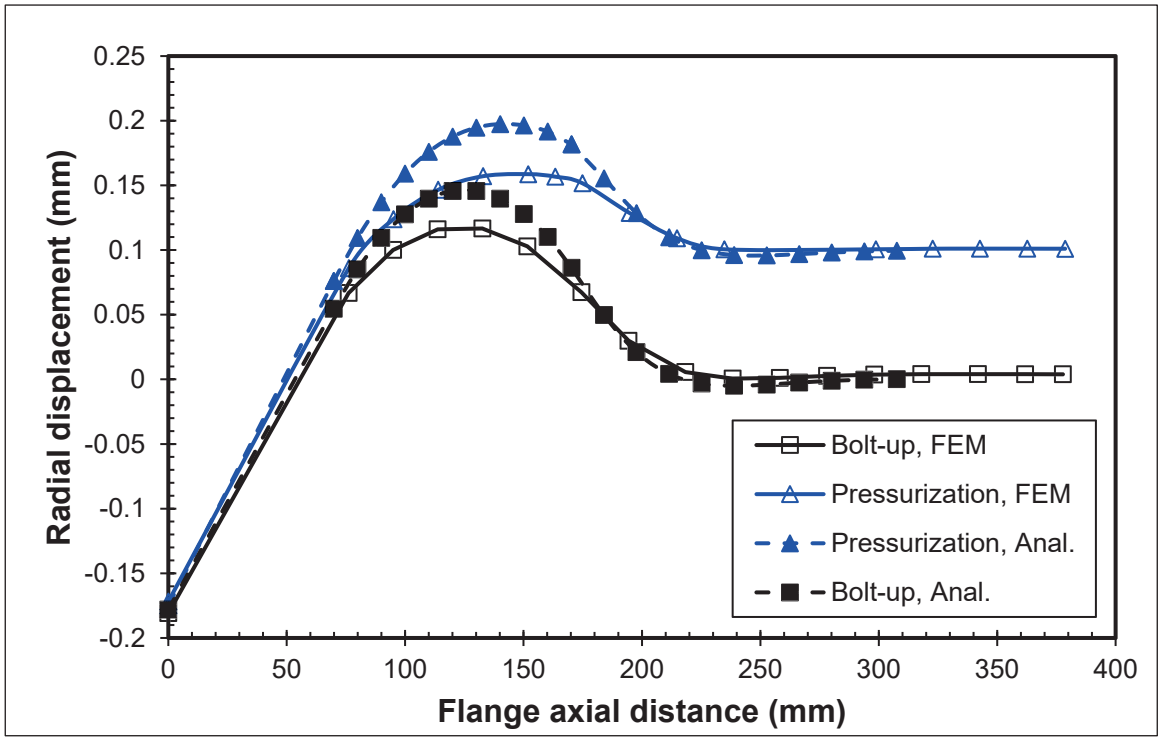

Figure 4-17 Radial displacement in function of the flange axial distance for NPS 10

NPS 14:

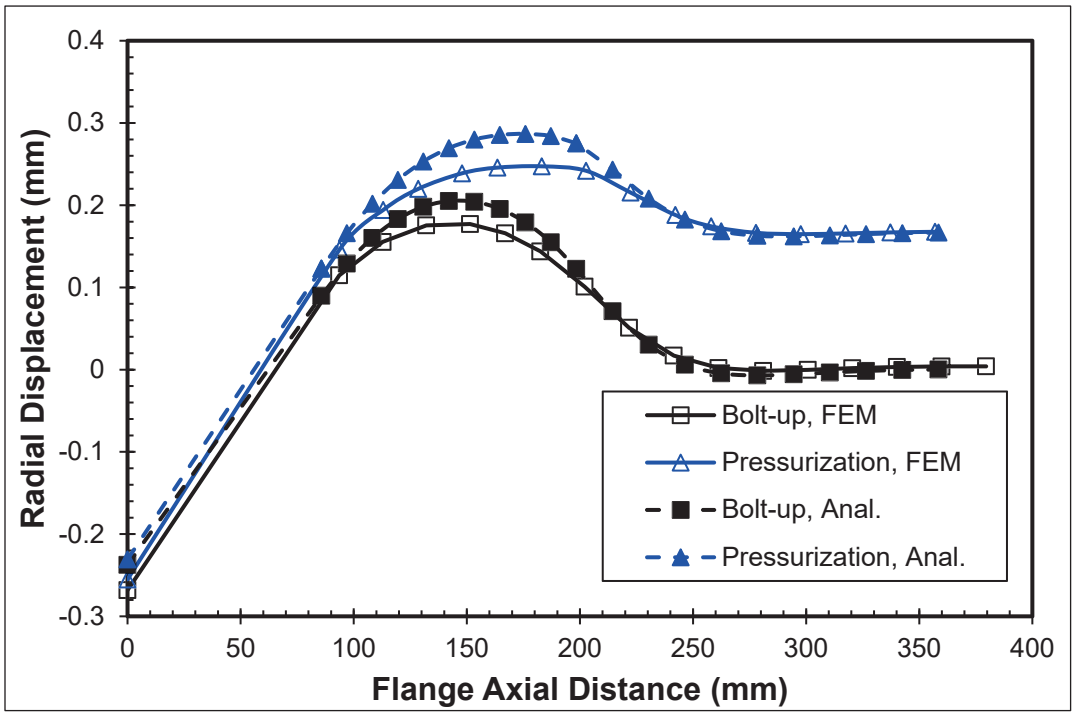

Figure 4-18 Radial displacement in function of the flange axial distance for NPS 14

NPS 16:

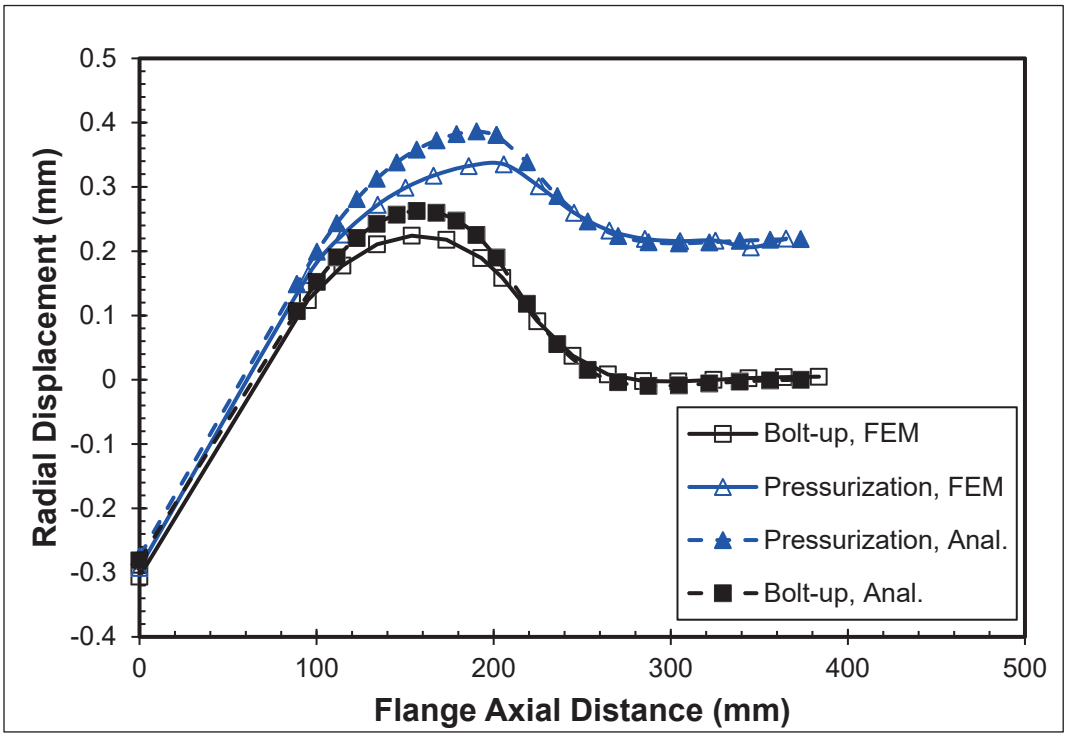

Figure 4-19 Radial displacement in function of the flange axial distance for NPS 16

NPS 20:

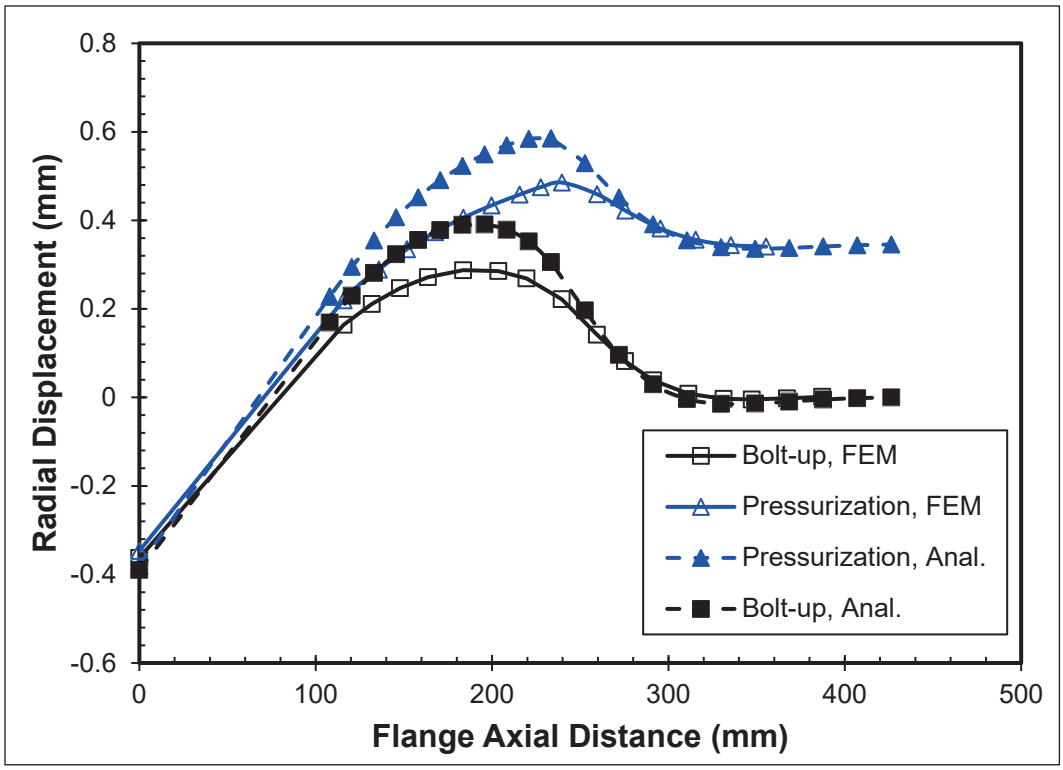

Figure 4-20 Radial displacement in function of the flange axial distance for NPS 20

NPS 24:

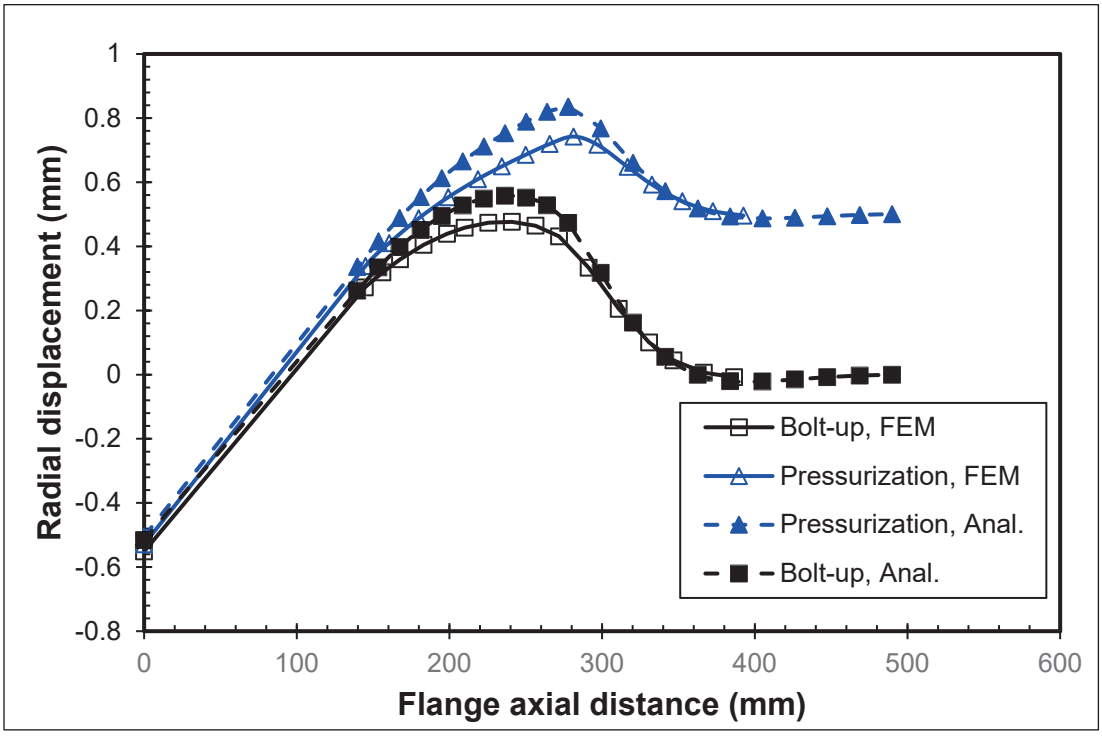

Figure 4-21 Radial displacement in function of the flange axial distance for NPS 24

Table 4-1 Results taken from ANSYS software for the different flange sizes

Flange	**Class 900**							
NPS		*4*	*8*	*10*	*14*	*16*	*20*	*24*
Initial σ_b (MPa)	*Ana.*	344.8	344.8	344.8	344.8	344.8	344.8	344.8
	FEM							
Final σ_b (MPa)	*Ana.*	345.2	336.3	332.6	326.8	319.1	313.5	316.2
	FEM	345.1	333.5	321.1	327	321.7	283.7	327.4
Initial σ_g (MPa)	*Ana.*	218	237.9	258.9	240.2	249.2	273.4	368.7
	FEM	232	239.3	256.3	246.7	247.7	242.5	375.6
Final σ_g (MPa)	*Ana.*	195	195.2	203.3	180.6	176.6	187.6	263.9
	FEM	211	207.5	209.1	193.2	189	172.9	286.7
Initial θ(°)	*Ana.*	0.136	0.1740	0.1908	0.2188	0.2501	0.2968	0.319
	FEM	0.2133	0.2250	0.2385	0.2806	0.303	0.3011	0.3676
Final θ(°)	*Ana.*	0.1448	0.1867	0.2058	0.2364	0.2732	0.323	0.3449
	FEM	0.2184	0.2297	0.2433	0.2877	0.313	0.3142	0.378

4.4 Flange Rotation

Flange rotation is considered one of the most important parameters from the integrity and leakage tightness point of view. Excessive rotation can cause damage to the gasket by crushing and lead to leakage because of the lift off and reduction in the area. The flange rotation for all the flanges sizes (NPS 4, 8, 10, 14, 16, 20, and 24) was obtained using Ansys. This was achieved by calculating the slope of the line obtained from the axial displacement of the flange

mating surfaces. Table 4-1 above displays the analytical and FEM results of the flange rotation for the selected flange sizes during bolt-up and pressurization.

Apparently, the flange rotation during bolt-up is smaller than the flange rotation during pressurization, but the flange rotation increases as the size of the flange increases. The analytical and FEM results were found to agree relatively well, specifically in concern to the small flange sizes.

4.5 Average Gasket Contact Stress

In addition to the flange rotation, the gasket contact stress is also an important parameter in flange design as it is directly linked to the level of leakage. The gasket contact stresses obtained from the FEM and shown in Figure 4-22 until Figure 4-28 are averaged through the gasket width. From the contact stress distributions, the curves show a continuous increase from the inner radius of the gasket to the outer radius of the gasket due to flange rotation. Adding to that, the gasket contact stress during bolt-up is seemingly greater than that during pressurization due to hydrostatic end thrust which causes the unloading of the gasket. Also, it is observed that the gasket contact stress increases with the flange size. Table 4-1 shows the comparisons between the analytical and FEM average values indicating a good agreement between the two.

NPS 4:

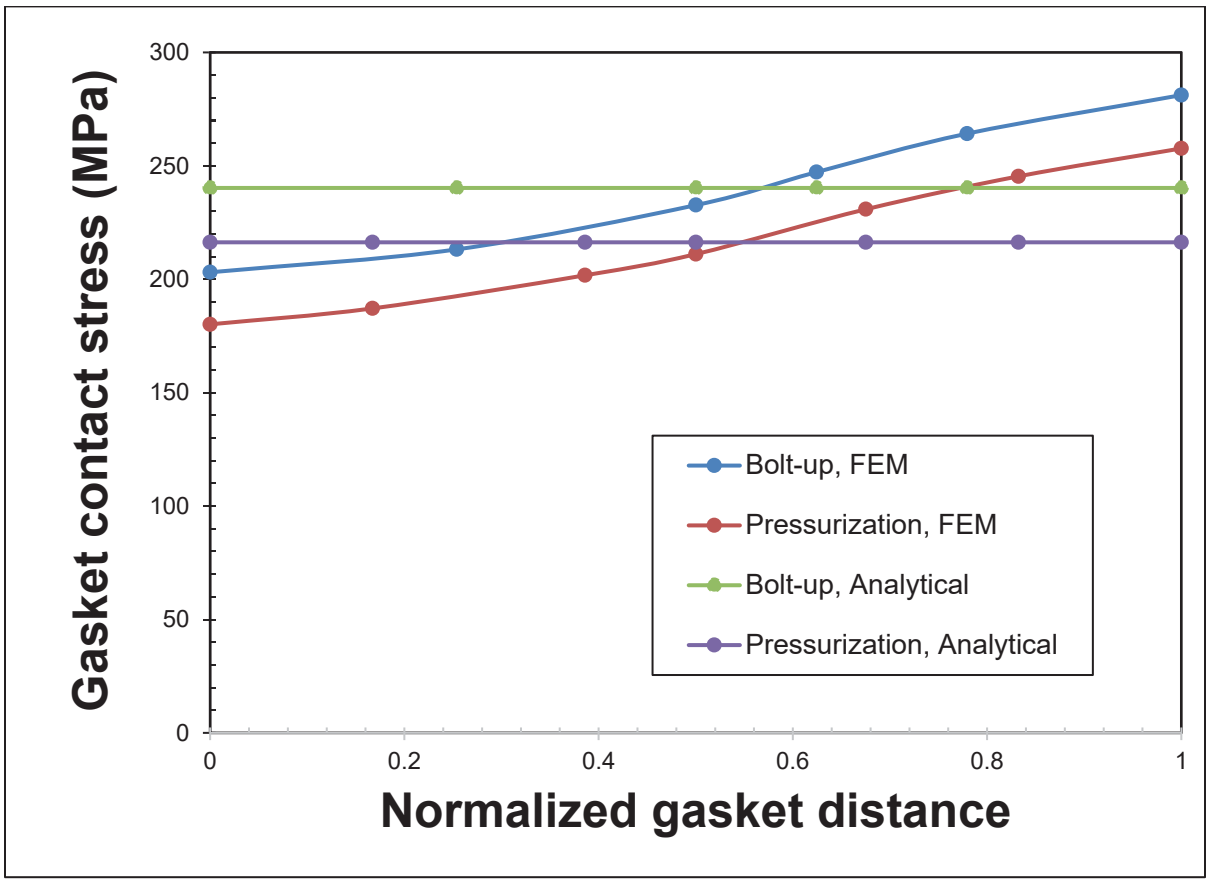

Figure 4-22 Gasket contact stress (MPa) in function of the Normalized gasket distance for NPS 4

NPS 8:

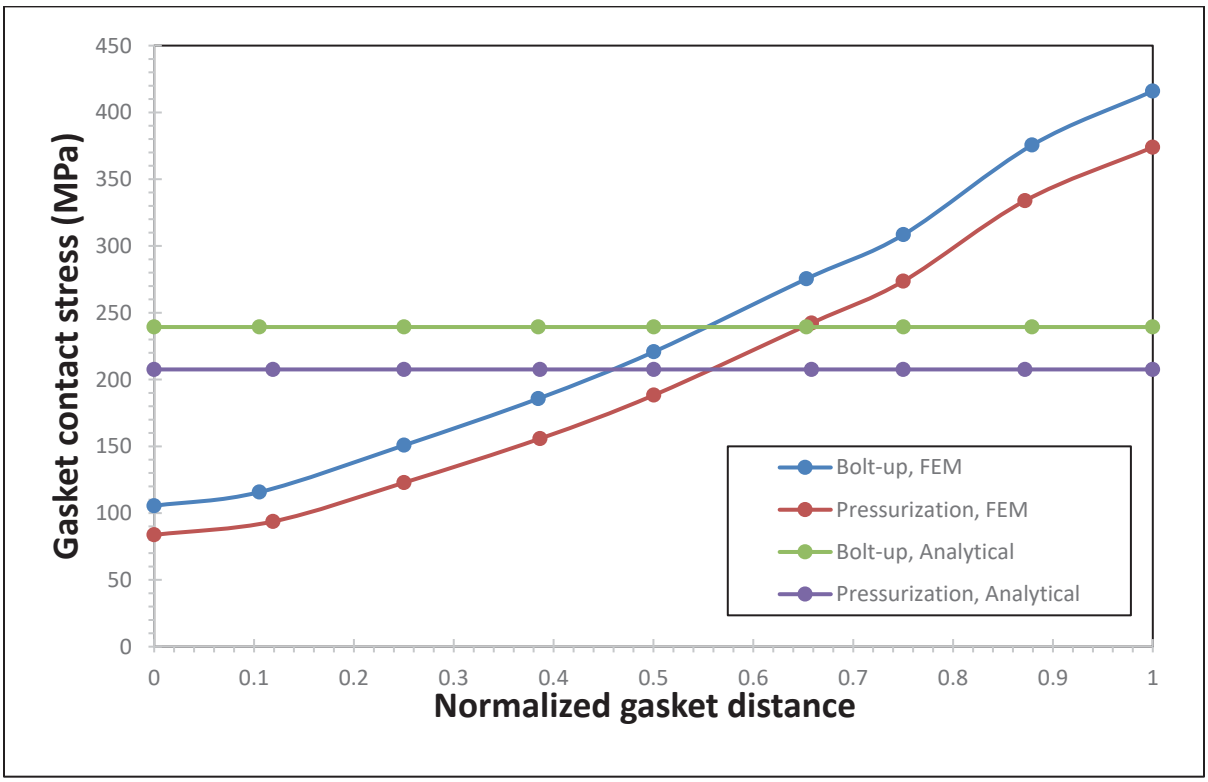

Figure 4-23 Gasket contact stress (MPa) in function of the Normalized gasket distance for NPS 8

NPS 10:

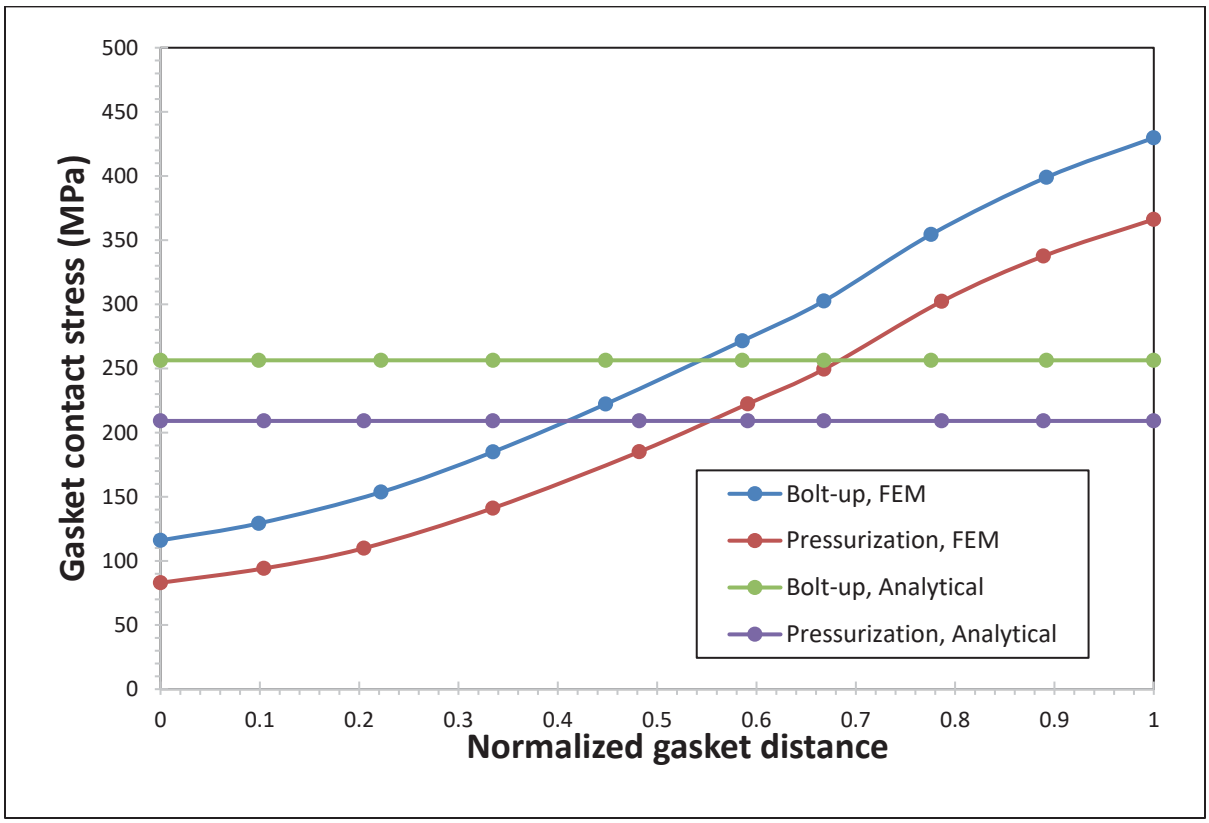

Figure 4-24 Gasket contact stress (MPa) in function of the Normalized gasket distance for NPS 10

NPS 14:

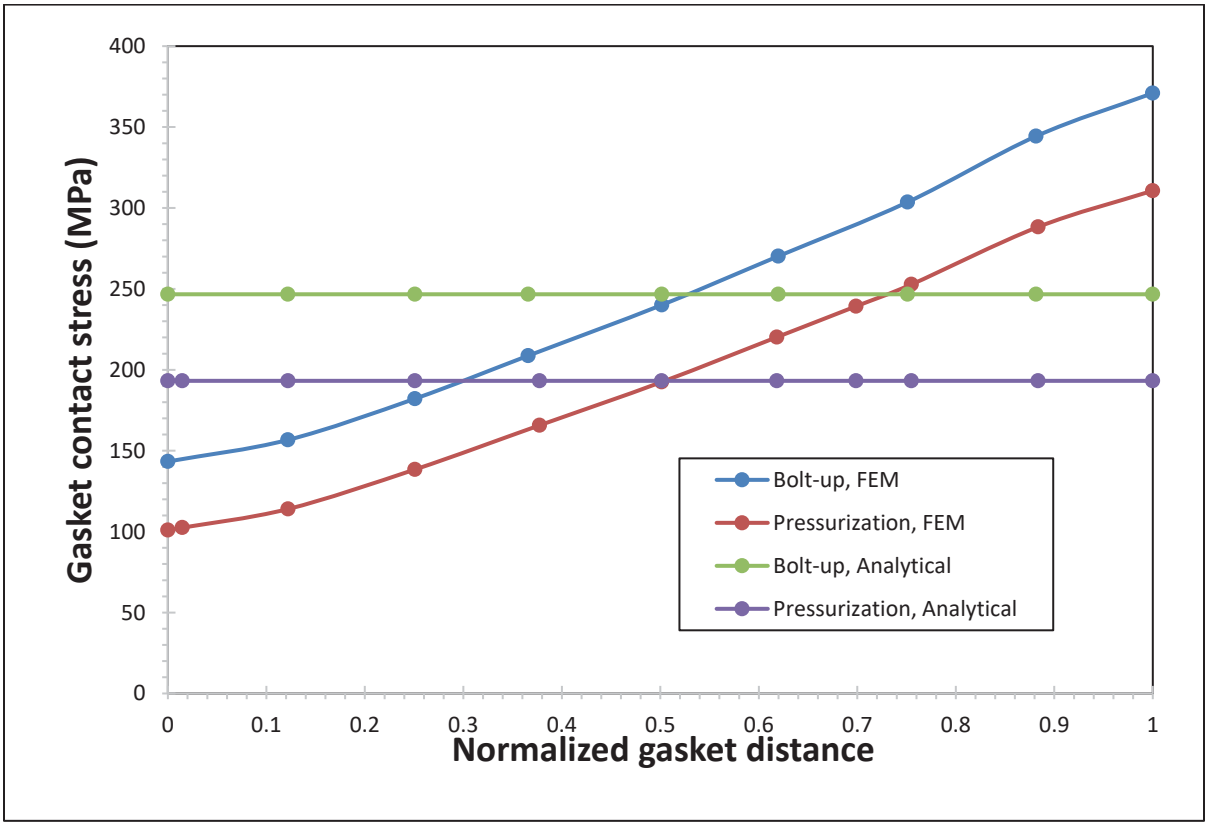

Figure 4-25 Gasket contact stress (MPa) in function of the Normalized gasket distance for NPS 14

NPS 16:

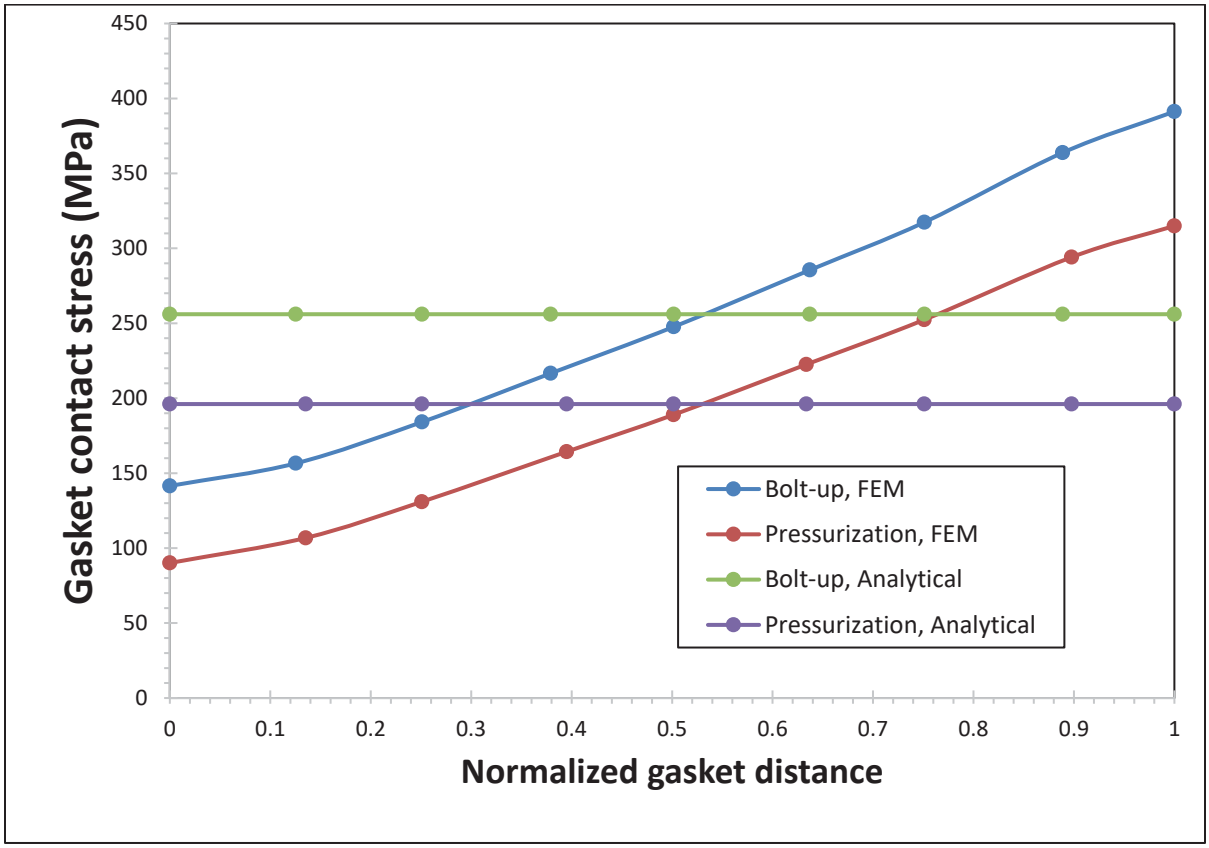

Figure 4-26 Gasket contact stress (MPa) in function of the Normalized gasket distance for NPS 16

NPS 20:

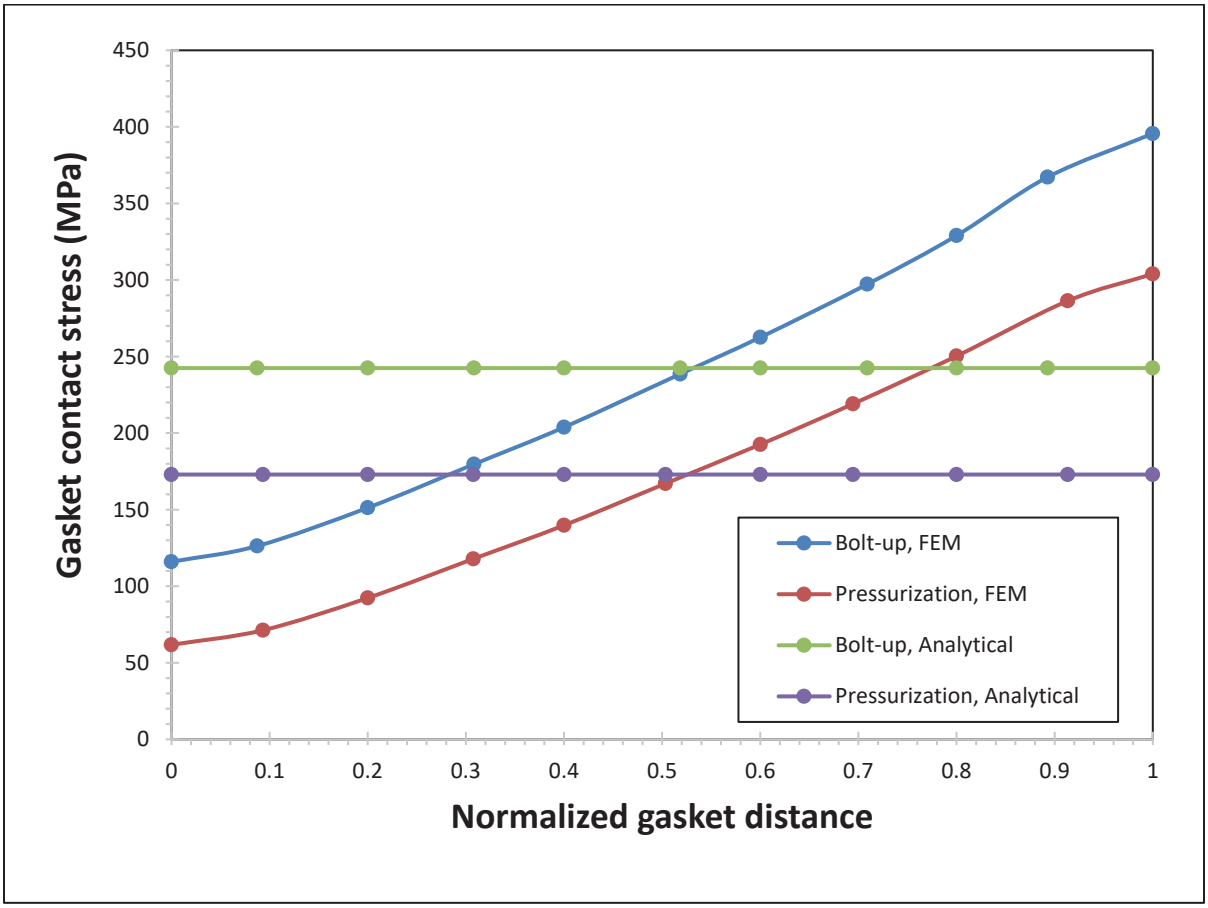

Figure 4-27 Gasket contact stress (MPa) in function of the Normalized gasket distance for NPS 20

NPS 24:

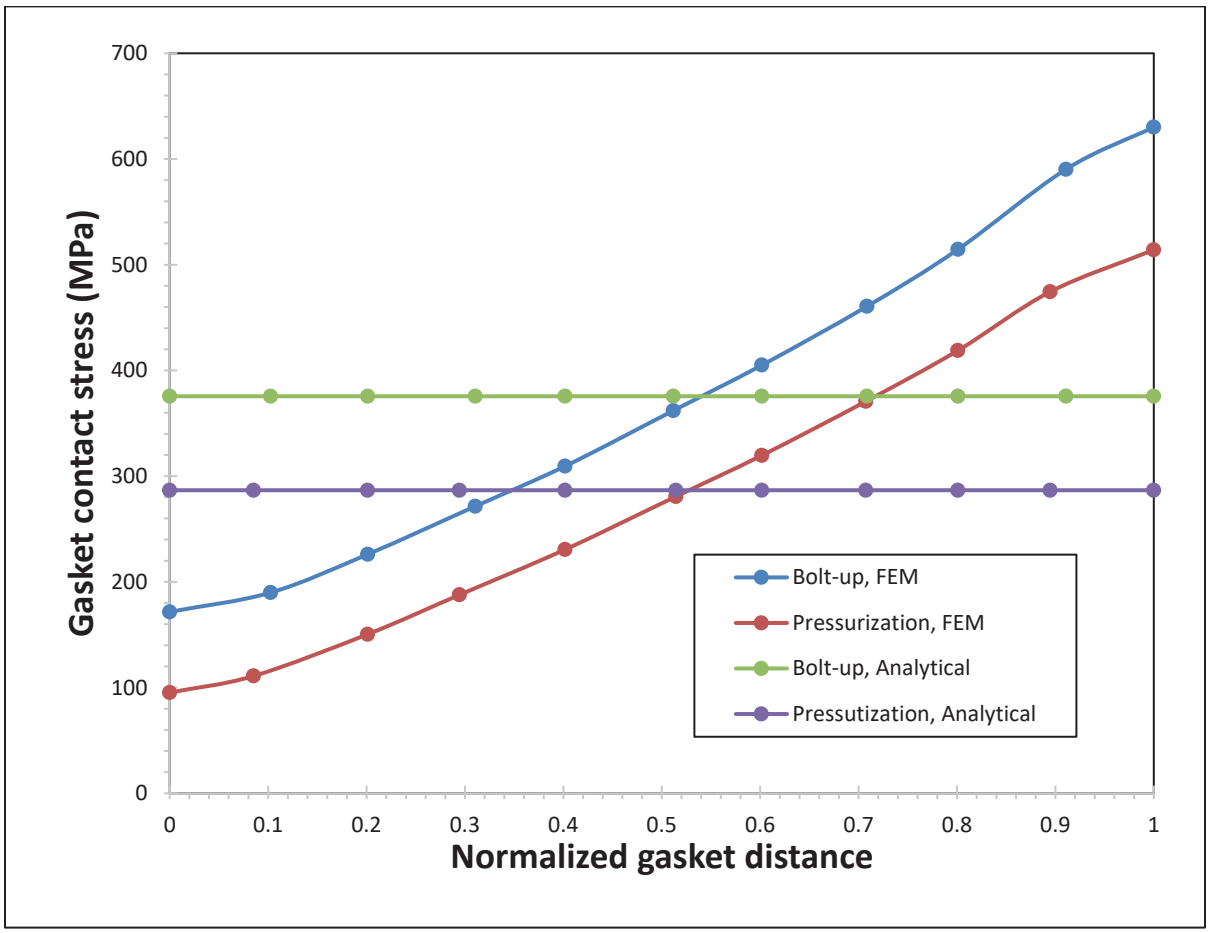

Figure 4-28 Gasket contact stress (MPa) in function of the Normalized gasket distance for NPS 24

4.6 Bolt Stress

As seen in Table 4-1, all the bolts have been tightened to the same amount of stress during bolt-up, which is 50 ksi or 344.8 MPa. The bolt stress is shown to decrease when the pressure is applied. For example: for NPS 8, the bolt stress decreases from 344.8 MPA during bolt-up to 336.3 MPA during pressurization. The bolt stress decrease is due to the lateral pressure that causes the barreling effect or a rotation of the hub and flange ring around the circumferential direction.

CONCLUSION

The main purpose of this study was to investigate the stresses and deformations of selected bolted flange joints of class 900. Different parts of the flange joint such as the flange ring, the hub and shell as well as the bolt and gasket are analyzed during bolt-up and pressurization. In particular, this work compares other important parameters of several bolted flange joints such as the gasket contact stress, the bolt stress, the radial displacement, and the flange rotation during bolt-up and pressurization given by both the analytical and FE methods.

For the purpose of the study, the following seven nominal pipe sizes were selected: NPS 4, 8, 10, 14, 16, 20, and 24, all of which belong to the same class of flanges of 900. All these flanges have the same boundary conditions, constraints and loading. Their bolts have been tightened to 50 ksi and they have been subjected to an internal pressure of 12.5 MPa. The stresses in the flange were confined to the longitudinal and the tangential stresses. Apparently, the radial stress doesn't have a significant effect on the hub and shell, yet it is important for the flange ring, and therefore it was evaluated at the inner and outer surfaces of the flange. During bolt-up, the longitudinal and the tangential stresses are reduced to zero in the shell far from the junction, except during pressurization where the longitudinal stress is half the tangential stress. It should be noted that the maximum stresses are in general located in the hub at its ends or in the junctions with the shell and flange ring. The tangential stress at the outside surface is maximum in the hub near the small end while the longitudinal stress is maximum at the big end.

Also, the maximum radial displacement which is in the hub decreases in shell until it reaches zero far from the junction during bolt-up. During pressurization, it is constantly far from the junction and increases in the hub before decreasing considerably due to the barreling effect.

The gasket contact stress during pressurization is always lower than during bolt-up because the hydrostatic end trust has the effect of unloading the joint. Along these lines, the FEM study shows that the distribution of the gasket contact stress is lower at the inner diameter of the gasket and higher at the outer diameter of the gasket. This trend is the result of the rotation of the flange ring caused by the bolt load and the lateral pressure. Nevertheless, the study shows

that the average gasket contact stress from both the FEM and analytical model are in good agreement.

On another note, the bolt stress during bolt-up is the same for all flanges because the initial tightening is done under the same level of stress; however, the bolt stress during pressurization is found to be reduced indicating that the barreling effect caused by the lateral pressure is present. During pressurization, it is observed that the bolt stress decrease is more important for large size flanges, the flange rotation is greater than during bolt-up, and the large size flange rotation is more significant.

Finally, the FE and analytical results are generally in good agreement. The results demonstrate that the final bolt load decreases in all cases depending on the relative rigidity of the different flange elements with the more rigid flanges showing higher decrease. In addition, there is a significant decrease in the operating gasket contact stress due to the hydrostatic end effect and barreling effect. The higher stresses seem to exist not only in the shell at the shell-to-hub junction, but also in the hub all around. The rotations are rather high above NPS 24 and therefore reaching ASME B16.47 with value exceeding the limiting value of 0.3° of ASME code.

RECOMMENDATIONS

This work examined the stresses and deformations of seven nominal pipe sizes associated with the same class of 900. The study shows a clear link of the size of the flange to the obtained results as the stresses and deformations increase with the diameter of the flange. Nevertheless, the subjectivity of this statement could have been tested had its flange been subjected to a different bolt-up load. A few more flange sizes and other classes should be studied to cover the whole flange standard before drawing general conclusions.

Moreover, future research can focus on studying the non-hubbed flanges in terms of testing the effects of the hub on the flange integrity in order to showcase its benefits as well as its disadvantages in comparison with the above studied integral flanges.

Future research might look at the long-term creep-relaxation behavior of bolted flange joints, focusing on the thermal impacts that occur at high temperatures. Furthermore, extreme environmental conditions, corrosion, and fluid properties are important factors impacting flange integrity and leakage tightness, necessitating a detailed examination. In order to broaden the scope of future research, two major topics should be highlighted. To begin, a thorough study of bolted flange joint durability should include a long-term performance evaluation of bolts and gaskets. This includes examining how they react to cyclic stress, different temperature profiles, and corrosive conditions. Such insights will shed light on probable failure processes and improve the accuracy of lifespan prediction. It is also advised to undertake experimental study on bigger flange joints to validate Finite Element Method (FEM) results. This confirmation will strengthen the credibility of FEM simulations, including those generated by ANSYS software, across a wider array of industrial applications.

APPENDIX

Appendix 1. Recommended Gasket Contact Surface Finish for Various Gasket Types (*PCC-1 Guidelines for Pressure Boundary Bolted Flange Joint Assembly.*, 2010)

Gasket Description	Gasket Contact Surface Finish [Note (1)]	
	μm	μin.
Spiral-wound	3.2–6.4	125–250
Corrugated metal jacket with corrugated metal core; full width and circumference of both sides to be covered with adhesive-backed flexible graphite tape	3.2–6.4	125–250
Grooved metal gasket with facing layers such as flexible graphite, PTFE, or other conformable materials	3.2–6.4	125–250
Flexible graphite reinforced with a metal interlayer insert	3.2–6.4	125–250
Grooved metal	1.6 max.	63 max.
Flat solid metal	1.6 max.	63 max.
Flat metal jacketed	2.5 max.	100 max.
Soft cut sheet, thickness ≤ 1.6 mm ($^1/_{16}$ in.)	3.2–6.4	125–250
Soft cut sheet, thickness > 1.6 mm ($^1/_{16}$ in.)	3.2–13	125–500

Figure 7-1 The appropriate gasket type according to the width of the gasket contact surface

REFRENCES

A Complete Guide to Hex Bolts. (n.d.). RS Components. [Webpage]. Retrieved from https://uk.rs-online.com/web/generalDisplay.html?id=ideas-and-advice/hex-bolts-guide#Hex_Bolt_Materials

Abid, M., & Hussain, S. (2008). Bolt preload scatter and relaxation behavior during tightening a 4 in-900# flange joint with spiral wound gasket. *Proceedings of the Institution of Mechanical Engineers, Part E: Journal of Process Mechanical Engineering, 222(2),* 123–134. https://doi.org/10.1243/09544089JPME160

Alkelani, A., Nassar, S., & Housari, B. (2009). Formulation of Elastic Interaction Between Bolts During the Tightening of Flat-Face Gasketed Joints. *Journal of Mechanical Design,131.* Retrieved from https://citeseerx.ist.psu.edu/

ASME. PCC-1-2010: Guidelines for pressure boundary bolted flange joint assembly. (2010).

ASME-B18.2.1. (2010). Square, Hex, Heavy Hex, and Askew Head Bolts and Hex, Heavy Hex, Hex Flange, Lobed Head, and Lag Screws.

ASME-B16.5. (2009). Pipe Flanges and Flanged Fittings NPS 1 / 2 Through NPS 24 Metric/Inch Standard. Retrieved from https://abangah-co.com/wp-content/uploads/2016/05/ASME-B16.5-2009.pdf

ASME Boiler and Pressure Vessel Code. (2001). Section VIII, Division 2, Appendix 2, "Rules for Bolted Flange Connections with Ring Type Gaskets."

Attoui, H., Bouzid, A.-H., & Waterland, J. (2014). PVP2014-28449 BUCKLING AND LATERAL PRESSURES IN SPIRAL WOUND GASKETS. Retrieved from https://vsptechnologies.com/wp-content/uploads/2018/11/PVP2014-28449-abstract.pdf

Bickford, J. (1998). *Gaskets and Gasketed Joints* (1st ed.). CRC Press. https://doi.org/10.1201/9781498709422

Bickford, J. H. (2008). *Introduction to the design and behavior of bolted joints* (4th ed.). CRC press, Taylor & Francis Group, Fourth edition

Bolts and Nuts for Flanged Connections. (n.d.). Wermac. Retrieved from https://www.wermac.org/bolts/bolts_stud-bolts_for-flanged-connections.html

Bouzid, A., & Nechache, A. (2005). An analytical solution for evaluating gasket stress change in bolted flange connections subjected to high temperature loading. *ASME Journal of Pressure Vessel Technology, 127 (4),* pp. 414-427. https://doi.org/10.1115/1.2042480

Bouzid, A., & Chaaban, A. (1993). Flanged joints analysis: A simplified method based on elastic interaction. *CSME Transactions, 17 (2),* pp. 181-196. https://doi.org/10.1139/tcsme-1993-0011

Bouzid, A., Chaaban, A., & Bazergui, A. (1995). The Effect of Gasket Creep-Relaxation on the Leakage Tightness of Bolted Flanged Joints. *Pressure Vessel Technology, 117(71)*. https://doi.org/10.1115/1.2842093

Bouzid, A.-H., Birembaut, Y., & Lejeune, H. (2009). On the Effect of External Bending Loads in Bolted Flange Joints. *ASME; American Society of Mechanical Engineers Digital Collection*. Retrieved from https://doi.org/10.1115/PVP2007-26039

Bouzid, S., Bouzid, A.-H., & Ngô, A. D. (2022). A Study of the Strength of ASME Section x FRP Flanges. *ASME; American Society of Mechanical Engineers Digital Collection*.

Brown, W. (2007). An Update on Improved Flange Design Methods. 2007 ASME Pressure *Vessels and Piping Division Conference.* https://proceedings.asmedigitalcollection.asme.org

Brown, W., & Lim, T. Y. (2017). Quantifying bolt relaxation during high temperature operation. *American Society of Mechanical Engineers, Pressure Vessels and Piping Division, 3A-2017*. https://doi.org/10.1115/PVP2017-65550

Chen, Y., Xu, Y. Y., Huang, L. Y., Xu, Y. H., & Guan, K. S. (2015). Creep Behavior of Metal-to-Metal Contact Bolted Flanged Joint. *Procedia Engineering, 130,* 214–220. https://doi.org/10.1016/j.proeng.2015.12.211

Choulaei, M., & Bouzid, A. (2021). Stress analysis of bolted flange joints with different shell connections. *ASME International Mechanical Engineering Congress and Exposition, Proceedings (IMECE), V.12,* https://doi.org/10.1115/IMECE2021-72063

Do, T. D. (2012). The effect of bolt spacing on the tightness behavior of bolted flange joints (dissertation). École de technologie supérieure.

Drago, J. (2013) Initial gasket compression is key to safe, reliable flange joints. *Sealing Technol 10–12.*

Eight Materials for Constructing Flanges. (2021). *Texas Flange*. Retrieved from https://www.texasflange.com/blog/8-materials-for-constructing-flanges/

Fukuoka T, Takaki T (2003). Finite element simulation of bolt-up process of pipe flange connections with spiral wound gasket. *J Pressure Vessel Technol 125:*371–378

Galai, H. (2009). Analyse des assemblages à brides boulonnées à face plate (dissertation). École de technologie supérieure.

Garlock. Legacy.garlock.com. (2004). [PDF] Retrieved from https://legacy.garlock.com/sites/default/files/documents/en/Gasket-Constants-for-the-Layman.pdf.

Grine, L., & Bouzid, A.-H. (2013). Analytical and Experimental Studies of Liquid and Gas Leaks through Micro and Nano-Porous Gaskets. *Materials Sciences and Applications, 04(08),* 32–42. https://doi.org/10.4236/msa.2013.48a004

Hamilton, S. (2021). Bolted Flange Joint Assembly: Learning the Technical Aspects – Hex Technology. Hex Technology. Retrieved from https://www.hextechnology.com/articles/bolted-flange-joint-assembly/.

Harrison, S. (2019, December 3). What is m and y gasket design constants, and how are they used? *Triangle Fluid Controls Ltd*. https://trianglefluid.com/what-is-m-and- y-gasket-designconstants-and-how-are-they-used/

Hasha, B. (2011). What Are M and Y Gasket Design Constants, and How Are They Used? *Pumps and Systems Magazine*. Retrieved from https://www.pumpsandsystems.com/what-are-m-and-y-gasket-design-constants-and-how-are-they-used

How to Choose the Best Flange Material | API International, Inc. (2021). *API International, Inc.* https://www.apiint.com/resource-center/how-to-choose-pipe-flange-materials/

Jaszak, P., & Adamek, K. (2019). Design and analysis of the flange- bolted joint with respect to required tightness and strength. *Open Engineering, 9(1),* 338–349. https://doi.org/10.1515/eng-2019-0031

Jenco, JM., Hunt, ES. (2000) Generic issues effecting spiral-wound gasket performance. *Int J Press Vessels Pip, 77*, 825–830

Joshi, T., Sharma, R., Parkash, O., Gupta, A., & Joshi, Preeti. (2021). Advances in engineering design: select proceedings of flame 2020. In Design and analysis of metal-to-metal contact bolted flange joint using fea tool (pp. 315–325). *Springer Singapore*. https://doi.org/10.1007/978-981-33-4684-0_32

Lidonnici, F. (2017). What will be the future of the new flange calculation methods? *Sant'Ambrogio Servizi Industriali*. Retrieved from https://www.sant-ambrogio.it/en/what-will-be-the-future-of-the-new-flange-calculation-methods/

Ma, K., Zhang, Y., Zhang, L., & Guan, K. (2014). Behavior of bolted joints with metal-to-metal contact type gaskets under bolting-up and loading conditions. *Proceedings of the Institution of Mechanical Engineers, Part E: Journal of Process Mechanical Engineering, 230(4),* 284–291. https://doi.org/10.1177/0954408914547931

Mathan, G., Siva Prasad N (2010). Evaluation of effective material properties of spiral wound gasket through homogenization. *Int J Press Vessel Pip, 87,* 704–713

Melone, L. (2013). Learn The Differences Between Studs and Bolts in Automotive Manufacturing. *Melfast.* Retrieved from https://www.melfast.com/blog/2013/12/learn-the-differences-between-studs-and-bolts-in-automotive-manufacturing

Metals, Ep. (n.d.). Flange Types: A Guide to Choosing the Right Flange. *China Piping Solution Supplier*. Retrieved from https://www.epowermetals.com/flange-types-a-guide-to-choosing-the-right-flange.html

Murali Krishna, M., Shunmugam, M. S., & Siva Prasad, N. (2007). A study on the sealing performance of bolted flange joints with gaskets using finite element analysis. *International Journal of Pressure Vessels and Piping, 84(6),* 349–357. https://doi.org/10.1016/j.ijpvp.2007.02.001

Nagy A (1996). Determination of the gasket load drop at large size welding neck flange joints in the case of nonlinear gasket model. *Int J Press Vessels Pip, 67*, 243–248

Nassar SA, Wu Z, Yang X (2010). Achieving uniform clamp load in gasketed bolted joints using a nonlinear finite element model. *J Press Vessel Technol, 132,* 031205

Nassar, S. A., & Alkelani, A. A. (2006). Effect of Tightening Speed on Clamp Load Distribution in Gasketed Joints. Www.sae.org. Retrieved from https://www.sae.org/publications/technical-papers/content/2006-01-1250/

Nechache, A., & Bouzid, A.-H. (2007). Creep analysis of bolted flange joints. International *Journal of Pressure Vessels and Piping, 84,* 185–194. https://doi.org/10.1016/j.ijpvp.2006.06.004

Nechache, A., & Bouzid A. (2008). On the use of plate theory to evaluate the load relaxation in bolted flanged joints subjected to creep. *International Journal of Pressure Vessels and Piping, 85(7),* pp. 486-497. https://doi.org/10.1016/j.ijpvp.2008.01.005

Nelson NR, Siva Prasad N, Sekhar AS (2016). Micromechanical modelling of spiral wound gasket under uniaxial compression. In: *International congress on computational mechanics and simulation*, pp 1116–1119

Nelson, N. R., Prasad, N. S., & Sekhar, A. S. (2017). Influence of Loading Rate on Deformation Behaviour and Sealing Performance of Spiral Wound Gasket in Flange Joint. *2nd International Conference on Mechanical, Manufacturing and Process Plant Engineering,* 83–93. https://doi.org/10.1007/978-981-10-4232-4_7

Nelson, N. R., Prasad, N. S., Sekhar, A. S., & Awang, Mokhtar (2017). 2nd international conference on mechanical, manufacturing and process plant engineering. *In Influence of loading rate on deformation behaviour and sealing performance of spiral wound gasket in flange joint,* 83–93. https://doi.org/10.1007/978-981-10-4232-4_7

Part modeling - Flange design by using revolve command. *Solidmaster.team.* (2021). Retrieved from https://www.solidmaster.team/2021/06/part-modeling-flange-design-by- using.html.

Peth, J., & Friedrich, C. (2018). DESIGN INFLUENCES OF PRELOAD RELAXATION BEHAVIOR IN BOLTED JOINTS USING ALUMINUM PARTS. *6th International Conference Integrity-Reliability-Failure.* https://paginas.fe.up.pt/~irf/Proceedings_IRF2018/data/papers/7242.pdf

Philipps, R. (2017, December 21). When Do Flanged Joints Leak? *LinkedIn.* https://www.linkedin.com/pulse/when-do-flanged-joints-leak-ray-phillips/

Pipe Material - A Complete Guide. (n.d.). *HardHat Engineer*. Retrieved from https://hardhatengineer.com/pipe-material-selection/

Roos, E., Kockelmann, H., & Hahn, R. (2002). Gasket characteristics for the design of bolted flange connections of metal-to-metal contact type. *International Journal of Pressure Vessels and Piping, 79(1)*, 45–52. https://doi.org/10.1016/S0308-0161(01)00127-2

Schaaf, M., & Bartonicek, J. (2008). Calculation of Bolted Flange Connections of Floating and Metal-to-Metal Contact Type. Asmedigitalcollection.asme.org; *American Society of Mechanical Engineers Digital Collection*. https://doi.org/10.1115/PVP2003-1874

Schaaf, M., Bartonicek, J. (2003). Analysis of bolted joints. In Calculation of bolted flange connections of floating and metal-to-metal contact type (pp. 59–64). Essay. *ASMEDC*. https://doi.org/10.1115/PVP2003-1874

Shu, C., U.S, A., & Shyu, M. (2001). Leakage Evaluated and Controlled from Industrial Process Pipeline by Optimum Gasket Assembly Stress.Flange Sealing Guide Gaskets and Bolted Connections. (2012). *A.W. Chesterton Company*. https://cdn2.hubspot.net/

Spetech. (2021). Effect of temperature on bolted flange assemblies. Spetech. Retrieved from https://www.spetech.com.pl/en/publications/effect-temperature-bolted-flangeassemblies.htm

Timoshenko, S., & Woinowsky-Krieger, S. (1989). *Theory of plates and shells* (2nd edition). McGrow-Hill Book Company.

US Hex Bolts - Inches. (n.d.). *The Engineering Toolbox*. Retrieved from https://www.engineeringtoolbox.com/hex-bolts-inches-d_2051.html

Vafadar, A. K., Bouzid, A.-H., & Ngô, A. D. (2020). An Analytical Anisotropic Model to Analyze Fiber Reinforced Polymer Bolted Flange Joints. *ASME; American Society of Mechanical Engineers Digital Collection*. https://doi.org/10.1115/PVP2020-21000

Wagner, H.N.R., Huehne, C., & Niemann S. (2018). Robust knockdown factors for the design of spherical shells under external pressure: Development and validation. *International Journal of Mechanical Sciences, 141,* pp.58–77. https://doi.org/10.1016/j.ijmecsci.2018.03.029

Wasmi, H., Abdullah, M., & Jassim, O. (2016). Development of Model for Creep Relaxation of Soft Gaskets in Bolted Joints at Room Temperature. *International Journal of Current Engineering and Technology, 6(4).* Retrieved from https://www.researchgate.net/publication/318700584_Development_of_Model_for_Creep_Relaxation_of_Soft_Gaskets_in_Bolted_Joints_at_Room_Temperature

Zacal, J., & Jancar, L. (2020). Effect of Temperature on Bolt Working Load of Pressure Vessels. 20 In S. Medvecký, S. Hrček, R. Kohár, F. Brumerčík, & V. Konstantová (Eds.), *Current Methods of Construction Design, Lecture Notes in Mechanical Engineering* (pp. 433–444). Springer. https://doi.org/10.1007/978-3-030-33146-7_50

Zhu, L., Bouzid, A. H., Hong, J., & Zhang, Z. (2018). Elastic interaction in bolted flange joints: An analytical model to predict and optimize bolt load. *Journal of Pressure Vessel Technology, Transactions of the ASME, 140(4).* https://doi.org/10.1115/1.404